Summer 2009

Investigating the impact of microbial interactions with geologic media on geophysical properties

Caroline A. Davis

INVESTIGATING THE IMPACT OF MICROBIAL INTERACTIONS WITH GEOLOGIC MEDIA ON GEOPHYSICAL PROPERTIES

by

CAROLINE ANN DAVIS

A DISSERTATION

Presented to the Faculty of the Graduate School of the

MISSOURI UNIVERSITY OF SCIENCE AND TECHNOLOGY

In Partial Fulfillment of the Requirements for the Degree

DOCTOR OF PHILOSOPHY

in

GEOLOGY AND GEOPHYSICS

2009

Approved by

Estella A. Atekwana, Advisor
Eliot A. Atekwana
Neil L. Anderson
Melanie R. Mormile
Lee D. Slater

PUBLICATION DISSERTATION OPTION

This dissertation has been prepared in the style utilized by the Geophysical Research Letters journal. Pages 51-62 have been submitted for publication in that journal. An Appendix has been added for purposes normal to dissertation writing.

ABSTRACT

The goals of this study were to investigate the effect of: (1) microbial metabolic byproducts, microbial growth, and biofilm formation on the low frequency electrical properties of porous media, (2) biofilm formation on acoustic wave properties, and (3) the natural electrical (self-potential) signatures associated with an *in-situ* biological permeable reactive barrier (PRB). The results suggest: (1) increases in electrolytic conductivity are consistent with increased concentrations of organic acids and biosurfactants; (2) mineral weathering promoted by organic acids causes increases in electrolytic conductivity, concomitant with increases in major cation concentrations; (3) interfacial conductivity generally parallels microbial cell concentrations and biofilm formation; (4) variations in microbial growth and biofilms causes spatiotemporal heterogeneity in the elastic properties of porous media; (5) SP signatures associated with the injection of groundwater into an in-situ biological PRB are dominated by diffusion potentials induced by the injections. The results suggest that electrolytic conductivity may be useful as an indicator of metabolism, while interfacial conductivity may be used as proxy indicator for microbial growth and biofilm formation in porous media. In addition, acoustic measurements may provide diagnostic spatiotemporal data for the validation of bioclogging models/simulations. Collectively, this study provides further evidence that geophysical measurements are sensitive to microbial-induced changes to geologic media, and may be useful for the detection and monitoring of subsurface microbial growth, activity, and distribution such as in microbial enhanced oil recovery, assessing biofilm barriers used for contaminant remediation, or as sealants for reservoirs in CO_2 sequestration studies.

ACKNOWLEDGMENTS

First and foremost, I would like to sincerely thank my advisor, Dr. Estella Atekwana, for all of her seemingly endless support, encouragement, and the extreme patience she has provided me during this long endeavor. I am very grateful for her mentorship and the fantastic research opportunities she has afforded me, and I honestly don't think I could have accomplished this major milestone in my life without her. I would also like to thank and acknowledge the guidance provided by my dissertation committee. Dr. Eliot Atekwana taught me how to defend my research, my opinion, and myself, and helped to make me a better scientist, and for this I am very appreciative. I thank Dr. Melanie Mormile and her students for lab assistance, and for teaching me the microbiological methods I needed for my research to succeed. Dr. Neil Anderson took a chance on me and encouraged me to do my Ph.D. research at UMR (now MS&T), and for this I will always be grateful. I thank Dr. Lee Slater for teaching me all I ever could possibly want to know about complex conductivity measurements, and for the fantastic opportunity to do field research in Northern Ireland.

I would like to send a big thank you to the GS&E Department at MS&T, in particular Katherine Mattison and Dr. Shari Dunn-Norman. I acknowledge the MS&T Chancellor's Fellowship I was awarded, the NSF grant that funded my Ph.D. research (OCE-0433869 and OCE-0433739), and the EPA Student Services Contract (EP07D000660). In addition, I thank Dr. Dale Werkema for his mentoring, support, and the opportunity to work on the EPA contract. I thank the OSU School of Geology for allowing me to complete my thesis work in their department. I need to thank the countless undergraduate and graduate students who assisted me with data collection, including Philip Bottrell, Joseph Heidenreich, Lindsay Chasten, Jeremiah Graber, and Marisa Haugen; and the numerous professors who I was able to collaborate with, including Drs. Laura Pyrak-Nolte, Bernd Kulessa, Rory Doherty, Andrew Ferguson, Robert Kalin, and Gamal Abdel Aal.

Finally, I thank my family, especially my parents Denny and Penny Davis for their endless love and support. I could not have done this without you. We did it!

TABLE OF CONTENTS

LIST OF FIGURES

LIST OF TABLES

NOMENCLATURE

Symbol	Description
σ_b	Bulk Conductivity
σ^*	Complex Conductivity
σ_w	Fluid Conductivity
σ_{el}	Electrolytic Conductivity
σ^*_{int}	Interfacial Conductivity
σ^*_{surf}	Complex Surface Conductivity
$\lvert\sigma\rvert$	Magnitude
ρ^*	Complex Resistivity
ε^*	Complex Permittivity
ω	Angular Frequency
φ	Phase Angle
σ'	Real Conductivity
σ''	Imaginary Conductivity
F	Formation Factor
h	Hydraulic Gradient
C	Streaming Coupling Coefficient
L	Reduced Coupling Coefficient
c_0	Medium Tortuosity
n	Medium Porosity
ε	Fluid Dielectric Constant
η	Fluid Viscosity
ζ	Zeta-potential
C_{comb}	Combined Electrochemical Coupling Coefficient
V	Volume
T	Temperature

1. INTRODUCTION

1.1. MOTIVATION

Microorganisms have played an integral role in Earth's evolution, and the transformations imparted to near-surface geologic systems by microbial activity are well documented in biogeochemical and geomicrobiology studies [e.g., *Chapelle and Bradley*, 1997; *Maier et al.*, 2000]. Geophysicists, however, are only now beginning to realize the importance of microorganisms and microbial processes on geophysical properties. Over the last decade, there has been growing interest in the field of geophysics to find relationships between microbial activity and geophysical signatures [e.g., *Atekwana et al.*, 2006]. As such, recent research has underscored the potential opportunities that exist for geophysical methods to investigate 'bio-geophysical' phenomena, and not just subsurface physicochemical properties as geophysical techniques are usually employed. This has lead to the emergence of a new sub-discipline of geophysics called 'biogeophysics', which is a multi-disciplinary fusion of the fields of biology, geology, and geophysics. Biogeophysics can be broadly defined as the study of geophysical signatures associated with subsurface biological activity [*Atekwana et al.*, 2006]. In particular, biogeophysics seeks to improve understanding of the geophysical response associated with (1) microbial cells, (2) microbial interactions with geologic materials, and (3) microbial-induced transformations of geologic media [e.g., *Atekwana et al.*, 2006]. Full realization of the underlying mechanisms responsible for these biogeophysical signatures, however, has not yet been achieved. Ultimately, a better understanding of biogeophysical signatures may allow for the utilization of geophysical methods to detect, characterize, and even monitor the growth and activity of microorganisms in the subsurface.

Microbial transformations of geologic media are complex, often coupled, and can occur over a wide range of spatial and temporal scales. Therefore, it is often difficult to predict the extent of these dynamic microbial-induced alterations in subsurface environments. A generalized conceptual diagram of the possible affects of microbial growth and activity on the physicochemical properties of porous media is shown in Figure 1.1. Current biogeochemical sampling and analytical methods can provide some

information regarding the extent and distribution of subsurface microbial activity by looking at trends in the concentration of biogeochemical indicators (e.g., electron acceptors, organic acids). These methodologies, however, are often expensive, laborious, and are limited in the spatial and temporal resolution needed to evaluate microbial activity at the field scale. Therefore, the ability to develop and employ cost effective, minimally invasive tools that span the spatiotemporal scales associated with microbial activity, such as geophysical methods, would have beneficial implications for studies aimed at assessing subsurface microbial processes. The geophysical signatures associated with subsurface microbial processes and microbial-induced alterations to geologic media, however, are not well understood. Figure 1.1 demonstrates that changes in the geophysical properties of geologic media are the end product of the integrated biogeochemical processes associated with microbial growth and activity. Thus, the challenge is decoupling the complex microbial-induced physical and chemical transformations inherent during microbial activity, and quantifying the magnitudes of the geophysical response.

1.2. PREVIOUS BIOGEOPHYSICAL STUDIES

Historically speaking, the idea of biogeophysics first began with research studies conducted at an aged hydrocarbon contaminated site. While lower bulk conductivity would be expected in hydrocarbon contaminated environments, consistent with the insulating properties of hydrocarbons [e.g., *Mazac et al.*, 1990], previous field studies observed anomalous elevated conductivity in zones with enhanced microbial activity [e.g., *Bermejo et al.*, 1997; *Sauck et al.*, 1998]. The elevated conductivity values were attributed to microbial degradation of the hydrocarbons and the associated microbial-induced alterations to the physicochemical properties of the subsurface media [e.g., *Bermejo et al.*, 1997; *Sauck et al.*, 1998; *Atekwana et al.*, 2000; *Werkema, et al.*, 2003].

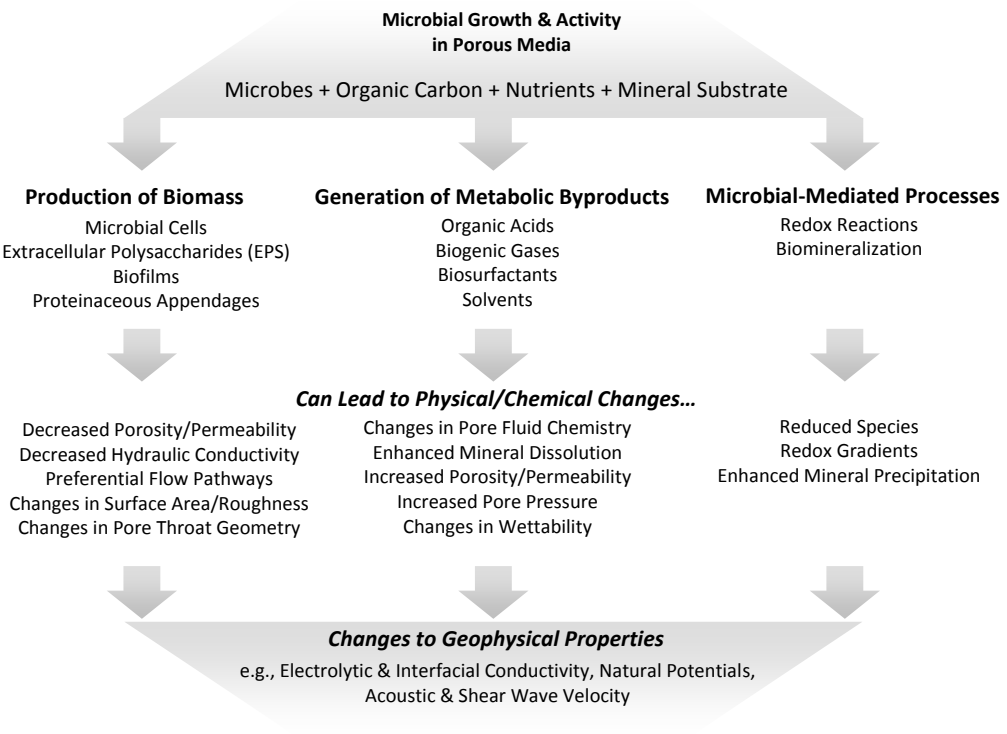

Figure 1.1. Generalized conceptual diagram showing that microbial growth and activity in porous media can alter the physicochemical properties, and thus the geophysical properties of porous media.

Motivated by the *Bermejo et al.* [1997] and *Sauck et al.* [1998] studies, microbial-induced alterations to the electrical properties of porous media have been the subject of a number of additional biogeophysical studies [e.g., *Atekwana et al.*, 2004a-d; *Naudet and Revil*, 2005; *Ntarlagiannis et al.*, 2005a&b; *Williams et al.*, 2005; *Slater et al.*, 2007a; 2007b]. Various microbial-induced physicochemical changes have been suggested to explain the elevated bulk conductivity, such as (1) increased ionic strength of pore fluid by addition of metabolic byproducts to solution [*Sauck et al.*, 1998; *Abdel Aal et al.*, 2004; *Atekwana et al.*, 2004a], (2) increased fluid conductivity and concentration of total dissolved solids (TDS) through enhanced mineral weathering by organic acids [*Sauck et al.*, 1998; *Atekwana et al.*, 2004b; 2005], (3) presence and activity of distinct microbial populations [*Allen et al.*, 2007]; and (4) increased microbial cell density [*Ntarlagiannis et al.*, 2005b] and enhanced attachment of microbes to mineral surfaces resulting in

alterations of the electrical properties at the cell-mineral interface [*Abdel Aal et al.*, 2004; 2006; 2009; *Davis et al.*, 2006]. While these studies all provide plausible, generally qualitative explanations for the generation of the anomalous conductivity, the relative contributions of the various different mechanisms remains unknown.

To date, most previous biogeophysical research has focused on geoelectrical methods to investigate microbe-sediment-geophysics relationships. In particular, laboratory studies have documented the sensitivity of dielectric spectroscopy [e.g., *Prodan et al.*, 2004] and induced polarization (IP) [e.g., *Ntarlagiannis et al.*, 2005b; *Abdel Aal et al.*, 2009] methods for the direct detection of microbial cells. In addition, the IP method has been found useful for the investigation of the presence of attached microbial cells [e.g., *Abdel Aal et al.*, 2009] and biofilms [e.g., *Davis et al.*, 2006; *Ntarlagiannis and Ferguson*, 2009], and microbial-induced mineral precipitation [e.g., *Ntarlagiannis et al.*, 2005a; *Slater et al.*, 2007a; *Personna et al*., 2008] in porous media. Further, the self-potential (SP) method has been employed for a number of field and laboratory studies to investigate the natural electrical signatures associated with microbial-induced subsurface transformations and redox gradients [e.g., *Naudet et al.*, 2003; 2004; *Naudet and Revil*, 2005; *Ntarlagiannis et al.*, 2007]. Additionally, while fewer in number, studies have also employed the use of acoustic (compressional) [e.g., *Williams et al.*, 2005] and shear wave [e.g., *DeJong et al.*, 2006] seismic for the investigation of biogeophysical phenomena. A more in-depth review of the geophysical methods employed for biogeophysical investigations can be found in *Atekwana et al.* [2006].

These previous geophysical studies have greatly advanced the field of biogeophysics, documenting the potential that exists for geophysical methods to explore microbial-induced phenomena in the subsurface. However, a mechanistic understanding of the cause of biogeophysical signatures is still lacking. Some of the outstanding questions that remain from these previous investigations include: (1) What are the relative contributions of microbial metabolic byproducts on geophysical signatures? (2) What is the effect of microbial growth and biofilm formation on geophysical properties? (3) What geophysical techniques are best suited for assessing microbial-geologic interactions?

Clearly, there is a knowledge gap in our understanding of not only the expected/predicted geophysical response, but also the mechanisms responsible for measured bio-geophysical responses, warranting further investigation.

1.3. RESEARCH OBJECTIVES

The primary goal of this thesis is to test the hypothesis that microbial growth and activity in geologic media can result in measurable changes to the geophysical properties of the media. To better understand the relationship between microbial activity and geophysical response, laboratory bench-scale column experiments and a field-scale experiment were conducted. The specific objectives of this thesis are to:

1. Determine the direct contribution of metabolic byproducts (organic acids and biosurfactants) to electrical conductivity magnitude and investigate the effect of mineral weathering promoted by organic acids on the temporal conductivity response of porous media.
2. Investigate the direct contribution and relative magnitude of the effect of microbial growth and biofilm formation on the low-frequency electrical properties of porous media.
3. Investigate the spatial and temporal changes in acoustic wave propagation associated with microbial growth and biofilm formation in porous media
4. Investigate the natural electrical signatures associated with an in-situ biological permeable reactive barrier in response to the injection of contaminated groundwater.

Understanding the geophysical response of microbial biosignatures in controlled laboratory investigations is the first step toward recognizing these biosignatures in field geophysical data. A fundamental understanding of the influence of microbial growth and activity on geophysical properties is needed as this biogeophysical approach will allow for more accurate interpretation of geophysical data from near-surface environments where microbial activity is enhanced or stimulated.

In addition, quantitative knowledge of the geophysical signatures associated with microbial activity may allow for minimally invasive geophysical techniques to be employed for monitoring the rates of subsurface biogeochemical processes. Such information would have beneficial implications for geomicrobiology investigations including bioremediation and microbial enhanced oil recovery (MEOR) activities.

1.4. OUTLINE OF THESIS

This introductory ***section (one)*** outlines the motivation and research objectives for this study. A description is given on microbial growth and activity in geologic media, and the potential effects of microbial-induced alterations to the physicochemical properties of the media.

Section two provides a brief literature review of the background, theory, and method of measurement for the geophysical techniques used in this thesis study.

Paper one describes the results of a laboratory experiment aimed at investigating the first objective of this study, to assess the direct contribution of metabolic byproducts to the low frequency (0.1-1000 Hz) electrical properties of porous media. The affect of mineral weathering promoted by organic acids is also investigated. The results of this experiment show that increases in electrolytic (fluid and real) conductivity are consistent with increases in concentrations of organic acids and biosurfactant. Increases in the electrolytic conductivity are also consistent with temporal increases major cation concentrations, which is indicative of mineral weathering, with a secondary affect on the interfacial conductivity. The results of this experiment suggest that electrolytic conductivity measurements may be useful as an indicator of microbial metabolism.

Paper two reports on the results of a laboratory experiment conducted to accomplish the second objective, to investigate the effect of microbial growth and biofilm formation on the low frequency electrical properties of porous media. The results of this experiment showed that interfacial conductivity generally paralleled the attached microbial cell concentrations in the biostimulated (bacteria + nutrients + diesel) columns. The results suggest that interfacial conductivity measurements may be used as proxy indicator for microbial growth and biofilm formation in porous media.

Paper three describes the results of a laboratory experiment aimed at

investigating the spatial and temporal changes in acoustic wave propagation associated with microbial growth and biofilm development in porous media. The results from the biostimulated column show an overall temporal decrease in acoustic wave velocity and exhibit variations in acoustic wave amplitude spatially over a 2D area of the column. While the exact mechanisms responsible for the differences in velocity and amplitude are yet unclear, the spatial variations appear to correlate with differences in the amount of attached biofilm and/or biofilm architecture.

Paper four describes the results of a field-scale experiment aimed at assessing the natural electrical (self-potential) signatures associated with the injection of contaminated and uncontaminated groundwater into an in-situ biological permeable reactive barrier. The results show that the self-potential (SP) signals are dominated by electrochemical (diffusion) potentials induced by the injections, though the affect of microbial activity can not be completely ruled out.

Section three provides a summary of the observations and conclusions of this study. This chapter also lists questions raised during this study and discusses future directions for research.

1.5. REFERENCES

Abdel Aal, G.Z., Atekwana, E.A., Slater, L.D., and Atekwana E.A. (2004), Effects of microbial processes on electrolytic and interfacial electrical properties of unconsolidated sediments, Geophys. Res. Lett., 31(12), L12505, doi:10.1029/2004GL020030.

Abdel Aal, G.Z., Slater, L.D., Atekwana, E.A. (2006), Induced-polarization measurements on unconsolidated sediments from a site of active hydrocarbon biodegradation, Geophysics, 71, H13-H24.

Abdel Aal, G., Atekwana, E., Radzikowski, S., Rossbach, S. (2009), Effect of bacterial adsorption on low frequency electrical properties of clean quartz sands and iron-oxide coated sands, Geophys. Res. Lett., 36, L04403, doi:10.1029/2008GL036196.

Allen, J.P., Atekwana, E.A., Atekwana, E.A., Duris, J.W., Werkema, D.D., and Rossbach, S. (2007), The microbial community structure in petroleum-contaminated sediments corresponds to geophysical signatures, Appl. Environ. Microbiol., 73, 2860-2870.

Atekwana, E.A., Sauck, W.A., and Werkema Jr., D.D. (2000), Investigations of geoelectrical signatures at a hydrocarbon contaminated site, J. Appl. Geophys., 44, 167-180.

Atekwana, E.A., Atekwana, E.A., Legall, F.D., and Krishnamurthy, R.V. (2004a), Field evidence for geophysical detection of microbial activity, Geophys. Res. Lett., 31, L23603, doi:10.1029/2004GL021576.

Atekwana, E.A., Atekwana, E.A., Rowe, R.S., Werkema, D.D., and Legall, F.D. (2004b), Total dissolved solids in groundwater and its relationship to bulk conductivity of soils contaminated with hydrocarbon, J. Appl. Geophys., 56, 281-294.

Atekwana, E.A., Atekwana, E.A., Werkema, D.D., Allen, J.P., Smart, L.A., Duris, J.W., Cassidy, D.P., Sauck, W.A., and Rossbach, S. (2004c), Evidence for microbial enhanced electrical conductivity in hydrocarbon-contaminated sediments, Geophys. Res. Lett., 31, L23501.

Atekwana, E.A., Werkema, D.D., Duris, J.W., Rossbach, S., Atekwana, E.A., Sauck, W.A., Cassidy, J.P., Means, J., and Legall, F.D. (2004d), In-situ apparent conductivity measurements and microbial population distribution at a hydrocarbon-contaminated site, Geophysics, 69, 56-63.

Atekwana, E.A., Atekwana, E.A., Legall, F.D., and Krishnamurthy, R.V. (2005), Biodegradation and mineral weathering controls on bulk electrical conductivity in a shallow hydrocarbon contaminated aquifer, J. Contam. Hydrol., 80, 149-167.

Atekwana, E.A., Atekwana, E.A., and Werkema, D.D. (2006), Biogeophysics: the effects of microbial processes on geophysical properties of the shallow subsurface. In Applied Hydrogeophysics, Vereecken, H., Binley, A., Cassiani, G., Revil, A., and Titov, K., (eds.), NATO Sci. Ser. IV, Springer: New York, pp. 161–193.

Bermejo, J.L., Sauck, W.A., and Atekwana, E.A. (1997), Geophysical discovery of a new LNAPL plume at the former Wurtsmith AFB, Ground Water Monit. Remed., 17, 131-137.

Chapelle, F.H., and Bradley, P.M. (1997), Alteration of aquifer geochemistry by microorganisms. In Hurst, C.J. (ed.), Manual of Environmental Microbiology, ASM Press, Washington, DC, pp. 558-564.

Davis, C.A., Atekwana, E.A., Atekwana, E.A., Slater, L.D., Rossbach, S., and Mormile, M.R. (2006), Microbial growth and biofilm formation in geologic media is detected with complex conductivity measurements, Geophys. Res. Lett., 33, L18403, doi:10.1029/2006GL027312.

DeJong, J.T., Fritzges, M.B., and Nusslein, K. (2006), Microbially induced cementation to control sand response to undrained shear, J. Geotech. Geoenviron. Eng., 132(11), 1381-1392.

Maier, R.M., Pepper, I.L., and Gerba, C.P. (2000), Environmental Microbiology, Academic Press, San Diego, CA, 585 p.

Mázac, O., Benes, L., Landa, I., and Maskova, A. (1990), Determination of the extent of oil contamination in groundwater by geoelectrical methods. In Ward, S.H. (ed.), Geotechnical. Env. Geo., 2, pp. 107-112.

Naudet, V., A. Revil, J.-Y. Bottero, and Bégassat, P. (2003), Relationship between self-potential (SP) signals and redox conditions in contaminated groundwater, Geophys. Res. Lett., 30(21), 2091, doi:10.1029/2003GL018096.

Naudet, V., A. Revil, E. Rizzo, J. Y. Bottero, and Begassat, P. (2004), Groundwater redox conditions and conductivity in a contaminant plume from geoelectrical investigations, Hydrol. Earth. Syst. Sci. 8(1), 8-22.

Naudet, V., and Revil, A. (2005), A sandbox experiment to investigate bacteria mediated redox processes on self-potential signals, Geophys. Res. Lett., 32, L11405, doi:10.1029/2005GL022735.

Ntarlagiannis, D., Williams, K.H., Slater, L., and Hubbard, S. (2005a), The low frequency electrical response to microbially induced sulfide precipitation, J. Geophys. Res., 110, G02009, doi:10.1029/2005JG000024.

Ntarlagiannis, D., Yee, N., and Slater, L. (2005b), On the low frequency induced polarization of bacterial cells in sands, Geophys. Res. Lett., 32, L24402, doi:10.1029/2005GL024751.

Ntarlagiannis, D., Atekwana, E.A., Hill, E.A., and Gorby, Y. (2007), Microbial nanowires: Is the subsurface "hardwired"?, Geophys. Res. Lett., 34(17).

Ntarlagiannis, D., and Ferguson, A. (2009), SIP response of artificial biofilms, Geophysics, 74(1), A1-A5.

Personna Y.R., Ntarlagiannis, D., Slater, L., Yee, N., O'Brien, M., and Hubbard, S. (2008), Spectral induced polarization and electrodic potential monitoring of microbially mediated iron sulfide transformations, J. Geophys. Res., 113, G02020, doi:10.1029/2007JG000614.

Prodan, C., F. Mayo, J. R. Claycomb, J. H. Miller, and Benedik, M.J. (2004), Low-frequency, low-field dielectric spectroscopy of living cell suspensions, J. Appl. Phys., 95, 3754-3756.

Sauck, W.A., Atekwana, E.A., and Nash, M.S. (1998), High conductivities associated with an LNAPL plume imaged by integrated geophysical techniques, J. Environ. Eng. Geophys., 2, 203-212.

Slater, L., Ntarlagiannis, D., Personna, Y.R., and Hubbard, S. (2007a), Pore-scale spectral induced polarization signatures associated with FeS biomineral transformations, Geophys. Res. Lett., 34, L21404, doi: 10.1029/2007GL031840.

Slater, L., Ntarlagiannis, Yee, N., O'Brien, M., Zhang, C., and Williams, K.H. (2007b), Electrodic voltages in the presence of dissolved sulfide: Implications for monitoring natural microbial activity, Geophysics, 73(2), 65-70.

Werkema, D.D., Atekwana, E.A., Enders A., Sauck, W.A., and Cassidy, D.P. (2003), Investigating the geoelectrical response of hydrocarbon contamination undergoing biodegradation, Geophys. Res. Lett., 30, 1647, doi: 10.1029/2003GL017346.

Williams, K.H., D. Ntarlagiannis, L. Slater, A. Dohnalkova, S.S. Hubbard, and Banfield, J.F. (2005), Geophysical imaging of stimulated microbial biomineralization, Environ. Sci. Technol., 39(19), 7592-7600.

2. REVIEW OF LITERATURE: GEOPHYSICAL METHODS

2.1. COMPLEX CONDUCTIVITY METHOD

2.1.1. Theory and Background. The complex conductivity or spectral induced polarization (SIP) method is a geophysical technique that extends upon the DC-resistivity method [e.g., *Olhoeft*, 1985] by measuring both the conductive and capacitive low-frequency (<1 kHz) electrical properties of earth materials. The electrical properties of porous earth materials can be described in terms of either complex conductivity (σ*), complex resistivity (ρ*), or complex permittivity (ε*) [e.g., *Slater*, 2006], where:

$$\sigma^* = \frac{1}{\rho^*} = i\omega\varepsilon^*, \tag{1}$$

$i = \sqrt{-1}$, and ω is the angular frequency. In terms of the in-phase or real (σ') and the out-of-phase or imaginary (σ") components of σ*:

$$\sigma^* = |\sigma| e^{i\varphi} = \sigma' + i\sigma'', \tag{2}$$

where |σ| and φ are the measured conductivity magnitude and phase angle, respectively. Further, the relationship between the measured |σ| and φ parameters and the σ' and σ" components can be described as:

$$|\sigma| = \sqrt{(\sigma')^2 + (\sigma'')^2}, \tag{3}$$

$$\varphi = \tan^{-1}\frac{\sigma''}{\sigma'} \cong \frac{\sigma''}{\sigma'}, \tag{4}$$

if the φ is < 100 mrad. Thus, for small phase angles the measured φ is the ratio of conduction to polarization.

The real part of σ* represents ohmic conduction currents (energy loss) that are in-phase with the applied electric field, whereas the out-of-phase imaginary part is a much smaller component which represents polarization or energy storage. In the absence of metallic minerals, there are two pathways available for electric charge transport within a porous medium, occurring by (1) electrolytic conduction (σ_{el}) via the fluid-filled pore spaces, and (2) interfacial conduction via ion migration within the electrical double layer (EDL) at mineral-fluid interfaces [*Lesmes and Morgan*, 2001]. At the low frequencies measured by the complex conductivity method these two pathways are commonly assumed to add in parallel [e.g., *Waxman and Smits*, 1968; *Vinegar and Waxman*, 1984], and can be modeled as:

$$\sigma^* = \sigma_{el} + \sigma^*_{surf}(\omega) = [\sigma_{el} + \sigma'_{surf}(\omega)] + i\sigma''_{surf}(\omega), \tag{5}$$

where (σ'_{surf}) and (σ''_{surf}) are the frequency-dependant real and imaginary parts of complex surface conductivity (σ^*_{surf}), respectively [*Lesmes and Frye*, 2001]. We assume that:

$$\omega\varepsilon_{el} << \sigma''_{surf}(\omega), \tag{6}$$

where ε_{el} is equivalent to the high frequency dielectric permittivity (ε_∞) [*Slater and Lesmes*, 2002]. Further, in coarse clay-free porous media $\sigma_{el} >> \sigma'_{surf}$, and as such $\sigma' \approx \sigma_{el}$, and can be expressed using Archie's equations [*Archie*, 1942]:

$$\sigma' = \sigma_{el} = \left(\frac{1}{F}\right)\sigma_w S_w^n = \sigma_w \phi_{eff}^m S^n, \tag{7}$$

where σ_w is the fluid conductivity, F represents the formation factor, S is the degree of saturation, ϕ_{eff} is the effective porosity, n is the saturation exponent, and m is the cementation exponent.

The real conductivity is dependent on both the electrolytic and interfacial

(surface) conduction, whereas the imaginary conductivity is uniquely sensitive to interfacial processes. Interfacial conduction and polarization are dependent on surface area, ionic charge density, and ionic mobility [e.g., *Vinegar and Waxman*, 1984; *Revil and Glover*, 1998; *Lesmes and Frye*, 2001]. In the absence of metallic minerals, the imaginary conductivity response is commonly attributed to ion migration within the electrical double layer (EDL) at mineral-fluid interfaces [*Lesmes and Morgan*, 2001]. However, other mechanisms can result in polarization effects, such as ion accumulation in pore throats and reduced ionic mobility [e.g., *Vinegar and Waxman*, 1984]. Further discussion of these polarization mechanisms can be found in *Telford et al.* [1991] and *Kearey et al.* [2002].

2.1.2. Method of Measurement. The complex conductivity measurements collected for this thesis study were obtained with a two-channel dynamic signal analyzer (DSA) by using a four-electrode technique [*Vanhala and Soininen*, 1995; *Slater and Lesmes,* 2002]. Figure 2.1 shows the DSA and the laboratory-scale column setup for experimental complex conductivity measurements. Current was injected through a pair of silver-silver chloride (Ag-AgCl) electrode coils placed at the ends of the experimental columns, and the electrical response was measured with two non-polarizing Ag-AgCl potential electrodes installed between the current electrodes. The potential electrodes were located in fluid-filled chambers outside of the current path in an effort to minimize any spurious polarization effects that may develop at the fluid-electrode interface [e.g., *Vanhala and Soininen*, 1995]. The distance between the current and potential electrodes varied depending on the column geometry for each specific experiment. Using this setup, the impedance magnitude ($|\sigma|$) and phase shift (φ) of the sample was measured between a measured voltage sinusoid and an impressed current sinusoid, relative to a high-quality resistor at 40 frequency intervals between 0.1 and 1000 Hz. The measured $|\sigma|$ and φ were then used to calculate the real (σ') and imaginary (σ'') conductivity as follows:

$$\sigma' = |\sigma| \cos\varphi \tag{8}$$

$$\sigma'' = |\sigma| \sin\varphi \tag{9}$$

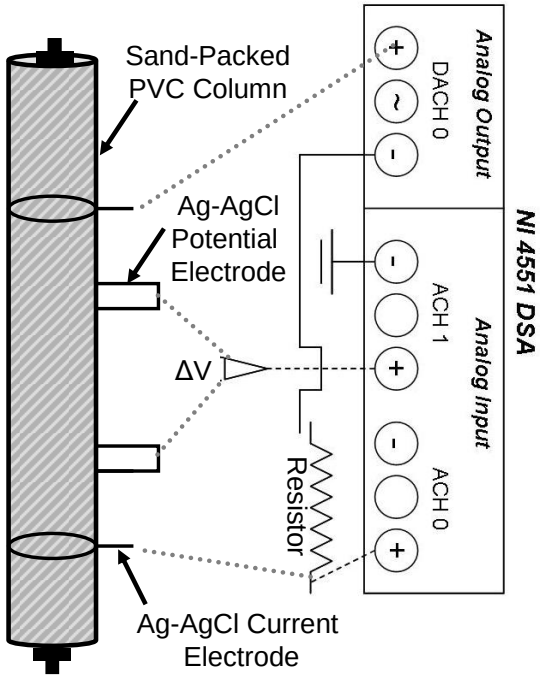

Figure 2.1: Drawing showing the general setup for collecting complex conductivity measurements using a dynamic signal analyzer.

2.2. SELF-POTENTIAL METHOD

2.2.1. Theory and Background. The self-potential (SP) method, or the spontaneous potential method, is a geophysical technique that is based upon the passive measurement of naturally occurring electric potentials in the subsurface with non-polarizable electrodes in contact with the ground surface. Natural electric potentials, or SP anomalies, can be generated by a variety of factors and/or mechanisms, and include electrokinetic, electrochemical, mineralization, redox, thermoelectric, and bioelectric potentials [e.g., *Nyquist and Corry*, 2002]. In natural environments, however, the SP response often results from a combination of mechanisms [e.g., *Darnet and Marquis*, 2004; *Kulessa et al.*, 2003; *Maineult et al.*, 2004].

An electrical field that develops in association with the flow of fluid through a porous medium is often called an electrokinetic or streaming potential [e.g., *Ernstson and*

Scherer, 1986]. Streaming potentials can arise from the drag of excess charge of the pore fluid during fluid flow through a porous medium [e.g., *Nyquist and Corry*, 2002; *Revil et al.*, 2003; *Boleve et al.*, 2007], and the resultant electrical field commonly parallels the direction of fluid flow. The potential that is generated is a function of the hydraulic gradient and the electrokinetic coupling coefficient. Based on the classical description of electrokinetic theory [e.g., *Sill*, 1983], the current density is related to pore fluid pressure gradients and a streaming current coupling coefficient which is dependent on the zeta-potential (ζ), an interfacial property of the porous media [e.g., *Boleve et al.*, 2007]. A proportional relationship exists between hydraulic gradient (Δh) and SP, which is described by a streaming coupling coefficient (C) [*Fournier*, 1989; *Revil et al.*, 2003]. Thus, streaming potential is equal to:

$$\Delta SP = C\Delta h \tag{10}$$

where

$$C = \frac{L}{\sigma_w}, \tag{11}$$

and

$$L = -\frac{c_0 n \varepsilon \zeta}{\eta}, \tag{12}$$

where L is the reduced coupling coefficient, σ_w is fluid conductivity, c_0 is material medium tortuosity, n is medium porosity, ε is fluid dielectric constant, η is fluid viscosity. A recently revised formulation of the electrokinetic theory developed by *Revil and Leroy* [2004] and *Revil et al.* [2005], and presented in *Boleve et al.* [2007], describes a direct dependence of streaming potential on the microstructure of porous media, and more specifically permeability. Herein, we will focus on the classic formulation of the streaming potentials, but it is worth mentioning the importance of the new formulation for investigating the effect of microstructure on SP signals.

Electrochemical potentials can arise from differences in chemical composition, such as concentration gradients and redox gradients, known as diffusion potentials and electro-redox potentials, respectively. Diffusion potentials can result from ionic

concentration gradients in solutions with ions of differing ionic mobilities [e.g., Reynolds, 1997]. This electrochemical effect is related to differences in fluid conductivity (σ_1/σ_2), and can be described by a combined electrochemical coupling coefficient (C_{comb}) [*Kulessa et al.*, 2003], where:

$$\Delta SP = C_{comb} \ln (\sigma_1/\sigma_2) \quad (13)$$

A 'geobattery' model has been used to describe the strong SP response measured over subsurface ore deposits, associated with oxidation-reduction reactions [e.g., *Sato and Mooney*, 1960]. Previous researchers have described this geobattery model as being the shuttling of electrons from oxidized zones above the water table to reduced zones below the water table [e.g., *Sato and Mooney*, 1960; *Timm and Moller*, 2001]. Previous studies have also observed a similar relationship between SP signals and redox potential gradients associated with contaminant plumes [e.g., *Naudet et al.*, 2003; 2004; *Arora et al.*, 2007]. While the mechanisms responsible for this relationship are still not well understood, it has been suggested that a geobattery model may be used to explain this phenomena [e.g., *Naudet et al.*, 2004]. According to *Naudet and Revil* [2005], biomass may act as a conductor to electrically connect the oxidized and reduced zones of contaminant plumes.

2.2.2. Method of Measurement. Collection of SP measurements is relatively non-trivial in that non-polarizing electrodes are placed at the ground surface, connected via wire to a high impedance (>10 MΩ) voltmeter, and the electric potential is measured. There are several different types of non-polarizing electrodes that can be used for SP measurement, but for this thesis study the lead-lead chloride (Pb-$PbCl_2$) type of non-polarizing electrodes were constructed (after *Petiau* [2000]) and employed. The SP method requires the use of non-polarizing electrodes to avoid any reactions (i.e., redox potentials) that may develop at the fluid-electrode interface.

The SP electrodes are placed in contact with the ground surface; one electrode is used for SP measurement (i.e., roving electrode), and another electrode is used as a reference electrode, which is situated at a location far from the SP survey site. For this thesis study, SP data were collected as differential values relative to a reference electrode, and by convention the reference electrode was connected to the negative terminal of the voltmeter.

2.3. ACOUSTIC WAVE METHOD

2.3.1. Background. The 2D acoustic wave scanning system (or the non-destructive testing (NDT) technique of ultrasonic testing) is a techniqe that uses the propagation of high frequency sound energy (or waves) through earth materials and measures the travel time and/or change in intensity of the wave over a constrained distance [e.g., *Blitz and Simpson*, 1996]. Measurement of acoustic wave properties (e.g., velocity and amplitude) can be used to characterize the elastic/viscoelastic properties of a material, as well as the distribution of mechanical properties. Acoustic properties of porous media are generally dependant on the bulk modulus of the saturating fluid [e.g., *Knight and Nolen-Hoeksema*, 1990], the elastic moduli of the solid media [e.g., *Ecker et al.*, 1998], and the solid-fluid interactions [e.g., *Clark et al.*, 1980]. Discussion of acoustic wave theory can be found in *Telford et al.* [1991] and *Kearey et al.* [2002].

Energy loss mechanisms for fluid-saturated porous media fall into three categories: viscoelastic loss, fluid-solid surface physiochemical loss, and scattering loss [*Li et al.*, 2001]. Generally, decreases in acoustic amplitude result from the weakening of grain contacts (physical/chemical alteration of surfaces and/or grain contacts [e.g., *Murphy et al.*, 1984; *Clark et al.*, 1980]) in porous media, both of which reduce the elastic moduli and are manifested by delays and attenuation of acoustic waves. Increases in acoustic amplitude may result from increases in the bulk modulus of the solid media [e.g., *Li et al.*, 2001] through the stiffening of grain contacts.

2.3.2. Method of Measurement. For this thesis study, a full-waveform acoustic wave imaging system was used to obtain two-dimensional point-by-point maps of the acoustic response of the samples [e.g., *Pyrak-Nolte et al.*, 1999]. The acoustic imaging system used two water-coupled plane-wave transducers (1 MHz central frequency) as

source and receiver. Water-coupled transducers were used to ensure the same coupling between the transducers and the sample at all locations on the sample and over time. Figure 2.2 shows the experimental setup and general components of the acoustic imaging system. Using the acoustic mapping mode (C-scan), computer-controlled linear actuators (Newport 850-B4 and Motion Master 2000) were used to move the source and receiver in unison over the area of interest. A high-voltage pulse generator (Panametrics PR1500) was used to excite the source and to receive the transmitted signal. At each point in the 2D scan region, a 50 microsecond window of the transmitted signal was recorded and digitized with an oscilloscope (Lecroy 9314L). The acoustic signals were then stored to a computer, and the velocity and amplitude of the acoustic wave signals are then analyzed.

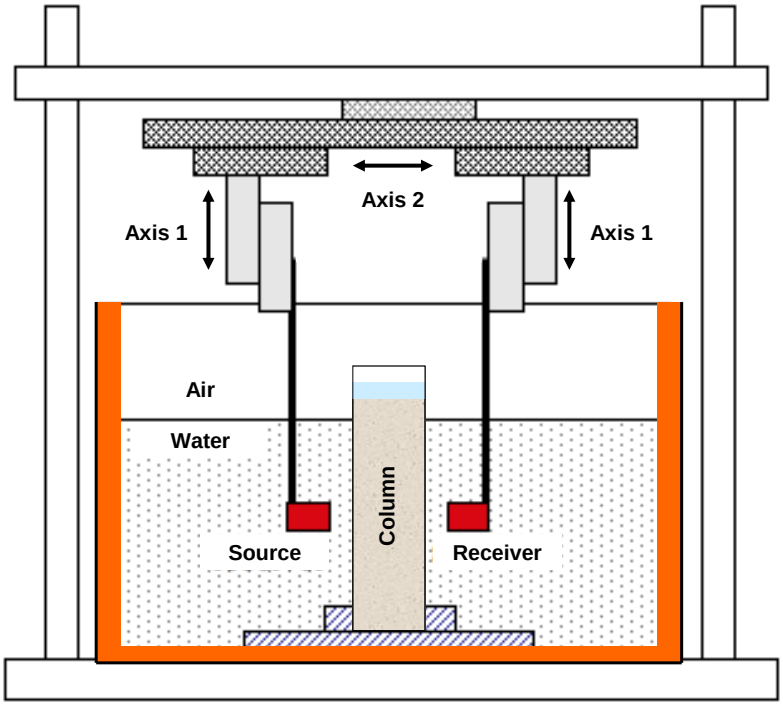

Figure 2.2: Drawing showing the general setup for collecting acoustic wave measurements.

2.4. REFERENCES

Archie, G.E. (1942), The electrical resistivity log as an aid in determining some reservoir characteristics, Transactions of the American Institute of Mining, Metallurgical and Petroleum Engineers, 146, 54-62.

Arora, T., Linde, N., Revil, A., and Castermant, J. (2007), Non-intrusive characterization of the redox potential of landfill leachate plumes from self-potential data, J. Contam. Hydrol., doi:10.1016/j.conhyd.2007.01.018.

Blitz, J., and Simpson, G. (1996), Ultrasonic methods of non-destructive testing, Springer, 264 p.

Boleve, A., Revil, A., Janod, F., Mattiuzzo, J.L., and Jardani, A. (2007), Forward modeling and validation of a new formulation to compute self-potential signals associated with ground water flow, Hydrol. Earth Syst. Sci., 11, 1661–1671.

Clark, V.A., Tittman, B.R., and Spencer, T.W. (1980), Effect of volatiles on attenuation (Q-1) and velocity in sedimentary rocks, J. Geophys. Res., 85, 5190-5198.

Darnet, M., and Marquis, G. (2004), Modelling streaming potential (SP) signals induced by water movement in the vadose zone, J. Hydrol. (Amsterdam), 285, 114-124.

Ecker, C., Dvorkin, J., and Nur, A. (1998), Sediments with gas hydrates: internal structure from seismic AVO, Geophysics, 63, 1659-1669.

Ernstson, K., and Scherer, H.U. (1986), Self-potential variations with time and their relation to hydrogeologic and meteorological parameters, Geophysics, 51, 1967–1977.

Fournier, C. (1989), Spontaneous potentials and resistivity surveys applied to hydrogeology in a volcanic area: case history of the Chaine des Puys (Puy-de-Dome, France), Geophys. Prospecting, 37, 647–668.

Kearey, P., Brooks, M., and Hill, I. (2002), An introduction to geophysical exploration, Blackwell Publishing, 262 p.

Knight, R., and Nolen-Hoeksema, R. (1990), A laboratory study of the dependence of elastic wave velocities on pore scale fluid distribution, Geophys. Res. Lett., 17, 1529-1532.

Kulessa, B., Hubbard, B., and Brown, G.H. (2003), Cross-coupled flow modeling of coincident streaming and electrochemical potentials and application to subglacial self-potential data, J. Geophys. Res., 108(B8), 2381, doi:10.1029/2001JB001167.

Lesmes, D.P., and Frye, K.M. (2001), Influence of pore fluid chemistry on the complex conductivity and induced polarization responses of Berea sandstone, J. Geophys. Res., 106, 4079-4090.

Lesmes, D.P., and Morgan, F.D. (2001), Dielectric spectroscopy of sedimentary rocks, J. Geophys. Res., 106, 13329-13346.

Li, X., Zhong, L.R., and Pyrak-Nolte, L.J. (2001), Physics of partially saturated porous media: residual saturation and seismic-wave propagation, Ann. Rev. Earth Planet. Sci., 29, 419-460.

Maineult, A., Bernabe, Y., and Ackerer, P. (2004), Electrical response of flow, diffusion, and advection in a laboratory sand box, Vadose Zone Journal, 3, 1180-1192.

Murphy III, W.F., Winkler, K.W., and Kleinberg, R.L. (1984), Frame modulus reduction in sedimentary rocks: the effect of adsorption on grain contacts, Geophys. Res. Lett., 1(9), 805-808.

Naudet, V., and Revil, A. (2005), A sandbox experiment to investigate bacteria-mediated redox processes on self-potential signals, Geophys. Res. Lett., 32, L11405, doi:10.1029/2005GL022735.

Naudet, V., Revil, A., Bottero, J., and Begassat, P. (2003), Relationship between self-potential (SP) signals and redox conditions in contaminated groundwater, Geophys. Res. Lett., 30(21), 2091, doi:10.1029/2003GL018096.

Naudet, V., Revil, A., Rizzo, E., Bottero, J., and Begassat, P. (2004), Groundwater redox conditions and conductivity in a contaminant plume from geoelectrical investigations, Hydrol. Earth Sys. Sci., 8(1), 8-22.

Nyquist, J.E., and Corry, C.E. (2002), Self-potential: the ugly duckling of environmental geophysics, Leading Edge, 446-451.

Olhoeft, G.R. (1985), Low-frequency electrical properties, Geophysics, 50(12), 2492-2503.

Petiau, G. (2000), Second generation of lead-lead chloride electrodes for geophysical applications, Pure Appl. Geophys., 157, 357-382.

Pyrak-Nolte, L.J., Mullenbach, B.L., Li, X., Nolte, D.D., and Grader, A.S. (1999), Detecting sub-wavelength layers and interfaces in synthetic sediments using seismic wave transmission, Geophys. Res. Lett., 26, 127-130.

Revil, A., and Glover, P.W.J. (1998), Nature of surface electrical conductivity in natural sands, sandstones, and clays, Geophys. Res. Lett., 25, 691-694.

Revil, A., Naudet, V., Nouzaret, J., and Pessel, M. (2003), Principles of electrography applied to self-potential electrokinetic sources and hydrogeological applications, Water Resour. Res., 39(5), 1114, doi:10.1029/2001WR000916.

Revil, A., and Leroy, P. (2004), Governing equations for ionic transport in porous shales, J. Geophys. Res., 109, B03208, doi:10.1029/2003JB002755.

Revil, A., Cary, L., Fan, Q., Finizola, A., and Trolard, F. (2005), Self potential signals associated with preferential ground water flow pathways in a buried paleo-channel, Geophys. Res. Lett., 32, L07401, doi:10.1029/2004GL022124.

Reynolds, J.M. (1997), An introduction to applied and environmental geophysics, John Wiley and Sons, 806p.

Sato, M., and Mooney, H.M. (1960), The electrochemical mechanism of sulfide self-potentials, Geophysics, 25(1), 226-249.

Sill, W.R. (1983), Self-potential modeling from primary flows, Geophysics, 48, 76-86.

Slater, L., (2006), Near surface electrical characterization of hydraulic conductivity: from petrophysical properties to aquifer geometries - a review, Surv. Geophys., 28, 169-197.

Slater, L., and Lesmes, D.P. (2002), IP interpretation in environmental investigations, Geophysics, 67, 77-88.

Telford, W.M., Geldart, I.P., and Sheriff, R.E. (1991), Applied geophysics, Cambridge University Press, 770 p.

Timm, F., and Moller, P. (2001), The relation between electric and redox potential: evidence from laboratory and field measurements, J. Geochem. Explor., 72(2), 115-128.

Vanhala, H., and Soininen, H. (1995), Laboratory technique for measurement of spectral induced polarization response of soil samples, Geophys. Prospect., 43, 655-676.

Vinegar, H.J., and Waxman, M.H. (1984), Induced polarization of shaly sands, Geophysics, 49(8), 1267-1287.

Waxman, M.H., and Smits, L.J.M. (1968), Electrical conductivities in oil-bearing shaly sands, Soc. Petrol. Eng. Journal, 8, 107-122.

1. ON THE CONTRIBUTION OF MICROBIAL METABOLIC BYPRODUCTS TO THE ELECTRICAL PROPERTIES OF POROUS MEDIA

1.1. ABSTRACT

The effect of microbial metabolic byproducts on the low frequency (0.1-1000 Hz) electrical properties of porous media was investigated in order to understand their contribution to the anomalous bulk electrical conductivity (σ_b) observed at hydrocarbon contaminated sites. To simulate the direct addition of metabolic byproducts to porous media, silica sand-packed columns were treated with varying concentrations of organic acids or biosurfactant (rhamnolipids) and complex conductivity (σ^*) measurements were collected for each treatment. The effects of mineral weathering by organic acids in porous media was investigated by saturating mixed mineral sand-packed columns with organic acids or water, and temporal σ^* measurements were collected for a total of 120 days.

A qualitative comparison of the results of this study to that of previous field studies showed that the direct addition of organic acids and biosurfactants at field concentrations only accounted for <5% of the total measured σ_b in the sand columns. This suggests that metabolic byproducts may only account for part of the anomalous σ_b observed at hydrocarbon contaminated field sites undergoing bioremediation. The results of the weathering experiment showed that temporal increases in the fluid and complex conductivity parameters are concomitant with temporal increases in Ca and Mg concentrations. Compared to mineral weathering products at field sites these products can account only in part for the elevated bulk conductivity values measured at hydrocarbon field sites. A qualitative comparison of our results to that of a laboratory investigation of hydrocarbon biodegradation showed that the magnitude of change in pH, fluid conductivity, and dissolved ion concentrations were similar but could not fully explain the σ^*. Since the increases in the electrolytic conductivity either by direct addition of metabolic byproducts or addition of ions via mineral weathering cannot fully account for the magnitude increase of the bulk electrical conductivity we measured, we suggest that the presence of microbes and the alteration of the petrophysical properties by microbial activity is an important variable to consider in the observed field σ_b response. Nonetheless, the results of this study suggest that σ^*, in particular electrolytic

conductivity measurements are sensitive to relatively low concentrations of organic acids and biosurfactants, and may be used as an indicator of microbial metabolism.

1.2. INTRODUCTION

Microbial-induced alterations to the electrical properties of porous media have been the subject of a number of geophysical studies [e.g., *Atekwana et al.,* 2004a-d; *Naudet and Revil,* 2005; *Ntarlagiannis et al.,* 2005b; *Williams et al.,* 2005; *Slater et al.,* 2007a; 2007b]. Growing interest in the use geophysical methods to evaluate subsurface microbial processes has been motivated by field and laboratory evidence suggesting that microbial degradation of hydrocarbon results in elevated bulk electrical conductivity (σ_b) [e.g., *Bermejo et al.,* 1998; *Sauck et al.,* 1998; *Werkema et al.,* 2003]. Various microbial-induced physicochemical changes have been suggested to explain the elevated σ_b, such as (1) increased ionic strength of pore fluid by addition of metabolic byproducts to solution [*Sauck et al.,* 1998; *Abdel Aal et al.,* 2004; *Atekwana et al.,* 2004a], (2) increased fluid conductivity (σ_w) and concentration of total dissolved solids (TDS) from enhanced mineral weathering by organic acids [*Sauck et al.,* 1998; *Atekwana et al.,* 2005], and (3) increased microbial cell density [*Ntarlagiannis et al.,* 2005b] and attachment of microbes to mineral surfaces that enhance the electrical properties at the cell-mineral interface [*Abdel Aal et al.,* 2004; 2006; *Davis et al.,* 2006].

During microbial utilization of organic carbon (e.g., hydrocarbons), fermentative anaerobes can produce an excess of intermediate products such as gases, organic acids, solvents [e.g., *Bartha and Atlas,* 1987; *Ollivier and Magot,* 2005] and biosurfactants [e.g., *Cassidy et al.,* 2001; 2002]. The accumulation of excess byproducts in pore water and void spaces can lead to alterations in the physicochemical properties of the subsurface environment. Microbial production of organic acids and the subsequent accumulation of acid in pore water have the potential to affect the physicochemical properties of porous media in a variety of ways [e.g., *McMahon and Chapelle,* 1991; *Cozzarelli et al.,* 1994; *McMahon et al.,* 1995; *Cozzarelli et al.,* 1995]. Elevated organic acid concentrations in groundwater promotes mineral dissolution [e.g., *Hiebert and Bennett,* 1992; *McMahon et al.,* 1995], releasing ions into solution [e.g., *Bennett et al.,* 1996], and thus changes the pore fluid chemistry. Further, enhanced mineral dissolution

catalyzed by increased organic acid concentration can lead to physical alterations, including changes in grain surface morphology and pore throat geometry which can result in the generation of microporosity or secondary porosity [e.g., *Lundegard and Land*, 1986; *Meshri*, 1986]. Such physical changes may in turn affect the hydraulic properties (e.g., permeability, hydraulic conductivity) of the subsurface environment [e.g., *McMahon and Chapelle*, 1991].

Biosurfactants can affect the physicochemical properties of contaminated media by adsorbing to and altering the conditions at interfaces [e.g., *Cassidy et al.*, 2001; 2002; *Ron and Rosenberg*, 2001]. Biosurfactants like solvents, can alter the wettability of interfaces (e.g., oil-rock interface), reducing the interfacial tension and aiding in the release of hydrocarbons from porous substrates [e.g., *Zhang et al.*, 1995; *Volkering et al.*, 1998; *Ron and Rosenberg*, 2001].

The physicochemical alterations imparted by organic acids and biosurfactants in porous media have the potential to translate into changes to the geophysical properties of the media, as suggested by *Cassidy et al.* [2001; 2002]. The *Cassidy et al.* [2001; 2002] studies, however, suggested this potential based on fluid conductivity measurements, attributing changes in fluid conductivity to increased presence of byproducts, but did not measure the subsequent geophysical response. The challenge is decoupling the complex microbial-induced physical and chemical transformations inherent during biodegradation and in quantifying the magnitude of the components of the geoelectrical response. In this study, we investigate the effects of two types of microbial metabolic byproducts, organic acids and biosurfactants, on the electrical properties of porous media. Complex conductivity measurements were employed for this study as this method is sensitive to changes in the surface and chemical properties of geologic media [e.g., *Lesmes and Frye*, 2001]. This permits the assessment of the relative contributions of microbial-induced changes to pore fluid chemistry and alterations at interfaces. In the absence of metallic minerals, and at frequencies <1 kHz, the complex conductivity (σ^*) of a porous medium is dependent on (1) electrolytic conductivity (σ_{el}) which describes the ohmic electric conductance through fluid-filled pore spaces, and (2) interfacial conductivity (σ^*_{int}) which is a complex term that represents the conduction and polarization mechanisms occurring at interfaces.

Here, we report on the results of laboratory experiments designed to investigate the contribution of microbial metabolic byproducts to the complex conductivity of porous media. Our objectives were to 1) determine the direct contribution of organic acids and biosurfactants to σ* magnitude, and 2) investigate the effect of mineral weathering by organic acids on the temporal σ* response. In addition to investigating the direct effect of the presence of organic acids, we were also interested in determining the relative magnitude of the electrical contribution of the organic acids (weak electrolytes) compared to that of strong electrolytes (i.e., salts). The results of our study are significant in that a fundamental understanding of the effects of microbial byproducts on geoelectrical properties will provide a framework for the interpretation of geophysical data from near subsurface environments where microbial activity is enhanced during bioremediation and in microbial enhanced oil recovery (MEOR).

1.3. METHODS

1.3.1 Experimental Column Setup. The experimental columns fabricated for this study were 24 cm long and constructed from 3.2 cm inner diameter polyvinyl chloride (PVC) pipe (Figure 1.1a). Three columns used to investigate the direct effect of metabolic byproducts (Figure 1.1a) were dry-packed with 20-30 mesh silica sand (Ottawa, IL) consisting of 99.8% silicon dioxide, 0.02% iron oxide, 0.06% aluminum oxide, and <0.01% each of magnesium oxide, sodium oxide, and potassium oxide. The three columns used to investigate the effect of mineral weathering by organic acids were modified with a fluid reservoir installed on top of each column (Figure 1.1b) to provide enough fluid to run the experiment in a closed system and allow for periodic fluid sampling from the reservoir. These columns were dry-packed with coarse (0.5-1 mm) natural sand (approximately 75% quartz, 10% feldspar, 5% chert, 5% carbonate, 5% rock fragments) collected from Burgher Branch Creek, Rolla, MO (Latitude 37°56’ N; Longitude 91°44’ W). All the sands were washed with deionized (DI) water, air-dried, and disinfected by autoclaving prior to use in the experiment.

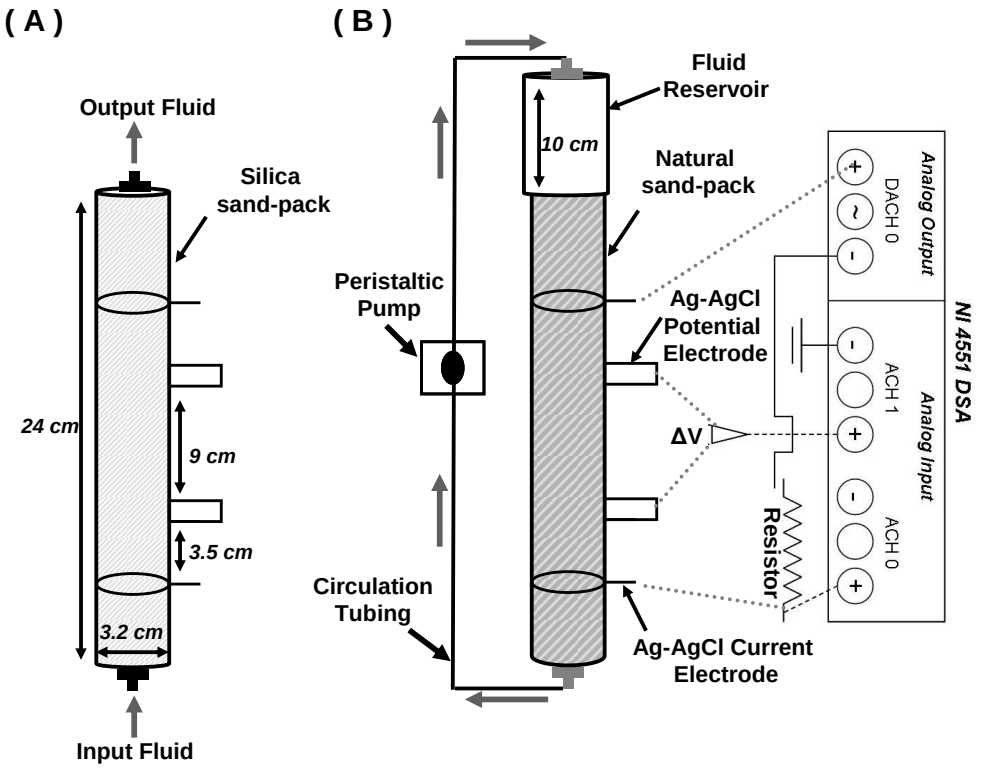

Figure 1.1. Schematic of the columns used for the (a) direct contribution of metabolic byproducts experiment, and (b) weathering by organic acids experiment. Complex conductivity measurements made with a dynamic signal analyzer as shown in (b).

1.3.2. Complex Conductivity Measurements. Low frequency electrical measurements (Figure 1.1b) were obtained with a two-channel dynamic signal analyzer (DSA) by using a four-electrode technique [*Vanhala and Soininen*, 1995; *Slater and Lesmes*, 2002]. Current was injected through a pair of silver-silver chloride (Ag-AgCl) electrode coils placed 16 cm apart in the column, and the electrical response was measured with two Ag-AgCl potential electrodes installed between the current electrodes (9 cm apart). We measured the impedance magnitude ($|\sigma|$) and phase shift (φ) of our sample between a measured voltage sinusoid and an impressed current sinusoid, relative to a high-quality resistor at 40 frequency intervals between 0.1 and 1000 Hz. The measured $|\sigma|$ and φ were used to calculate the real ($\sigma' = |\sigma| \sin \varphi$) and imaginary ($\sigma'' = |\sigma| \cos \varphi$) parts of σ^*. The real component of σ^* depends on both the σ_{el} and surface conductivity (σ'_{surf}), and represents conduction loss in the sample ($\sigma' = \sigma_{el} + \sigma'_{surf} = \sigma_w/F$

+ σ'_{surf}) [*Lesmes and Frye*, 2001]. Where F represents the formation factor of the sediment sample, and σ'_{surf} results from various factors at the mineral-fluid interface, such as surface area, surface charge density, and/or ionic mobility [e.g., *Revil and Glover*, 1998]. In addition, the imaginary part of σ^* is an interfacial component and energy storage term which relates to the polarization phenomena that occurs at interfaces (σ^*_{int}) [e.g., *Lesmes and Frye*, 2001].

Prior to starting the experiments, tests were carried out on the columns to determine the variability in the σ^* measurements between the three columns in each column set (either silica sand or mixed mineral sand column set). Each column was saturated with NaCl solutions of known σ_w (30-3000 μS/cm) and σ^* measurements were collected. For each column set, the φ and $|\sigma|$ data were averaged at each σ_w value and the variability is reported as the standard deviation from the average. After the variability tests, the columns were flushed with DI water prior to injection of the experimental solutions.

1.3.3. Varying concentrations of metabolic byproducts. The silica sand-packed columns were saturated with either organic acid, biosurfactant, weak organic acid salt, or strong electrolytic inorganic salt solutions (Table 1.1). The following organic acids were used in this study: acetic ($C_2H_4O_2$), butyric ($C_4H_8O_2$), formic (CH_2O_2), and propionic ($C_3H_6O_2$) acid. Each acid solution was prepared individually in concentrations of 10, 100, and 1000 μN. The biosurfactant solutions were prepared using a stock solution of 15% rhamnolipids in distilled water (JBR 515; Jeneil Biosurfactant Company), consisting of a 50 w/v% combination of monorhamnolipids ($C_{26}H_{48}O_9$) and dirhamnolipids ($C_{32}H_{58}O_{13}$), or RL1 and RL2, respectively. The solutions of biosurfactants (rhamnolipids) were prepared in concentrations of 0.01, 0.5, 0.1, and 0.5%, or 0.057, 0.28, 0.57, and 2.88 g/L, respectively, by diluting the original 15% rhamnolipid solution in DI water to the desired concentrations. The individual organic acid salt included calcium acetate ($Ca(C_2H_3O_2)_2$), calcium formate ($Ca(HCOO)_2$), and calcium propionate ($Ca(C_2H_5COO)_2$) and the inorganic salts included sodium chloride (NaCl), calcium chloride ($CaCl_2$), and aluminum chloride ($AlCl_3$). The salt solutions were prepared by dissolving the solid salts in DI water at the same equivalent (normal) concentration as the acids.

Table 1.1. Experimental treatments for the six different columns used in this study.

Column #	Sand Type	Experimental Treatment(s)
1	Silica	butyric acid, calcium chloride, calcium acetate, or calcium propionate
2	Silica	acetic acid, propionic acid, calcium formate, or aluminum chloride
3	Silica	sodium chloride, formic acid, or biosurfactant
4	Mixed Mineral	10% tap water water for 120 days
5	Mixed Mineral	100 µN acetic acid for 120 days
6	Mixed Mineral	20 µN acid mix for 120 days

All of the silica sand-packed columns were saturated with solutions (10, 100, or 1000 µN) of organic acids, organic acid salts, inorganic salts, or biosurfactants using a peristaltic pump. Beginning with the least concentrated solution, σ* measurements were collected once for each acid, salt, or biosurfactant solution/concentration. The σ_w, pH, and temperature of each solution were measured at the input and output into the sand-packed columns using microelectrodes. The average value of each variable was determined. Experimental uncertainty in the σ_w and pH measurements was calculated by averaging the input and output solution value, and calculating the standard deviation from the average. The columns were flushed with DI water (< 1 µS/cm) until the σ_w of the output DI water measured < 3 µS/cm before changing the type of solution.

1.3.4. Mineral weathering by organic acids. Two natural sand-packed columns were saturated with 100 µN acetic acid or a mix of 20 µN each of acetic ($C_2H_4O_2$), benzoic ($C_7H_6O_2$), citric ($C_6H_8O_7$), formic (CH_2O_2), and propionic ($C_3H_6O_2$) acid (Table 1.1). In addition, a third column was saturated with a solution consisting of 10% tap water in DI water (pH ~6.8) to collect electrical measurements for comparison with the organic acid solutions. The natural sand-packed columns were saturated with the acetic acid, mixed acid, and 10% tap water solutions using a peristaltic pump, and the fluid in the columns was circulated for 30 min prior to collecting electrical and geochemical measurements. Electrical measurements were collected twice a week for the first three weeks of the experiment, then once every two weeks for the duration of the experiment. Fluid samples were collected periodically from the fluid reservoir for analysis of major

cations by ion chromatography. The σ_w, pH, and temperature were measured immediately after the electrical measurements were collected, using microelectrodes inserted through the removable cap on the fluid reservoir at the top of each column. The columns were stored at room temperature (23-25˚C) on a laboratory bench-top for the 120 day duration of the experiment.

1.4. RESULTS

The results of the variability tests conducted prior to the experiments indicate that errors were generally less than 0.4 mrad and 0.6% for the phase and magnitude, respectively, at 1 Hz. In addition, the temperature corrected experimental σ' and σ" (25˚C) are reported at 1 Hz, as this frequency is close to typical frequencies used in field electrical measurements. Temperature correction factors for the σ' and σ" were determined from laboratory experiments [*Davis et al.*, 2006], and the σ_w measurements were automatically normalized to 25˚C by the conductivity microelectrode. Column variability and experimental uncertainty are shown as error bars in the figures.

1.4.1. Contribution of Metabolic Byproducts to σ*.

1.4.1.1 Effect of organic acids and salts. The results from the silica sand-packed columns saturated with organic acids are presented in Figure 1.2. The σ' values ranged from 4.15 x 10^{-4} S/m to 1.06 x 10^{-3} S/m at 10 µN, and 3.13 x 10^{-3} S/m to 1.78 x 10^{-2} S/m at 1000 µN, and increase with increasing strength for each organic acid (Figure 1.2a). In contrast, the σ" values ranged from 2.97 x 10^{-7} S/m to 7.06 x 10^{-7} S/m over the acid strength range measured, and show a slight decrease with increase in the acid strength (Figure 1.2b). Compared to the σ" values, the σ' showed a greater relative magnitude of change (up to one order of magnitude) with increasing organic acid concentration. The σ_w values ranged from 1.67 x 10^{-3} S/m to 6.35 x 10^{-3} S/m at 10 µN, and 1.85 x 10^{-2} S/m to 9.76 x 10^{-2} S/m at 1000 µN, and increased with increasing acid strength (Figure 1.2c). There is a decrease in the pH values from 3.4 to 4.2 at 10 µN and 2.5 to 3.4 at 1000 µN with increasing acid concentration (Figure .2d). Of the four organic acids measured, formic acid showed the highest σ' and σ_w magnitude and lowest pH at the different concentrations (Figure 1.2).

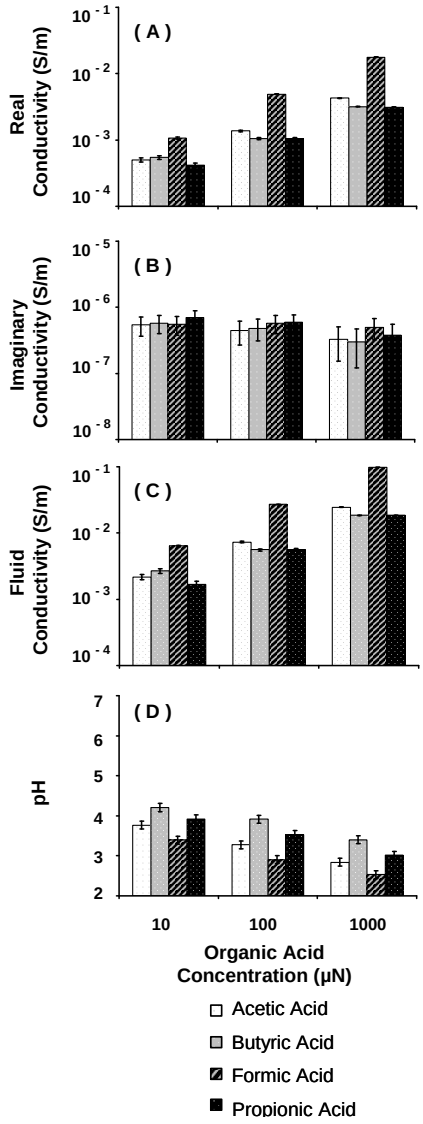

Figure 1.2. Bar graphs showing the direct effect of varying concentrations of organic acids on (a) real conductivity, (b) imaginary conductivity, and (c) fluid conductivity magnitude, and (d) pH. Complex conductivity measurements are reported at 1Hz.

The results of measurements from silica sand-packed columns saturated with varying concentrations of organic acid salts and inorganic salts are presented in Figure 1.3. Similar to the organic acids, increases in the σ' values are concomitant with increasing concentration of organic acid salts (Figure 1.3a) and inorganic salts (Figure 1.3b). The organic acids, however, have higher σ' magnitudes at 10 µN and 100 µN

compared to the salts of equivalent concentration. Over the concentration range measured, σ" values range from 2.45 x 10^{-7} S/m to 7.22 x 10^{-7} S/m for the organic acid salts, and 2.91 x 10^{-7} S/m to 6.81 x 10^{-7} S/m for the inorganic salts. The σ" values show no consistent trend with increasing concentration for the organic acid salts (Figure 1.3c) or the inorganic salts (Figure 1.3d). The σ_w values for the organic acid salts and inorganic salts range from 3.37 x 10^{-4} S/m to 6.11 x 10^{-4} S/m at 10 μN, and 7.38 x 10^{-3} S/m to 2.02 x 10^{-2} S/m at 1000 μN. Similar to the σ' trends, the σ_w values increased with increasing concentration for the organic acid salts (Figure 1.3e) and inorganic salts (Figure 1.3f) , and both showed similar magnitudes of increase in σ_w values over the concentration range measured. The pH values range from a pH of 5.4 to 6.3 for the organic acid salts (Figure 1.3d), and a pH of 4.2 to 6.3 for the inorganic salts (Figure 1.3h) and of the salt solutions do not show a consistent trend with increasing concentration.

1.4.1.2. Effect of biosurfactants. The results of measurements for the silica sand-packed columns saturated with varying concentrations of biosurfactants are presented in Figure 1.4. The σ' (Figure 1.4a) and σ" (Figure 1.4b) values increased with increasing biosurfactant concentration, although to a greater extent for the σ' (one order of magnitude) compared to σ". The σ' increased from 6.23 x 10^{-4} S/m at 0.01%, to 1.32 x 10^{-2} S/m at 0.5% biosurfactant concentration. Whereas, the σ" increased from 9.00 x 10^{-7} S/m at 0.01%, to 1.80 x 10^{-6} S/m at 0.5% biosurfactant concentration. In addition, increases are also observed in both the σ_w (Figure 1.4c) and pH (Figure 1.4d) values with increasing concentration. The σ_w of the biosurfactant solutions increase from 2.43 x 10^{-3} S/m to 6.38 x 10^{-2} S/m, and the pH values increase from 6.1 to 6.9 over the concentration range measured.

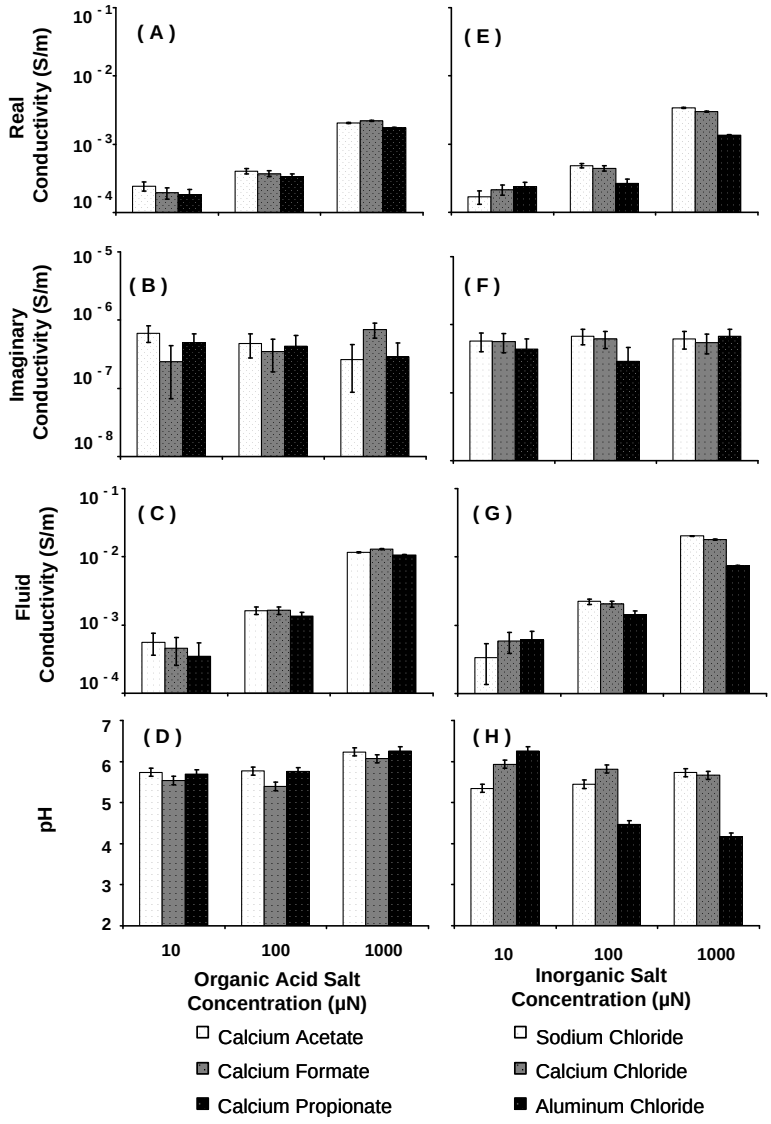

Figure 1.3. Bar graphs showing the effect of varying concentrations of organic acid salts and inorganic salts on (a,e) real conductivity, (b,f) imaginary conductivity, and (c,g) fluid conductivity magnitude, and (d,h) pH. Complex conductivity measurements are reported at 1 Hz.

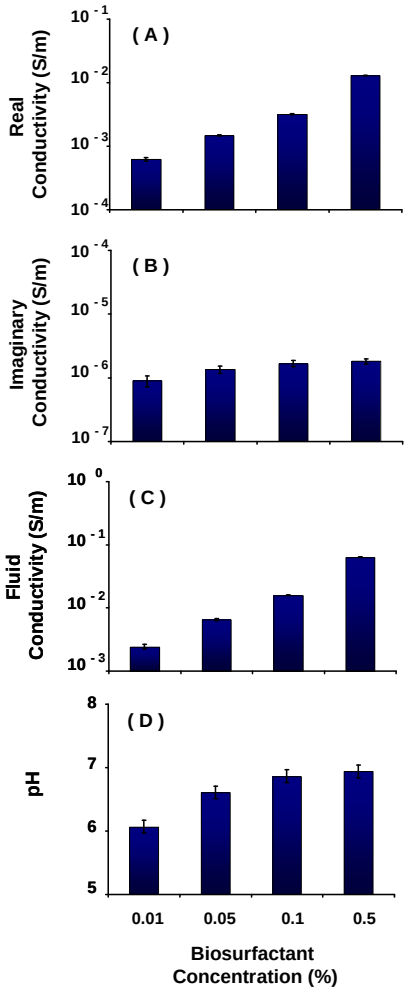

Figure 1.4. Bar graphs showing the direct effect of varying concentrations of biosurfactants (RL1 + RL2) on (a) real conductivity, (b) imaginary conductivity, and (c) fluid conductivity magnitude, and (d) pH. Complex conductivity reported at 1 Hz.

1.4.2. Effect of Mineral Weathering by Organic Acids on σ*. The temporal pH and σ_w measurements collected during the weathering experiment are shown in Figure 1.5a and 1.5b, respectively. The pH values for the acetic acid and mixed acid treatments increased from 3.2 and 3.5, respectively, to near 7 on the second day of the experiment. The pH values continued to increase to maximum values of ~7.4 with the acetic acid treatment, and ~7.8 for the mixed acid treatment, before both column treatments decreased to ~7.3 by the end of the experiment. The pH values measured from

the 10% tap water column increased from an initial value of 6.8 to 8.1 on day 2, before decreasing to ~7.3 by the end of the experiment. The σ_w values increased for all treatments (Figure 1.5b), most noticeably during the first week of the experiment. During the first six days, the σ_w measured for the acetic acid treatment increased from 7.56×10^{-3} to 3.28×10^{-2} S/m, while the mixed acid and 10% tap water treatments increased by a similar σ_w magnitude over the first 14 days. The σ_w continued to increase for the mixed acid and 10% tap water treatments (by ~1.21×10^{-2} S/m), and to a lesser extent for the acetic acid treatment (by ~7.6×10^{-3} S/m) through the end of the experiment. The σ' measured for the acetic acid treatment (Figure 1.5c) increased from an initial value of 8.30×10^{-3} to 1.15×10^{-2} S/m on day 6, and continued to increase at a slow rate to the end of the experiment. The σ' values for the mixed acid and 10% tap water treatments increased from 3.10×10^{-3} to 9.13×10^{-3} S/m by the end of the experiment. The σ'' values increased by ~2.00×10^{-5} S/m from initial values through day 18 for all three treatments, then increased to the end of the experiment (Figure 1.5d).

Temporal changes in calcium (Ca), potassium (K), and magnesium (Mg) concentrations during the weathering experiment are shown in Figure 1.6. Ca and Mg concentrations increased for all treatments (>10 mg/L), with the largest increase in Ca (41 mg/L) and Mg (26 mg/L) observed for the acetic acid treatment (Figure 1.6b).

1.5. DISCUSSION

1.5.1. Contribution of Metabolic Byproducts to σ*. The organic acid and biosurfactant solutions used in this experiment are comparable in type and concentration to those measured at hydrocarbon contaminated field sites undergoing biodegradation [e.g., *Cozzarelli et al.*, 1994; *Cozzarelli et al.*, 1995; *McMahon et al.*, 1995; *Atekwana et al.*, 2004c], and in laboratory biodegradation studies [e.g., *Cassidy et al.*, 2001]. The results of this experiment showed that the σ' and σ_w increase with increasing ionic strength of the metabolic byproduct. The σ' shows a positive correlation ($R^2 > 0.99$) on σ_w for all organic acids, biosurfactant (Figure 1.7a), and salt (Figure 1.7b) solutions.

These relationships are expected, as the σ' parameter is largely dependent on σ_{el} associated with variations in σ_w [*Archie*, 1942], and increases in electrolyte concentration generally increase electrolytic conduction, and consequently the σ' component of σ* [e.g., *Lesmes and Frye*, 2001; *Slater and Lesmes*, 2002].

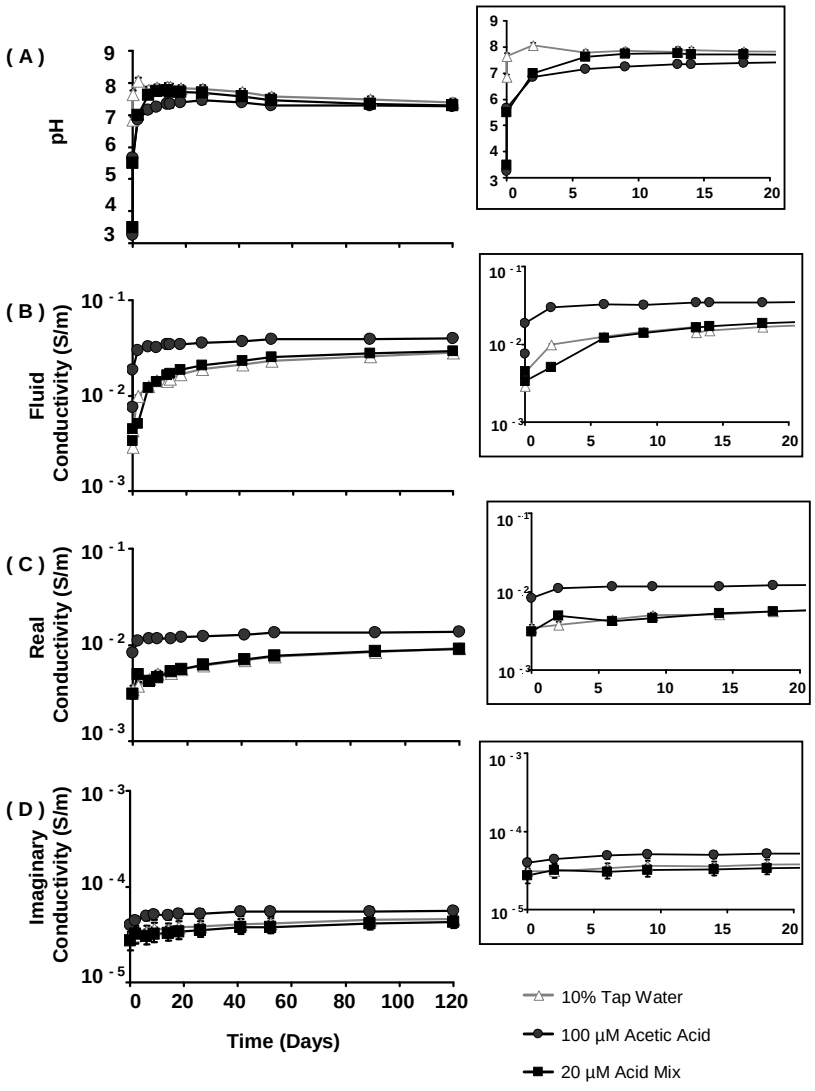

Figure 1.5. Measured temporal (a) pH, (b) fluid conductivity, (c) real conductivity, and (d) imaginary conductivity during weathering by 10% tap water, 100 µM acetic acid, and 20 µM acid mix in natural mixed mineral composition sands. Complex conductivity measurements at shown at 1 Hz. Insert to the right of each graph shows the temporal data through 20 days.

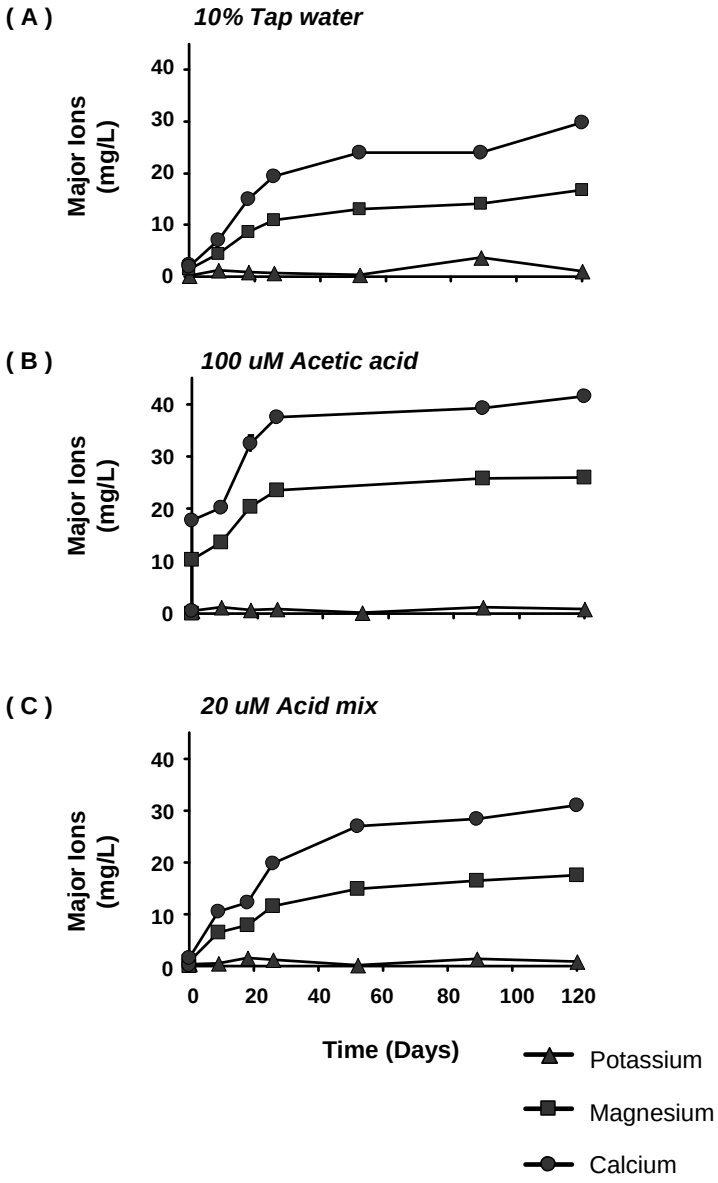

Figure 1.6. Temporal major cation concentrations measured during weathering by (a) 10% tap water, (b) 100 µM acetic acid, and (c) 20 µM acid mix in natural mixed mineral composition sands.

Our results also show that organic acids within the concentration range found in hydrocarbon biodegradation environments contributes more to σ_w magnitude and thus the σ' magnitude than strong electrolytes (i.e., organic and inorganic salt solutions) of the same concentration (Figure 1.2 vs. 1.3). This observation is consistent with Ostwald's

law whereby the equivalent electrical conductivity of weak electrolytes (i.e., organic acids) increases more rapidly with dilution than strong electrolytes such as salts [e.g., *Tower*, 1905]. The highest σ', σ_w, and pH magnitude was associated with formic acid compared to the other organic acids and salts which suggests that the σ_{el} magnitude is dependent on the organic acid present in addition to it's concentration. Further, the observation that formic acid contributes more to σ_w than the other acids measured in this study, is consistent with previous studies that show the equivalent conductivity (at infinite dilution) decreases with the increasing number of atoms in the acid molecule [e.g., *Tower*, 1905]. Therefore, the contribution of organic acids to the σ_w magnitude at field sites may also be dependent on the major acid type present in pore water.

In contrast to the σ' results, the σ" results do not show a consistent response for organic acids, or organic and inorganic salts. While the solution concentration and the σw increase, we observe a slight decrease in the σ" for organic acids (Figure 1.7c), a slight increase in the σ" for biosurfactants, and no clear trend in the σ" for the salts (Figure 1.7d). A possible explanation for the increase in the σ" for the biosurfactant solutions may result from the adsorption of the ionic surfactants at the surface of the aqueous solution leading to a reduction in the surface tension, an increase of the surface electric charge density, and the development of an electric double layer [*Lesmes and Frye*, 2001; *Kolev et al.*, 2002]. In addition, previous studies have demonstrated that biosurfactants can alter the nature of interfaces (e.g., wettability) by aggregating at the interface of fluid phases (e.g., water/hydrocarbon, or water/air) and reduce the surface tension or interfacial tension at the interface [e.g., *Rosen*, 1989; *Desai et al.*, 1997]. In contrast to the increased σ" response observed for the biosurfactants, there is a slight decrease in the σ" response from increasing concentrations of organic acids. The slight decrease in the σ" magnitude for the organic acids is coincident with decreased pH and increased σ_w (Figure 1.7e). While previous studies have shown that the effect of pH on σ* is secondary to ionic strength effects [*Lesmes and Frye*, 2001], we speculate that at relatively low concentrations of acids, variations in pH may have affected the properties at the fluid-mineral interface (e.g., surface ionic mobility) and thus the σ" response. Further, *Lesmes and Frye* [2001] observed reductions in surface conductance and polarization at relatively low pH (pH 3), which was attributed to the pH being at the zero point charge for quartz

systems. This general observation is consistent with our results for organic acids, where increased concentration results in decreased pH and a slight decrease in the trend of σ" values.

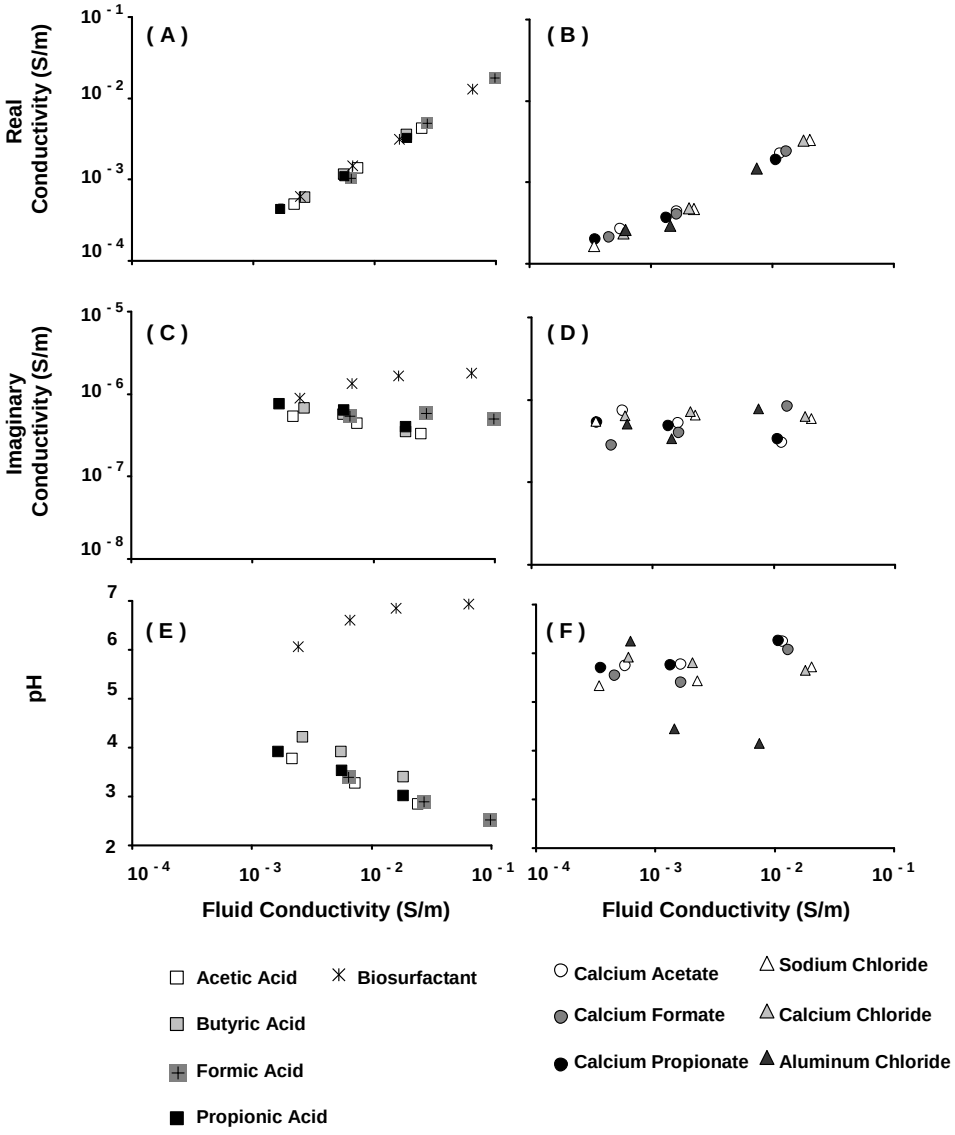

Figure 1.7. Graphs showing the relationship between (a, b) real conductivity, (c, d) imaginary conductivity, (e, f) pH and fluid conductivity for sand with different treatments of organic acids, salts, and biosurfactant solutions. Complex conductivity measurements are reported at 1 Hz.

The results of this experiment show that σ' measurements are sensitive to relatively low concentrations of organic acids and biosurfactants, such as those found in hydrocarbon biodegradation environments. While the concentrations of organic acids used in this study are similar to those found in field situations, these concentrations are in excess of that which is consumed or needed by the microorganisms in field environments [e.g., *Cozzarelli et al.*, 1994]. We speculate that σ' measurements may be useful for monitoring variations in metabolic byproduct concentration in field settings, in addition to other analytical geochemical techniques such as direct fluid sampling.

1.5.2. Contribution of Mineral Weathering Products to σ*. Acetic acid was chosen for single organic acid leaching as it is commonly reported in groundwater at hydrocarbon contaminated environments [e.g., *Welch and Ullman*, 1993; *Cozzarelli et al.*, 1994; *McMahon et al.*, 1995; *Cassidy et al.*, 2001; *Atekwana et al.*, 2004d]. The concentration of acetic acid used was intermediate in value between the values reported by *Atekwana et al.* [2004d; ~215-270 μN] and *Cozzarelli et al.* [1994; ~2.13-12.5 μN]. The mixed acid solution consisted of common organic acids found in hydrocarbon biodegradation environments [e.g., *Welch and Ullman*, 1993; *Cozzarelli et al.*, 1994; *McMahon et al.*, 1995; *Atekwana et al.*, 2004d], and consisted of the combination of the five acids (at 20 μN each) which was designed to represent a total organic acid concentration of 100 μN. The 10% tap water solution was used for background measurements as a comparison with the organic acid solutions, as experimental measurements at a near neutral pH would allow us to investigate the effect of the acidity of the experimental solutions on the electrical measurements.

The results of the weathering experiment show that the acetic acid (100 μN) treatment contributed more to conductivity magnitude (Figure 1.5), directly by increasing ionic strength and indirectly through mineral weathering (Figure 1.6), than lower concentrations of mixed acids (20 μN) or near-neutral solution (10% tap water). The temporal increases in the σ_w values are consistent with increases in ionic strength (concentration of cations) of the solutions (Figure 1.8a) and the relatively good linear correlation is observed (R^2 >0.73) between σ_w and cation concentrations (Ca and Mg) suggest that cation concentration exerts a primary control on the σ_w values. The similarity of the results obtained from the mixed acid and 10% tap water (background) columns

suggest that the pH and electrical parameters were enhanced by more than just the presence of organic acids. We observed weathering of sands in the 10% tap water (background) column (Figure 1.6a), though the pH at the start of the experiment was near neutral (~6.8). Our results are consistent with those of *Huang and Keller* [1970] who observed a temporal increase in cation concentrations and increases in pH for silicate minerals (e.g., plagioclase feldspars) in DI water (with a starting pH of ~5.7-8.6). Hence, the presence alone of fluid in the mixed mineral-composition sand may have caused some mineral dissolution, similar to *Huang and Keller* [1970]. *Huang and Keller* [1970] noted, however, that the solubilities of major cations (e.g., calcium, magnesium) were higher in organic acid solutions compared to that of DI water. Furthermore, although we attribute the increase in cation concentrations to mineral weathering/leaching, we cannot exclude the role of ion exchange.

There is a relatively good positive linear correlation between the temporal conductivity parameters (σ_w, σ', and σ'') and cation concentrations (acetic acid column R^2 >0.73; mixed acid column R^2 >0.96; 10% tap water column R^2 >0.91) (Figure 1.8). The correlation between cation concentrations and the conductivity parameters suggests that the observed variations in σ_w values are primarily responsible for the changes in measured σ'. Further, the relatively weak dependence of σ'' on σ_w may be attributed to increased surface charge density in the diffuse part of the electrical double layer [e.g., *Lesmes and Frye*, 2001; *Slater and Lesmes*, 2002].

1.5.3. Application of Results to Previous Studies. Our results suggest that organic acids contribute more to σ_w than strong electrolytes at low concentrations. However, the contribution of organic acids to σ_w in field settings is unknown. For example, at a field site undergoing intrinsic hydrocarbon biodegradation *Atekwana et al.* [2004d] observed elevated σ_w (~8.4 x 10^{-2} S/m) and σ_b (~4.9 x 10^{-3} S/m) values, and measured elevated organic acids concentrations (~215 – 270 μN measured as acetic acid) in contaminated groundwater. While we cannot make a direct quantitative comparison of the σ_b results from *Atekwana et al.* [2004d] to our current study due to the fact that the sediment samples/conditions are not identical we can, however, present a general qualitative analysis based on the relationship between σ_w and concentration of acetic acid between the two studies. Based on our relationship between σ_w and concentration of

acetic acid ($y = 0.000025x + 0.0035$; $R^2 > 0.98$), we suggest that the acetic acid concentration measured by *Atekwana et al.* [2004d] will impart ~7.8 x 10^{-3} to ~8.9 x 10^{-3} S/m, or ~9-11% to the total σ_w measured. Further, based on the relationship between σ' and acetic acid concentration ($y = 0.000004x + 0.0007$; $R^2 > 0.98$), the organic acid concentration measured in the field by *Atekwana et al.* [2004d] will impart ~1.6 x 10^{-3} to ~1.8 x 10^{-3} S/m, or ~3-4% to the total σ_b. Similarly, based on our σ' results for biosurfactants ($y = 0.0254x + 0.0004$; $R^2 > 0.99$), the magnitude of biosurfactants at field concentrations of ~0.01% [*Cassidy et al.*, 2002] likely imparts ~6.5 x 10^{-4} S/m to the total σ_b magnitude. We argue that although organic acids and biosurfactants contribute to ionic strength and thus the fluid and bulk conductivity, the cumulative effect of these metabolic byproducts is likely <12% of the total σ_w, and <5% of the total σ_b. Therefore, the direct addition of organic acids and biosurfactants to pore fluids cannot explain the total magnitude of the elevated bulk conductivity observed in hydrocarbon contaminated field sites undergoing biodegradation [e.g., *Atekwana et al.*, 2004d].

The results of weathering experiments support the findings of a field study by *Atekwana et al.* [2005], where a positive linear relationship was observed between total dissolved solids (TDS) and σ_b measured in a hydrocarbon contaminated aquifer. Elevated TDS values in the contaminated groundwater were coincident with higher dissolved ion concentrations. However, *Atekwana et al.* [2005] observed that zones with the highest σ_b did not correspond to the highest TDS values in pore water in those zones, and that only ~50-60% of the measured σ_b from the contaminant fringe and core could be explained by TDS concentrations. Similarly, the results of the weathering experiment conducted during this study shows a positive correlations between the conductivity parameters and cation concentrations, suggesting that leaching of ions from the sands of mixed mineral composition is primarily responsible for the measured conductivity response. The results of our study further validate the conclusions presented by *Atekwana et al.* [2005], that mineral weathering is likely the primary contributor to the measured fluid conductivity response measured in the field. We infer from these observations that another mechanism, besides the contribution from mineral weathering, must be at work here.

We speculate that the presence of microorganisms and the physical alterations imparted by the microbes (i.e., biofilm formation), also contribute to the measured bulk conductivity response [e.g., *Davis et al.*, 2006].

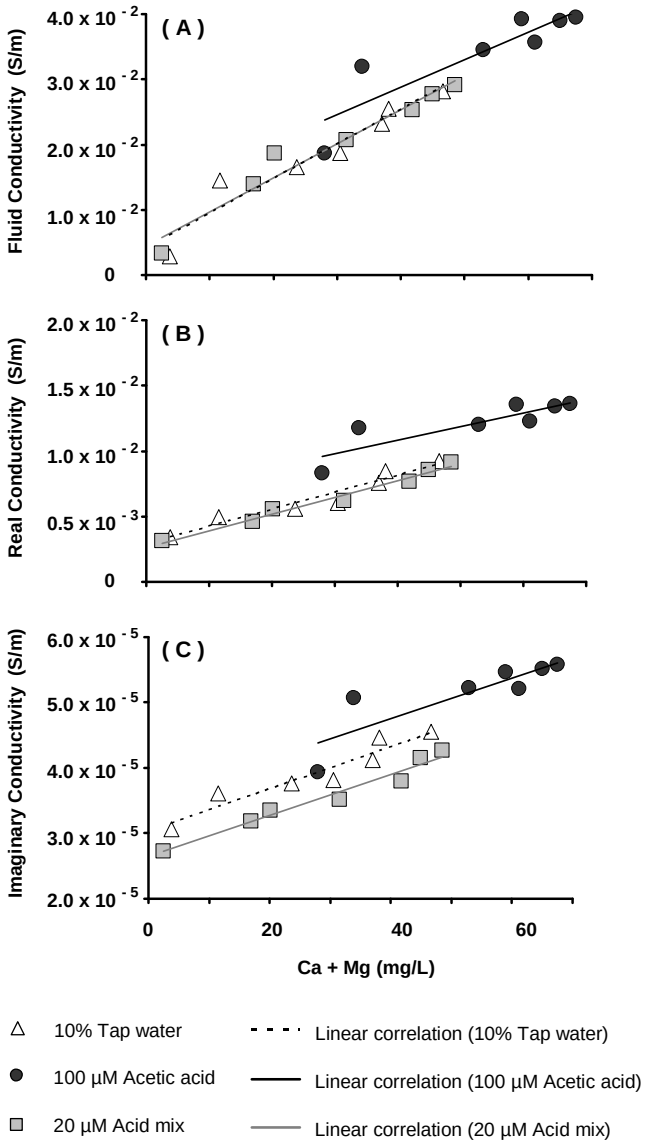

Figure 1.8. Cross plots of Ca + Mg vs. (a) fluid conductivity, (b) real conductivity, and (c) imaginary conductivity measured during weathering by 10% tap water, 100 µM acetic acid, and 20 µM acid mix in natural sand of mixed mineral composition. Complex conductivity measurements are reported at 1 Hz.

In a study by *Abdel Aal et al.* [2004], increases in σ_{el} in biotic columns was attributed to variations in σ_w due to the addition of ions (e.g., Ca) from enhanced mineral weathering by organic acids. There was a decrease in pH (~16%), and an increase in Ca concentration (120%), σ_w (80%), σ' (100%), and σ" (120%) in biotic sand columns after 36 weeks of active microbial metabolism. While the *Abdel Aal et al.* [2004] study did not measure organic acid concentrations, the authors attributed the decreased pH and increased Ca to organic acid production and weathering by the acids. The pH, Ca concentration, and σ_w results are similar in magnitude of change relative to the results of our current study from sands treated once with 100 μN acetic acid for 17 weeks. In the weathering experiment, we observed an increase in the pH (29%), Ca concentration (133%), σ_w (112%), σ' (63%), and σ" (42%). The magnitude of change in the σ' and σ" observed by *Abdel Aal et al.* [2004] are larger than the values measured in this study, perhaps underscoring the important role of the direct presence of microbes on σ* [e.g., *Ntarlagiannis et al.*, 2005b; *Davis et al.*, 2006]. This difference may result from the fact that our experiments were abiotic, while the experiments conducted by *Abdel Aal et al.* [2004] were biotic. The presence or absence of microbes may explain the differences observed between the σ' and σ" response between the two studies. We suggest that the results of our abiotic experiments may provide further evidence for the importance of the direct contribution by microbes with regards to the measured σ' and σ" in biotic laboratory studies [*Abdel Aal et al.*, 2004].

1.6. SUMMARY AND CONCLUSIONS

The primary purpose of this research was to decouple the complex microbial-induced physical and chemical transformations inherent during biodegradation, specifically the contribution of metabolic byproducts, and quantify the magnitudes of the geoelectrical response. The results presented here suggest the following important points:

1. The direct presence of organic acids and biosurfactants contributes to the σ_{el} of porous media to a greater extent than the interfacial properties.
2. Organic acids and biosurfactants directly contribute to conductivity magnitude, but their pure presence alone may only account for <12 % of the fluid conductivity and 5% of the bulk conductivity and therefore

cannot explain the total magnitude of the anomalous conduction and polarization observed in previous field [e.g., *Atekwana et al.*, 2004] and laboratory studies [e.g., *Abdel Aal et al.*, 2004].

3. Mineral weathering promoted by organic acids may be the primary contributor to the elevated conductivity values observed in previous field studies such as *Atekwana et al.* [2005], however, the contribution by mineral weathering products cannot completely account for the anomalous bulk conductivity response.
4. In addition to mineral weathering products, we suggest that the conductivity response observed in hydrocarbon biodegradation studies [e.g., *Abdel Aal et al.*, 2004] may also result from the direct presence and activity of microbes (i.e., presence of biofilms and alteration of pore structure).

Our study provides further fundamental understanding of the effect of microbial activity on electrical properties of geologic media. The results of our laboratory investigations suggest that σ^* measurements, in particular σ_{el}, may be used as an indicator of microbial metabolism in porous media. Up-scaling these measurements may be of significant interest to investigations aimed at assessing subsurface microbial activity and presence of metabolic byproducts in MEOR and gas hydrate studies. For example, MEOR practices can employ the use of microorganisms that produce biosurfactants in-situ to help mobilize entrapped oil in reservoirs, improving oil recovery [e.g., *McInerney et al.*, 2005; *Youssef et al.*, 2007]. There are problems associated with the application of biosurfactant-mediated oil recovery, however, as insufficient quantitative evidence exists regarding the in situ production of biosurfactants at the appropriate quantities and rates needed to mobilize the oil [e.g., *Bryant and Lockhart*, 2002; *Youssef et al.*, 2007]. The results of our current study suggest that geophysical data, and in particular geoelectrical measurements, may provide the additional information needed to assess the production of biosurfactants in field environments.

1.7. ACKNOWLEDGMENTS

This material is based in part on work supported by the National Science Foundation under Grant No. OCE-0433869 and Grant No. OCE-0433739.

1.8. REFERENCES

Abdel Aal, G.Z., Atekwana, E.A., Slater, L.D., and Atekwana E.A. (2004), Effects of microbial processes on electrolytic and interfacial electrical properties of unconsolidated sediments, Geophys. Res. Lett., 31(12), L12505, doi:10.1029/2004GL020030.

Abdel Aal, G.Z., Slater, L.D., and Atekwana, E.A. (2006), Induced-polarization measurements on unconsolidated sediments from a site of active hydrocarbon biodegradation, Geophysics, 71(2), H13-H24.

Archie, G.E. (1942), The electrical resistivity log as an aid in determining some reservoir characteristics, Transactions of the American Institute of Mining, Metallurgical and Petroleum Engineers, 146, 54-62.

Atekwana, E.A., Atekwana, E.A., Legall, F.D., and Krishnamurthy, R.V. (2004a), Field evidence for geophysical detection of microbial activity, Geophys. Res. Lett., 31, L23603, doi:10.1029/2004GL021576.

Atekwana, E.A., Atekwana, E.A., Rowe, R.S., Werkema, D.D., and Legall, F.D. (2004b), Total dissolved solids in groundwater and its relationship to bulk conductivity of soils contaminated with hydrocarbon, J. Appl. Geophys., 56, 281-294.

Atekwana, E.A., Atekwana, E.A., Werkema, D.D., Allen, J.P., Smart, L.A., Duris, J.W., Cassidy, D.P., Sauck, W.A., and Rossbach, S. (2004c), Evidence for microbial enhanced electrical conductivity in hydrocarbon-contaminated sediments, Geophys. Res. Lett., 31, L23501.

Atekwana, E.A., Werkema, D.D., Duris, J.W., Rossbach, S., Atekwana, E.A., Sauck, W.A., Cassidy, J.P., Means, J., and Legall, F.D. (2004d), In-situ apparent conductivity measurements and microbial population distribution at a hydrocarbon-contaminated site, Geophysics, 69, 56-63.

Atekwana, E.A., Atekwana, E.A., Legall, F.D., and Krishnamurthy, R.V. (2005), Biodegradation and mineral weathering controls on bulk electrical conductivity in a shallow hydrocarbon contaminated aquifer, J. Contam. Hydrol., 80, 149-167.

Bartha, R., and Atlas, R.M. (1987), Transport and transformations of petroleum: biological processes. In Boesch, D.F., and Rabalais, N.N. (eds.), Long-term environmental effects of offshore oil and gas development, Elsevier Applied Science, London, pp. 287-341.

Bennett, P.C., Hiebert, F.K., Choi, W.J. (1996), Microbial colonization and weathering of silicates in a petroleum-contaminated groundwater, Chem. Geol., 132, 45-53.

Bermejo, J. L., Sauck, W. A., and Atekwana, E. A. (1998), Geophysical discovery of a new LNAPL plume at the former Wurtsmith AFB, Oscoda, Michigan, Ground Water Mon. Remed., 17, 131–137.

Bryant, S.L., and Lockhart, T.P. (2002), Reservoir engineering analysis of microbial enhanced oil recovery, SPE Reservoir Eval. Eng., 5, 365-374

Cassidy, D.P., Werkema, D.D., Sauck, W.A., Atekwana, E.A., Rossbach, S., and Duris, J. (2001), The effects of LNAPL biodegradation products on electrical conductivity measurements, J. Env. Eng. Geophysics, 6, 47-52.

Cassidy, D.P., Hudak, A.J., Werkema, D.D., Atekwana, E.A., Rossbach, S., Duris, J.W., Atekwana, E.A., and Sauck, W.A. (2002), In-situ rhamnolipid production at an abandoned petroleum refinery by Pseudomonas aeruginosa, J. Soil Sed. Contam., 11, 769-787.

Cozzarelli, I.M., Baedecker, M.J., Eganhouse, R.P., and Goerlitz, D.F. (1994), The geochemical evolution of low-molecular-weight organic acids derived from the degradation of petroleum contaminants in groundwater, Geochim. Cosmo. Acta, 58, 863-877.

Cozzarelli, I.M., Herman, J.S., and Baedecker, M.J. (1995), Fate of microbial metabolites of hydrocarbons in a coastal plain aquifer: the role of electron acceptors, Environ. Sci. Tech., 29, 458-469.

Davis, C.A., Atekwana, E.A., Atekwana, E.A., Slater, L.D., Rossbach, S., and Mormile, M.R. (2006), Microbial growth and biofilm formation in geologic media is detected with complex conductivity measurements, Geophys. Res. Lett., 33, L18403, doi:10.1029/2006GL027312.

Desai, J.D., and Banat, I.M. (1997), Microbial production of surfactants and their commercial potential, Microbiol. Mol. Bio. Rev., 61(1), 47-64.

Hiebert, F.K., and Bennett, P.C. (1992), Microbial control of silicate weathering in organic-rich groundwater, Science, 258, 278-281.

Huang, W.H., and Keller, W.D. (1970), Dissolution of rock-forming silicate minerals in organic acids: simulated first-stage weathering of fresh mineral surfaces, Amer. Mineral., 55, 2076-2094.

Kolev, V. L., Danov, K.D., Kralchevsky, P.A., Broze, G., and Mehreteab, A., (2002), Comparison of the van der waals and frumkin adsorption isotherms for sodium dodecyl sulfate at various salt concentrations, Langmuir, 18(23), 9106-9109, doi:10.1021/la0259858.

Lesmes, D.P., and Frye, K.M. (2001), Influence of pore fluid chemistry on the complex conductivity and induced polarization responses of Berea sandstone, J. Geophys. Res., 106, 4079-4090.

Lundegard, P.D., and Land, L.S. (1986), Carbon dioxide and organic acids: their role in porosity enhancement and cementation, Paleogene of the Texas Gulf Coast. In Gautier, D.L. (ed.), Roles of Organic Matter in Sediment Diagenesis, SEPM Special Pub., 38, pp. 129-146.

McInerney, M.J., Nagle, D.P., and Knapp, R.M. (2005), Microbially enhanced oil recovery: past, present, and future. In Ollivier, B., and Magot, M. (eds.), Petroleum Microbiology, ASM Press, 365 p.

McMahon, P.B., and Chapelle, F.H. (1991), Microbial production of organic acids in aquitard sediments and its role in aquifer geochemistry, Nature, 349, 233-235.

McMahon, P.B., Vroblesky, D.A., Bradley, P.M., Chapelle, F.H., and Gullet, C.D. (1995), Evidence for enhanced mineral dissolution in organic acid-rich shallow groundwater, Ground Water, 33, 207-216.

Meshri, I.D. (1986), On the reactivity of carbonic and organic acids and generation of secondary porosity, SEPM Special Pub., 38, pp. 123-128.

Naudet, V., and Revil, A. (2005), A sandbox experiment to investigate bacteria mediated redox processes on self-potential signals, Geophys. Res. Lett., 32, L11405, doi:10.1029/2005GL022735.

Ntarlagiannis, D., Yee, N., and Slater, L. (2005), On the low frequency induced polarization of bacterial cells in sands, Geophys. Res. Lett., 32, L24402, doi:10.1029/2005GL024751.

Ollivier, B., and Magot, M., (eds.) (2005), Petroleum Microbiology, ASM Press, 365 p.

Revil, A., and Glover, P.W.J. (1998), Nature of surface electrical conductivity in natural sands, sandstones, and clays, Geophys. Res. Lett., 25, 691-694.

Ron, E.Z., and Rosenberg, E. (2001), Natural roles of biosurfactants, Environ. Microbiol., 3(4), 229, doi:10.1046/j.1462-2920.2001.00190.x.

Rosen, MJ. (1989), Surfactants and Interfacial Phenomena. 2nd Ed. New York: Wiley-Interscience, 393–419.

Sauck, W.A., Atekwana, E.A., and Nash, M.S. (1998), High conductivities associated with an LNAPL plume imaged by integrated geophysical techniques, J. Env. Eng. Geophys., 2, 203-212.

Slater, L., and Lesmes, D.P. (2002), IP interpretation in environmental investigations, Geophysics, 67, 77-88.

Slater, L., Ntarlagiannis, D., Personna, Y.R., and Hubbard, S. (2007a), Pore-scale spectral induced polarization signatures associated with FeS biomineral transformations, Geophys. Res. Lett., 34, L21404, doi: 10.1029/2007GL031840.

Slater, L., Ntarlagiannis, Yee, N., O'Brien, M., Zhang, C., and Williams, K.H. (2007b), Electrodic voltages in the presence of dissolved sulfide: Implications for monitoring natural microbial activity, Geophysics, 73(2), 65-70.

Tower, O.F. (1905), The conductivity of liquids: methods, results, chemical applications, and theoretical considerations, Chemical Publishing Co., Easton, PA., 182.

Vanhala, H., and Soininen, H. (1995), Laboratory technique for measurement of spectral induced polarization response of soil samples, Geophys. Prospect., 43, 655-676.

Volkering, F., Breure, A.M., and Rulkens, W.H. (1998), Microbiological aspects of surfactant use for biological soil remediation, Biodegradation, 8, 401-417.

Welch, S.A., and Ullman, W.J. (1993), The effect of organic acids on feldspar dissolution rates and stoichiometry, Geochim. Cosmo. Acta, 57, 2725-2736.

Werkema, D.D., Atekwana, E.A., Enders, A., Sauck, W.A., and Cassidy, D.P. (2003), Investigating the geoelectrical response of hydrocarbon contamination undergoing biodegradation, Geophys. Res. Lett., 30, 1647, doi: 10.1029/2003GL017346.

Williams, K.H., D. Ntarlagiannis, L.D. Slater, A. Dohnalkova, S.S. Hubbard, and Banfield, J.F. (2005), Geophysical imaging of stimulated microbial biomineralization, Environ. Sci. Tech., 39(19), 7592-7600.

Youssef, N., Simpson, D.R., Duncan, K.E., McInerney, M.J., Folmsbee, M., Fincher, T., and Knapp, R.M. (2007), In Situ Biosurfactant Production by *Bacillus* Strains Injected into a Limestone Petroleum Reservoir, Appl. Environ. Microbiol., 73(4), 1239–1247, doi:10.1128/AEM.02264-06.

Zhang, Y., and Miller, R.M. (1995), Effect of rhamnolipid (biosurfactant) structure on solubilization and biodegradation of n-alkanes, Appl. Environ. Microbiol., 61, 2247-2251.

2. MICROBIAL GROWTH AND BIOFILM FORMATION IN GEOLOGIC MEDIA IS DETECTED WITH COMPLEX CONDUCTIVITY MEASUREMENTS

Caroline A. Davis, Estella Atekwana, Eliot Atekwana, Lee D. Slater, Silvia Rossbach, Melanie R. Mormile, 2006, Microbial growth and biofilm formation in geologic media is detected with complex conductivity measurements, Geophys. Res. Lett., 33, L18403, doi: 10.1029/2006GL027312.

2.1. ABSTRACT

Complex conductivity measurements (0.1-1000 Hz) were obtained from biostimulated sand-packed columns to investigate the effect of microbial growth and biofilm formation on the electrical properties of porous media. Microbial growth was verified by direct microbial counts, pH measurements, and environmental scanning electron microscope imaging. Peaks in imaginary (interfacial) conductivity in the biostimulated columns were coincident with peaks in the microbial cell concentrations extracted from sands. However, the real conductivity component showed no discernible relationship to microbial cell concentration. We suggest that the observed dynamic changes in the imaginary conductivity (σ") arise from the growth and attachment of microbial cells and biofilms to sand surfaces. We conclude that complex conductivity techniques, specifically imaginary conductivity measurements are a proxy indicator for microbial growth and biofilm formation in porous media. Our results have implications for microbial enhanced oil recovery, CO_2 sequestration, bioremediation, and astrobiology studies.

2.2. INTRODUCTION

Several laboratory studies have demonstrated the utility of geophysical methods for the investigation of microbial-induced changes in porous geologic media. The primary suggestion of these studies was that temporal variations in the geophysical signatures corresponded with microbial-induced changes in the geologic media, such as changes in pore fluid chemistry [*Atekwana et al.*, 2004], redox conditions [*Naudet and*

Revil, 2005], sulfide mineral precipitation [*Ntarlagiannis et al.*, 2005a; *Williams et al.*, 2005], increase in surface area resulting from attachment of microbes to mineral surfaces [*Abdel Aal et al.*, 2004], or pore clogging due to the presence of microbial cells [*Ntarlagiannis et al.*, 2005b]. Although the above studies have increased our understanding of microbial-induced changes on the geophysical response of geologic media, the direct contribution of microbial growth and biofilm formation on the geophysical response of geologic media remains unknown.

Notable is the use of electrical conductivity in conjunction with other methods (e.g., pH), to detect changes in the chemical properties of pore solutions caused by microbial growth and metabolism in geologic media [e.g., *Silverman and Munoz*, 1974; *Abdel Aal et al.*, 2004]. A laboratory column experiment by *Ntarlagiannis et al.* [2005b] showed a 15% enhanced polarization associated with the direct presence of dormant live (pure culture) bacterial cells in silica sands. *Ntarlagiannis et al.* [2005b] tentatively attributed this polarization enhancement at high cell densities to a combination of decreased ionic mobility and electron transfer associated with cell accumulation in pore throats.

The work described in this letter advances the work of *Ntarlagiannis et al.* [2005b] by using an environmental (mixed) bacterial culture, and allowing for microbial growth and biofilm formation, being more similar to typical field conditions. Understanding the effect of microbial growth and biofilm formation on the geophysical response of geologic media has implications for microbial enhanced oil recovery (MEOR), CO_2 sequestration, and bioremediation investigations, as well as studies focused on the development of techniques for the detection of extraterrestrial life. Here we show an apparent correlation between imaginary conductivity and microbial growth, and infer that imaginary conductivity measurements can be used as an indicator of microbial growth and biofilm formation in porous geologic media.

2.3. METHODS

2.3.1. Experimental Column Setup. The experimental columns used in this study were 30 cm long (Figure 2.1) and constructed from 3.2 cm inner diameter polyvinyl chloride pipe (PVC). Two Ag-AgCl current injection electrode coils were installed 16 cm

apart in the column, and two Ag-AgCl potential electrodes (9 cm apart) were installed between the current electrodes. A fluid reservoir constructed of 7.6 cm PVC pipe was installed on top of each column to allow for fluid sampling. Columns were dry-packed with 20-30 mesh silica sand (99.8% silicon dioxide, 0.020% iron oxide, 0.06% aluminum oxide, 0.01% titanium oxide, <0.01% calcium oxide, <0.01% magnesium oxide, <0.01% sodium oxide, <0.01% potassium oxide). The sands were washed with deionized water and disinfected by autoclaving prior to being packed in the columns. All columns, tubing, and accessories were disinfected by rinsing with 70% ethanol.

Two sets of electrical columns were constructed in duplicate, and a third column was constructed for solid phase analysis. One set was used for unstimulated (background) measurements (nutrients + diesel fuel) and one set for biostimulated (experimental) measurements (nutrients + diesel fuel + bacterial culture). Columns were saturated with a sterile 25% Bushnell Haas (BH) nutrient broth (Becton Dickinson; 50 mg/L magnesium sulfate, 5 mg/L calcium chloride, 250 mg/L monopotassium phosphate, 250 mg/L diammonium hydrogen phosphate, 250 mg/L potassium nitrate, 12.5 mg/L ferric chloride), diesel fuel, and the biostimulated columns were amended with a mixed bacterial culture that was cultured from sediments collected at a hydrocarbon contaminated site in Carson City, MI, USA. The mixed culture is known to contain hydrocarbon degraders such as strains of *Variovorax* and *Stenotrophomonas*. The fluid in each column was circulated for 30 min by using a peristaltic pump prior to electrical measurements, fluid sampling, and sand sampling.

2.3.2. Complex Conductivity Measurements. Complex conductivity measurements (0.1-1000 Hz) were obtained by using a four-electrode technique (Figure 2.1) based around a National Instruments (NI) 4551 dynamic signal analyzer [*Vanhala and Soininen*, 1995; *Slater and Lesmes*, 2002]. The impedance magnitude $|\sigma|$ and the phase shift φ (between a measured voltage sinusoid and an impressed current sinusoid) of the sample were measured relative to a high-quality resistor. The real ($\sigma' = |\sigma| \cos \varphi$) and imaginary ($\sigma'' = |\sigma| \sin \varphi$) parts of the sample complex conductivity were then calculated.

The electrical measurements were made twice a week for the 60 day duration of the experiment. Experimental uncertainty in the electrical measurements was calculated by averaging the electrical data for duplicate columns, and calculating the standard deviation from the average.

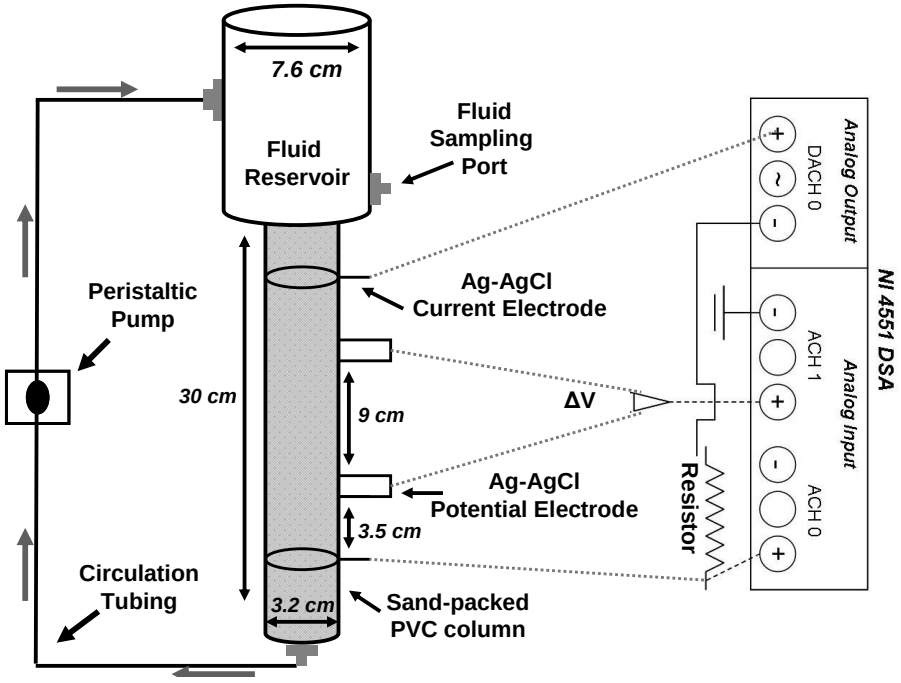

Figure 2.1. Schematic diagram showing the experimental set up. A digital signal analyzer (DSA) was used to collect the low frequency electrical measurements.

2.3.3. Sampling and Analyses. Fluid conductivity (σ_w) and pH were measured using microelectrodes immediately after fluids were withdrawn from the fluid reservoirs at the top of the columns. BH broth was periodically added (day 18, and 31) to the fluid reservoir to maintain the fluid volume in the reservoir. Experimental uncertainty in the geochemical measurements was calculated by averaging the geochemical data for duplicate columns, and calculating the standard deviation from the average.

Sand samples were collected from the sand sampling columns beginning on day

13 of the experiment, immediately after fluid samples were collected. The sand samples were used for (1) extraction of bacterial cells for direct microbial counts, and (2) environmental scanning electron microscope (ESEM) imaging of grain surface characteristics. Live and dead microbial cell numbers were determined by direct counting using an epifluorescent microscope [*Bunthof et al.*, 2001]. Bacterial cells were extracted from 0.5g of wet sand using an extraction technique modified after *Lehman et al.* [2001]. After extraction, the bacterial cells were washed with 0.85% NaCl solution, stained, and prepared for direct counts using a Live/Dead BacLight Bacterial Viability Kit. The average live cell concentrations and average dead cell concentrations were calculated, and experimental uncertainty was determined by calculating the standard deviation from the average of duplicate counts.

A portion of the sand samples collected from the columns were imaged using an ESEM. Images of the sand surface characteristics and attached microbial cells and biofilms were obtained by Hitachi High Technologies America, Inc. using a Hitachi S3400 ESEM fitted with secondary and backscattered electron detectors. The ESEM operating parameters varied depending on the surface characteristic being imaged, and ranged from 2.5-8.0 kV, 5.9-11.1 mm, 700x-3000x, for accelerating voltage, working distance, and magnification, respectively.

2.4. RESULTS

2.4.1. Complex Conductivity. The complex conductivity measurements were corrected for changes in temperature effects using correction equation $y = 0.0003x + 0.0084$ ($R^2 = 0.99$) and $y = 0.0000001x + 0.000002$ ($R^2 = 0.98$) at 25C, for the real and imaginary conductivity, respectively. Temperature correction equations were determined from laboratory experiments designed to measure the effect of temperature variations on the complex conductivity measurements. Fluid conductivity values were automatically corrected for changes in temperature by the conductivity microelectrode.

The complex conductivity measurements are shown in Figure 2.2a and 2.2b. We show the electrical data at 2 Hz, as this frequency is close to typical frequencies used in field electrical measurements. This was also the frequency at which our measurement error was lowest. The σ" in the biostimulated columns increased by ~280% from

~$2.0x10^{-6}$ S/m on day 0 to peak values (~$7.8x10^{-6}$ S/m) between day 18 and 23, before steadily decreasing to ~$2.0x10^{-6}$ S/m on day 40. The magnitude of the σ" response in the unstimulated columns was relatively small compared to the biostimulated columns, increasing slightly and varying by ~$1.5x10^{-7}$ S/m over the duration of the experiment and rarely exceeding the initial values at the start of the experiment. The σ' (Figure 2.2b) showed a relatively steady increase over the duration of the experiment for both the unstimulated (up to ~$1.5x10^{-2}$ S/m or ~28% increase) and biostimulated (up to ~$1.6x10^{-2}$ S/m or ~18% increase) columns. The σ_w (Figure 2.2c) of the biostimulated columns decreased slightly for the first few days (by ~5%) to ~$8.0x10^{-2}$ S/m, before increasing slightly for the rest of the experiment. The σ_w of the unstimulated columns varied to a greater degree (~12%) than the biostimulated columns, decreasing for the first 20 days by ~12% to $7.5x10^{-2}$ S/m, before increasing to ~ $8.3x10^{-2}$ S/m by day 60.

2.4.2. Microbial and Geochemical Analyses. Temporal variations in the live and dead microbial cell concentrations (presented as cells/gram of wet sand weight) for both biostimulated and unstimulated columns are shown in Figure 2.2d. Live cell concentrations in the biostimulated column increased by ~230%, from ~$3.6x10^4$ cells/g on day 13 to peak concentrations on day 23 (~$1.2x10^5$ cells/g), before declining to ~$3.0x10^4$ cells/g on day 40. Although the dead cell concentrations within the biostimulated columns were generally lower than the live cell concentrations, they displayed a similar trend to the live cell concentrations, albeit to a lesser degree. The dead cell concentrations increased from ~$4.6x10^3$ cells/g on day 13 to peak concentrations on day 23 (~$1.9x10^4$ cells/g), and decreased to ~$6.0x10^3$ cells/g on day 40. The microbial cell concentrations from the unstimulated column initially decreased during the first 30 days of the experiment before increasing with values varying between ~$2x10^3$ cells/g and $2x10^4$ cells/g for the duration of the experiment (both live concentrations and dead concentrations). The error associated with the cell concentrations was less than $1.8x10^4$ cells/g and $1.5x10^4$ cells/g for the biostimulated column live and dead cell concentrations, respectively, and less than $1.2x10^4$ cells/g and $1.0x10^4$ cells/g for the unstimulated column live and dead cell concentrations, respectively.

A temporal decrease in pH was observed for both the biostimulated and unstimulated columns (Figure 2.2e). The biostimulated columns showed a relatively greater decrease (~7-6.3) than the unstimulated columns (~7-6.6).

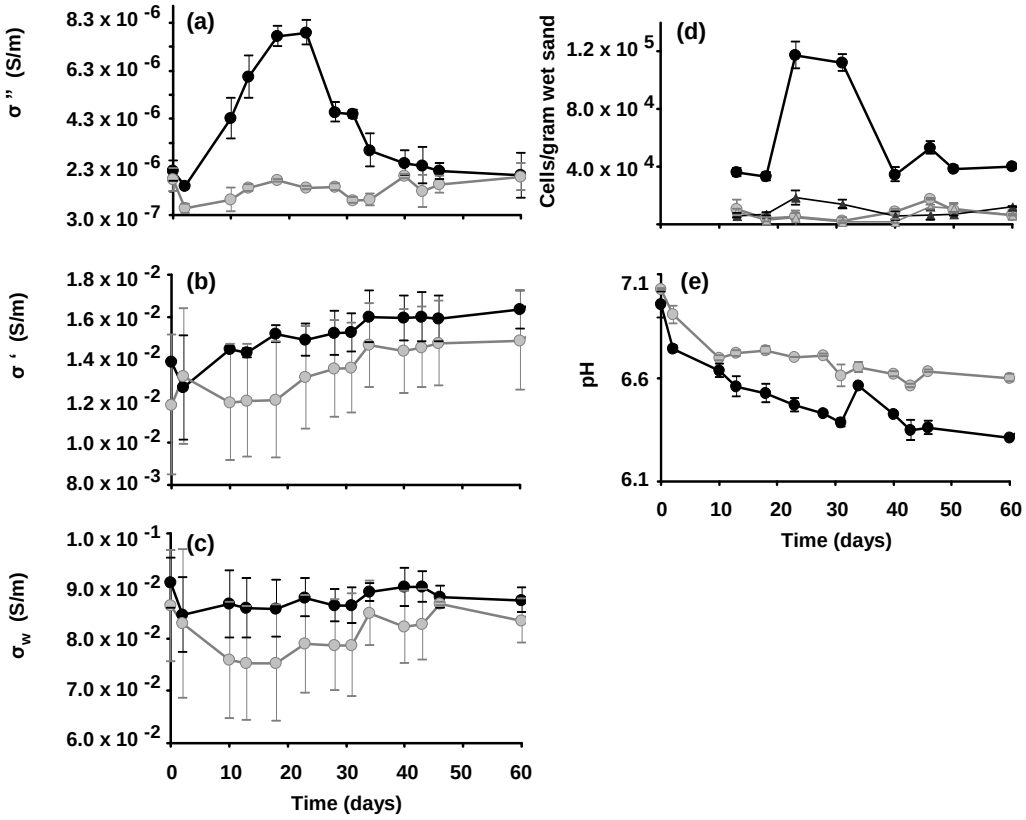

Figure 2.2. Results of the measured (a) σ", (b) σ', and (c) σ_w, (d) microbial cell concentrations, and (e) pH. (a-c and e) Closed black circles represent biostimulated column measurements, and closed gray symbols represent unstimulated column measurements. Microbial cell concentrations (d) are shown as biostimulated column live cells (black closed circle), unstimulated live cells (gray closed circles), biostimulated column dead cells (black closed triangle), and unstimulated column dead cells (gray closed triangle). Error bars represent measurement uncertainty reported as standard deviation from average of duplicate measurements.

2.4.3. Grain Surface Characteristics. We show four representative ESEM images of surfaces of sand samples obtained on day 23 and day 46 (Figure 2.3). The images from day 23 of the biostimulated column show a network of extracellular structures between sand grains (Figure 2.3a), as well as the attachment of individual bacterial cells (Figure 2.3b) to the sand surfaces. The image from day 23 of the unstimulated column (Figure 2.3c) shows the relatively smooth, uncolonized surface of a sand grain. Figure 2.3d shows a backscattered electron composition image of the surface of a sand grain from day 46 of the biostimulated column with features that may represent extracellular or biomat-like structures.

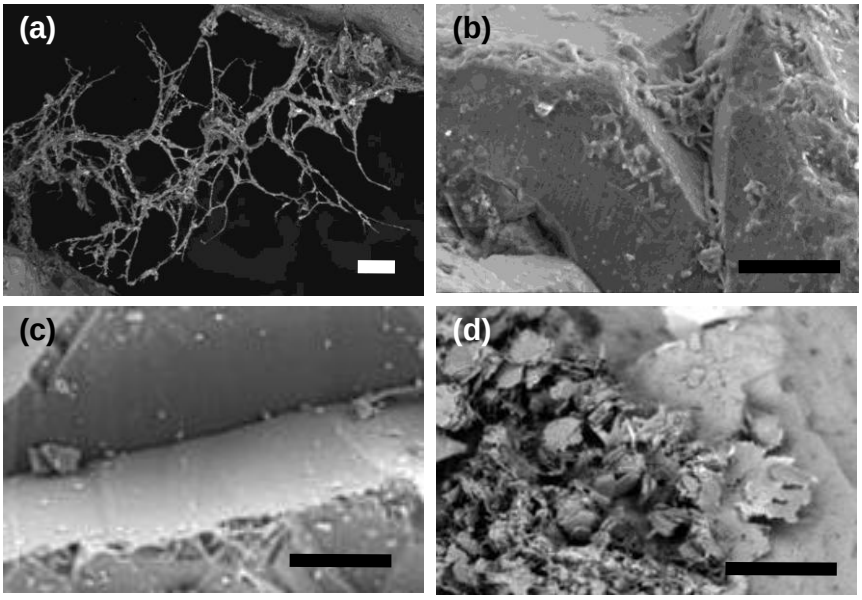

Figure 2.3. Environmental scanning electron microscope images of sand from (a & b) day 23 of the biostimulated column, (c) day 23 of the unstimulated column, and (d) day 46 of the biostimulated column. Scale bar on each image represents 10 μm.

2.5. DISCUSSION

ESEM images confirm microbial growth and biofilm formation in the biostimulated column. The complex conductivity measurements show that changes in σ" generally paralleled those of the microbial counts, with a close correspondence in the

peaks and magnitude (up to 280%) of the σ" and that of the cell concentrations (up to 230%) in the biostimulated columns (Figure 2.2a and 2.2d). Since the microbial cell concentrations were measured from microbial cells extracted from sand grains, the close correspondence of the peaks and magnitudes of change of both parameters suggest that the σ" response resulted directly from the microbial growth and attachment. The unstimulated column, however, did not show any close correspondence between cell concentration and σ".

From our results, we infer the following: the increase in microbial cell concentration (Figure 2.2d) and σ" observed in the biostimulated column (day 13-23) may be in whole or in part due to the increased attachment of cells/biofilms to the surface of sand grains, and/or the increased aggregation of cells into microcolonies [e.g., *Watnick and Kolter*, 2000]. The subsequent decrease in the live microbial cell concentration (day 23-60), and corresponding decrease in σ" may be due to an increased rate of detachment [e.g., *Watnick and Kolter*, 2000] or death and lysis of cells [*Mai-Prochnow et al.*, 2004], possibly due to limited nutrients/carbon source or from excessive cell density. The idea of cell death and lysis, the process in which the cell disintegrates and the contents enter the bulk fluid, is a plausible explanation for not observing an increase in the dead cell concentration after day 30.

This suggestion is further supported by the ESEM images of sand from the biostimulated column, which showed high numbers of attached cells and extracellular structures on day 23 (Figure 2.3a), while less attached biomass is apparent on day 46 (Figure 2.3d). Whereas *Ntarlagiannis et al.* [2005] investigated the electrical response of live dormant cells and speculated on the cause of the electrical response, the ESEM images (Figure 2.3a) presented in this study, provides strong evidence to support our findings that the σ" response is associated with cell aggregation/biofilm formation. The ESEM image from day 23 of the biostimulated column (Figure 2.3a) showing the extracellular material between sand grains, looks similar to the conductive extracellular structures known as nanowires that have been found in recent studies [i.e., *Reguera et al.*, 2005; *Gorby et al.*, 2006]. The nanowire structures have been documented to facilitate electron transport from cells to solid phase electron acceptors and typically develop under nutrient (terminal electron acceptor) limiting conditions [*Gorby et al.*, 2006].

Consequently, they may provide the necessary connections needed for charge transfer in microbially active systems and thus be responsible in part for the geoelectrical response observed in biostimulated porous material. However, more laboratory studies are needed to confirm or refute this hypothesis.

A relatively steady temporal increase in the σ' was observed in both the biostimulated and unstimulated columns. We used pure silica sands to minimize weathering in the columns and therefore did not expect to observe any significant changes in σ'. Hence, we are not sure as to the cause for the changes in σ'. However, we speculate that the temporal increase in the σ' may be due to the periodic addition of BH nutrients (Day 18 and 31) to the columns, which would increase the ionic concentration of the pore fluid. This increase in the ionic concentration of the pore fluid is observed in the σ_w, albeit to a lesser magnitude. We note that *Ntarlagiannis et al.* [2005b] also observed changes in the σ' in their experimental columns not explained by the fluid conductivity data.

In conclusion, the results from this study provide evidence that complex conductivity measurements, specifically imaginary conductivity measurements, can be used as a proxy indicator of microbial growth, attachment, and biofilm formation in porous geologic media. We surmise that the observed polarization (σ") response arises from the direct interaction of the attachment of microbial cells and biofilm development on mineral grain surfaces. These results further our understanding of the direct effect of microbial growth on electrical measurements, and have implications for geoelectrical investigations of environments with enhanced microbial growth/activity. Our work may lead to the application of complex conductivity measurements to field investigations, such as studies aimed at assessing the (1) integrity of subsurface biofilm barriers (biobarriers) used to remediate contaminants or seal reservoirs for CO_2 sequestration and (2) progress of microbial activity during enhanced oil recovery. Furthermore, our work suggests the possibility of applying electrical measurements to investigations of life on other planets.

2.6. ACKNOWLEDGMENTS

This material is based in part on work supported by the National Science Foundation under Grant No. OCE-0433869 and Grant No. OCE-0433739. We thank two summer Research Experience for Undergraduates (REU) students, Philip Bottrell and Joseph Heidenreich, for their laboratory assistance. We also thank Jessica Christiansen for assistance with the microbial analyses. Discussions with Y. Gorby on nanowires are greatly appreciated.

2.7. REFERENCES

Abdel Aal, G.Z., Atekwana, E.A., Slater, L.D., and Atekwana E.A. (2004), Effects of microbial processes on electrolytic and interfacial electrical properties of unconsolidated sediments, Geophys. Res. Lett., 31(12), L12505, doi:10.1029/2004GL020030.

Atekwana, E.A., Atekwana, E.A., Werkema, D.D., Allen, J.P., Smart, L.A., Duris, J.W., Cassidy, D.P., Sauck, W.A., and Rossbach, S. (2004), Evidence for microbial enhanced electrical conductivity in hydrocarbon-contaminated sediments, Geophys. Res. Lett., 31, L23501.

Bunthof, C.J., van Schalkwijk, S., Meijer, W., Abee, T., and Hugenholtz, J. (2001), Fluorescent method for monitoring cheese starter permeabilization and lysis, Appl. Environ. Microbiol., 67, 4264-4271.

Gorby, Y.A., Yanina, S., McLean, J.S., Rosso, K.M., Moyles, D., Dohnalkova, A., Beveridge, T.J., Chang, I., Kim, B.H., Kim, K.S., Culley, D.E., Reed, S.B., Romine, M.F., Saffarini, D.A., Hill, E.A., Shi, L, Elias, D.A., Kennedy, D.W., Pinchuk, G., Watanabe, K., Ishii, S., Logan, B., Nealson, K.H., and Fredrickson, J.K. (2006), Electrically conductive bacterial nanowires produced by Shewanella oneidensis strain MR-1 and other microorganisms, Proc. Natl. Acad. Sci. USA, 103(30), 11358-11363.

Lehman, M.R., Colwell, F.S., and Bala, G.A. (2001), Attached and unattached microbial communities in a simulated basalt aquifer under fracture- and porous-flow conditions, Appl. Environ. Microbiol., 67(6), 2799-2809.

Mai-Prochnow, A., Evans, F., Dalisay-Saludes, D., Stelzer, S., Egan, S., James, S., Webb, J.S., and Kjelleberg, S. (2004), Biofilm development and cell death in the marine bacterium Pseudoaltermonas tunicate, Appl. Environ. Microbiol., 70, 3232-3238.

Naudet, V., and Revil, A. (2005), A sandbox experiment to investigate bacteria-mediated redox processes on self-potential signals, Geophys. Res. Lett., 32, L11405, doi:10.1029/2005GL022735.

Ntarlagiannis, D., Williams, K.H., Slater, L., and Hubbard, S. (2005a), The low frequency electrical response to microbially induced sulfide precipitation, J. Geophys. Res., 110, G02009, doi:10.1029/2005JG000024.

Ntarlagiannis, D., Yee, N., and Slater, L. (2005b), On the low frequency induced polarization of bacterial cells in sands, Geophys. Res. Lett., 32, L24402, doi:10.1029/2005GL024751.

Reguera, G., McCarthy, K.D., Mehta, T., Nicoll, J.S., Tuominen, M.T., and Lovely, D.R. (2005), Extracellular electron transfer via microbial nanowires, Nat. Lett., 435(23), 1098-1101.

Silverman, M.P., and Munoz, E.F. (1974), Microbial metabolism and dynamic changes in the electrical conductivity of soil solutions: a method for detecting extraterrestrial life, Appl. Microbiol., 28(6), 960-967.

Slater, L., and Lesmes, D.P. (2002), IP interpretation in environmental investigations, Geophysics, 67, 77-88.

Vanhala, H., and Soininen, H. (1995), Laboratory technique for measurement of spectral induced polarization response of soil samples, Geophys. Prospect., 43, 655-676.

Watnick, P., and Kolter, R. (2000), Biofilm, city of microbes, J. Bacteriol., 182(10), 2675-2679.

Williams, K.H., Ntarlagiannis, D., Slater, L., Dohnalkova, A., Hubbard, S.S., and Banfield, J.F. (2005), Geophysical imaging of stimulated microbial biomineralization, Environ. Sci. Tech., 39(19), 7592-7600.

3. EFFECTS OF MICROBIAL GROWTH AND BIOFILM FORMATION ON ACOUSTIC WAVE PROPAGATION IN POROUS MEDIA

3.1. ABSTRACT

Acoustic wave data were acquired over a two-dimensional region of a microbial-stimulated and an unstimulated sand column to assess the spatiotemporal changes in a porous medium caused by growth of a biofilm forming bacteria culture. Concurrent measurements of complex conductivity and fluid chemistry (i.e., pH) were also collected on the columns to assess the progress of the stimulated microbial growth. Acoustic signals recorded for the unstimulated sample were relatively uniform over the 2D scan region for the 29 day experiment duration. The biostimulated sample, however, exhibited a high degree of spatial variation in the acoustic amplitude measurements, with portions of the sample exhibiting increased attenuation (up to 73%) while other portions exhibited decreased attenuation (up to 45%) compared to baseline values. The acoustic amplitude changed significantly in the biostimulated sample between Days 5-7 of the experiment, consistent with a peak in the imaginary conductivity values. Peaks in the imaginary conductivity response associated with microbial growth in porous media have been previously shown to parallel peaks in attached cell concentrations and biofilm formation. Environmental scanning electron microscope imaging verified microbial cell attachment to sand surfaces and showed apparent differences in the structure and/or texture of attached biomass between regions of increased and decreased acoustic wave amplitude. We conclude from these observations that spatial and temporal variations in microbial growth and/or biofilm structure caused heterogeneity in the elastic properties, and therefore changes to the acoustic wave propagation in the porous media. Our results have significant implications for the use of acoustic measurements for assessing spatial and/or temporal variations in biomass distribution in subsurface environments necessary for validating bioclogging models.

3.2. INTRODUCTION

Bioclogging of porous media due to biofilm development is a phenomenon that can cause significant changes in the porosity and permeability of subsurface systems,

influencing fluid flow and transport. [e.g., *Vandevivere and Baveye*, 1992; *Brovelli et al.*, 2009], groundwater recharge [e.g., *Rinck-Pfeiffer et al.*, 2000], and remediation efforts [e.g., *Baveye et al.*, 1998]. Several numerical models and simulations have been developed to qualitatively forecast changes to the hydraulic properties of porous media from bioclogging [e.g., *Taylor and Jaffé*, 1990; *Kildsgaard and Engesgaard*, 2001; *Thullner et al.*, 2004; *Brovelli et al.*, 2009]. Limitations exist with the application of these models, however, as bioclogging processes are dynamic and influenced by many phenomena including the presence of initial heterogeneities in biomass distribution as well as in the physical properties of the porous medium [e.g., *Brovelli et al.*, 2009]. One of the difficulties inherent with experimental modeling approaches is that quantitative information from the direct observation of biological growth and bioclogging is required from the subsurface. However, it is difficult to obtain these data at the appropriate spatiotemporal scales needed to validate or test the predictive models [*Dupin and McCarty*, 2000]. Therefore, further development of diagnostic techniques such as minimally invasive geophysical methods, which can provide information on the spatiotemporal distribution of subsurface heterogeneities and the effect on hydrogeological properties as a result of microbial growth, is essential. Development of such techniques would allow for the further validation of predictive models, such as bioclogging models, with implications for monitoring microbial growth, biofilm formation, and bioclogging distribution in situ.

To date, most biogeophysical investigations have focused on geoelectrical techniques [*Atekwana et al.*, 2006]. Apart from a few studies [e.g., *Williams*, 2002; *Williams et al.*, 2005; *DeJong et al.*, 2006; 2009], less attention has been given to explore the effects of microbial interactions with geologic media on seismic properties. While the *Williams et al.* [2005] and *DeJong et al.* [2006] studies have improved our understanding of the seismic signatures associated with microbial-mediated mineral precipitation, there is a need to expand these previous works to understand the fundamental seismic response of bacteria growth and biofilm formation in porous media in the absence of enhanced precipitation.

The work described here advances the *Williams et al.* [2005] and *DeJong et al.* [2006] studies by investigating the influence of microbial growth and biofilm formation

on the spatiotemporal seismic properties of porous media using an acoustic two-dimensional scanning method [e.g., *Li et al.*, 2001] in the absence of enhanced precipitation. We show for the first time that variations in microbial growth and biofilm structure/texture can cause heterogeneity in the elastic properties of porous media, and thus variations in acoustic wave propagation. We suggest that acoustic measurements may (1) provide diagnostic semi-quantitative data for testing and validation of bioclogging models and numerical simulations used for assessing microbial induced changes in flow and transport properties, and (2) be used for assessing spatial and/or temporal variations in biomass distribution in subsurface environments (i.e., microbial enhanced oil recovery (MEOR), and engineered biobarriers).

3.3. METHODS

3.3.1. Experimental Column Setup. Rectangular experimental columns were fabricated using 0.32 cm thick clear acrylic (Figure 3.1), and measured 10.2 cm by 5.1 cm by 25.4 cm (width x depth x height). Two sets of experimental columns were constructed; two columns for acoustic wave measurements (e.g., Figure 3.1a) and two columns for complex conductivity (electrical) measurements (e.g., Figure 3.1b). The electrical columns were constructed with two Ag-AgCl current injection electrode coils (16 cm apart), and two Ag-AgCl potential electrodes (9 cm apart) which were installed between the current electrodes (Figure 3.1b). In addition, a plastic divider was installed in the center of the electrical columns (Figure 3.1b,c), constructed from a 19 cm long section of 3.2 cm inner diameter (0.1 cm thick) polyvinyl chloride pipe cut lengthwise. Emplacement of the divider was deemed necessary to reduce noise in the electrical data, after calibration measurements using NaCl solutions of known fluid conductivity without the divider showed that the phase shift (φ) error exceeded 1 mrad at 10 Hz. This φ error is in excess of what has previously been reported by other studies using similar complex conductivity equipment (<0.5 mrad below 10 Hz) [e.g., *Ntarlagiannis et al.*, 2005; *Abdel Aal et al.*, 2006], and well beyond the relative φ accuracy (~0.2 mrad below 100 Hz) reported for this instrumentation by *Slater and Lesmes* [2002]. After placing the divider in the electrical columns the φ error decreased to <0.5 mrad, which was deemed to be an acceptable level.

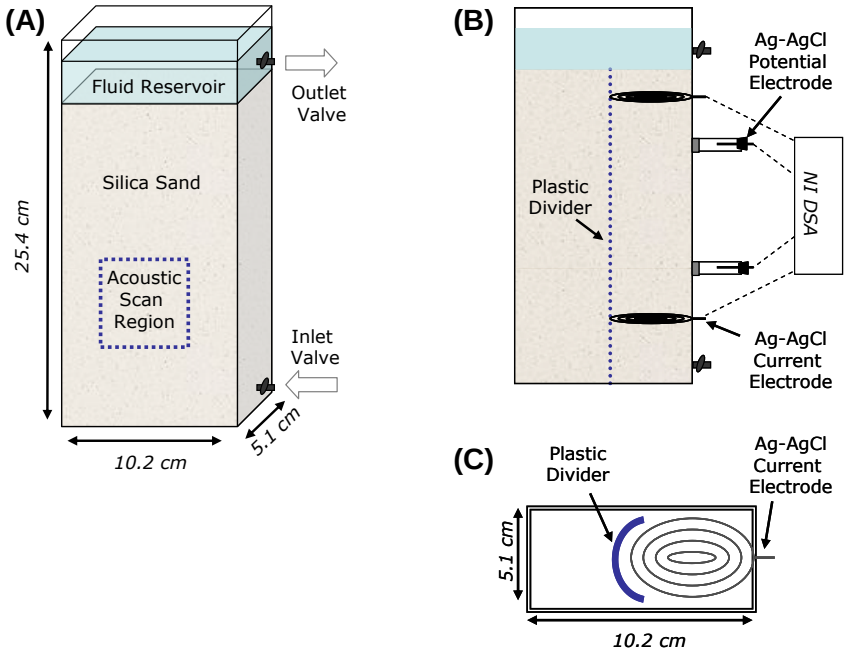

Figure 3.1. Schematic drawing showing a side view of the column setup for the (a) acoustic and (b) complex conductivity measurements. (c) Shows a top view of the complex conductivity columns. The 2D acoustic scan region measures 6cm x 7cm (width x height).

The columns were wet-packed with 20-30 mesh silica sand (Ottawa, IL) consisting of 99.8% silicon dioxide, 0.020% iron oxide, 0.06% aluminum oxide, 0.01% titanium oxide, <0.01% calcium oxide, <0.01% magnesium oxide, <0.01% sodium oxide, <0.01% potassium oxide. Prior to packing, the sands were washed with deionized (DI) water and disinfected by autoclaving. Columns and accessory equipment were also disinfected by rinsing with a 70% ethanol solution. Prior to saturation with the experimental fluids, the sand-packed columns were saturated with sterile 25% Bushnell Haas (BH) nutrient broth (Becton Dickinson; 50 mg/L magnesium sulfate, 5 mg/L calcium chloride, 250 mg/L monopotassium phosphate, 250 mg/L diammonium hydrogen phosphate, 250 mg/L potassium nitrate, 12.5 mg/L ferric chloride) and baseline acoustic and electrical measurements were collected. After the initial background measurements were recorded, microbial growth was stimulated in two sand columns (one electrical and one seismic) by saturating with 25% BH nutrient broth, 30 mM glucose,

Pseudomonas aeruginosa PAO1 bacteria inocula, and 30 µg/mL Gentamicin antibiotic. The PAO1 strain is a Gram-negative, rod-shaped, biofilm forming bacteria culture [e.g., *Klausen et al.*, 2003] commonly found in soil and water. The bacteria strain (specifically PAO1 Tn7-Gm-gfp) was obtained from the University of Denmark (Lyngby, Denmark), where previous studies with this bacteria strain have been conducted [e.g., *Pamp and Tolker-Nielsen*, 2007]. The other two columns (unstimulated columns) were used for background measurements and were saturated with 25% BH and Gentamicin antibiotic. Antibiotics were added to both the biostimulated and unstimulated columns to inhibit the growth of microorganisms other than the *P. aeruginosa* in the biostimulated column. As this was a static experiment, the fluid in the columns remained stagnant during this experiment and the columns were not fed with additional nutrients.

3.3.2. Acoustic Wave Measurements. A full-waveform acoustic wave imaging system was used to obtain two-dimensional point-by-point maps of the acoustic response of the samples [e.g., *Pyrak-Nolte et al.*, 1999]. The acoustic imaging system used two water-coupled plane-wave transducers (1 MHz central frequency) as source and receiver. Water-coupled transducers were used to ensure the same coupling between the transducers and the sample at all locations on the sample and over time. The columns were placed in a water tank to a depth 2/3 the length of a column. Using the acoustic mapping mode (C-scan), computer-controlled linear actuators (Newport 850-B4 and Motion Master 2000) were used to move the source and receiver in unison over a 60 mm by 70 mm region in 5 mm increments (Figure 3.1a). A high-voltage pulse generator (Panametrics PR1500) was used to excite the source and to receive the transmitted signal. At each point in the 2D scan region, a 50 microsecond window of the transmitted signal was recorded and digitized with an oscilloscope (Lecroy 9314L). The entire 2D region of each column was scanned 2-3 times per week for the 29 day duration of the experiment.

3.3.3. Complex Conductivity Measurements. Complex conductivity (σ^*) measurements were collected at 40 frequency intervals between 0.1 and 1000 Hz using instrumentation based around a two-channel National Instruments (NI) dynamic signal analyzer [e.g., *Slater and Lesmes*, 2002]. Current was injected through Ag-AgCl current electrode coils (Figure 3.1b), and the impedance magnitude ($|\sigma|$) and phase shift φ (between a measured voltage sinusoid and an impressed current sinusoid) of the sample

were measured at the Ag-AgCl potential electrodes relative to a high-quality resistor. The imaginary ($\sigma'' = |\sigma| \sin \varphi$) part of the complex conductivity was then calculated from the measured $|\sigma|$ and φ, and the imaginary conductivity (σ'') is related to the polarization that occurs at interfaces [e.g., *Lesmes and Frye*, 2001]. Prior to starting the experiments, experimental uncertainty in the electrical measurements was determined from calibration measurements using NaCl solutions of known fluid conductivity (30-3000 μS/cm). The columns were then flushed with DI water prior to injection of the background and experimental solutions. Upon starting the experiment, electrical measurements were collected 2-3 times per week for the 29 day duration of the experiment.

3.3.4. Sampling and Analyses. Fluid samples were collected 1-2 times per week from the bottom valve of the columns. The fluid conductivity, pH, and fluid temperature were measured using bench-top probes immediately after fluids were withdrawn. Upon termination of the experiment, the columns were destructively sampled by withdrawing fluid from the bottom valve, and then withdrawing cores of the wet sand (core diameter ~0.6 cm) in a grid-like fashion (1.5 cm by 1.5 cm grid) from the acoustic scan region. The sand cores were used for environmental scanning electron microscope (ESEM) imaging to characterize the surfaces of the sand grains. An FEI Quanta 600 ESEM operating at 25 kV, 14-89%, 5-20 °C, for accelerating voltage, relative humidity, and temperature, respectively, was used to image the sand grains.

3.4. RESULTS

3.4.1. Acoustic Wave Measurements. The 2D acoustic scan images of the peak-to-peak transmitted amplitude obtained from the biostimulated and unstimulated columns are shown in Figures 3.2 and 3.3, respectively. The 2D scans obtained from the biostimulated column Day 1 reveal the transmitted compressional wave amplitude as relatively uniform over the scan region with an average amplitude of 0.99 ± 0.03 V (Figure 3.2a). However, over time the amplitudes varied spatially within the scan region through the first week, and by Day 5 and 6 the average amplitudes measured 1.00 ± 0.24 V and 0.80 ± 0.22 V, respectively. The 2D images began to show a persistent spatial trend in the amplitude values by Day 6 (Figure 3.4a), which remained relatively consistent through the end of the experiment on Day 29. The 2D image obtained on Day

29 exhibited an increase in amplitude up to 45% in some regions (i.e., Figure 3.2a; Location A), while other regions showed a decrease in amplitude of up to 73% (i.e., Figure 3.2a; Location E) compared to baseline values (Figure 3.4a). Figure 3.2b shows a 30 microsecond waveform window collected from the biostimulated column (Figure 3.2a) which documents amplitude changes. Overall, the compressional waves transmitted through the biostimulated column showed a decrease in amplitude (an average of 0.74 ± 0.25 V), and a slight decrease in acoustic wave velocity (~4%).

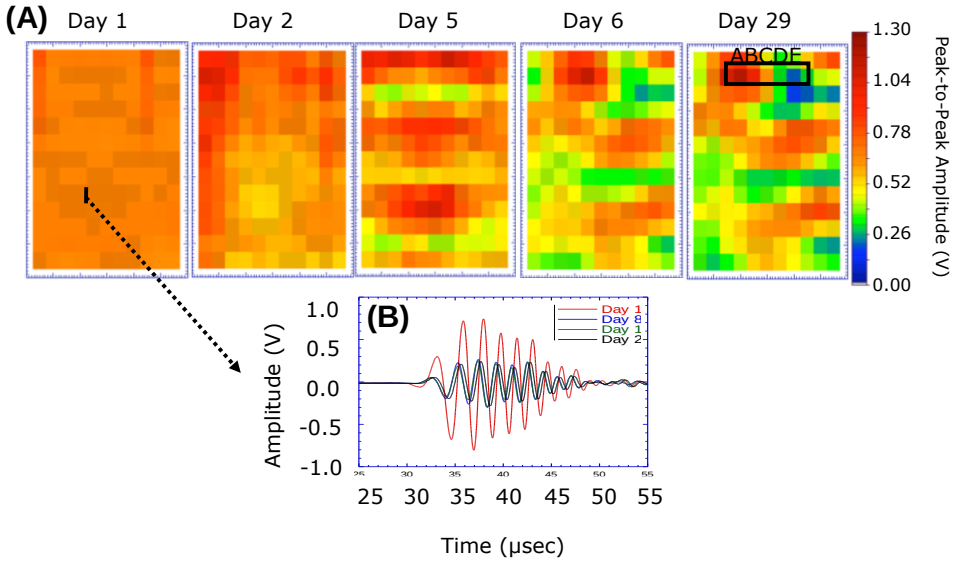

Figure 3.2. (a) 2D acoustic wave amplitude scans from the biostimulated column for Days 1, 2, 5, 6, and 29. (b) Shows the acoustic waveforms collected from the biostimulated column for the same respective five days. Black vertical line on Day 1 scan shows the data location for the waveform plot; black box on Day 29 scan denotes location of data plotted in Figure 3.4 and ESEM images shown in Figure 3.6.

Similar to the biostimulated column, the baseline 2D image from Day 1 of the unstimulated column (Figure 3.3a) was relatively uniform except the lower edges where slightly lower amplitudes were measured. Unlike the results from the biostimulated column, the 2D images collected from the unstimulated column (Figure 3.3a) show the amplitudes became more spatially uniform over time. The average amplitudes remained

relatively consistent and measured 0.92 ± 0.13 V and 0.90 ± 0.03 V for Day 1 and Day 29, respectively. In addition, the acoustic wave arrival times (Figure 3.3b) show a relative temporal consistency with no significant change in acoustic wave velocity observed.

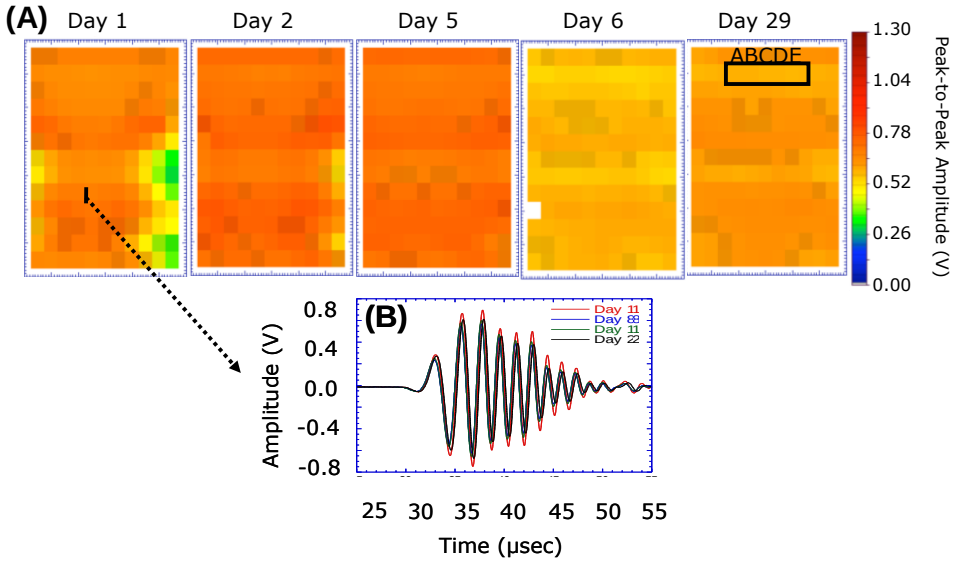

Figure 3.3. (a) 2D acoustic wave amplitude scans from the unstimulated column for Days 1, 2, 5, 6, and 29. (b) Shows the acoustic waveforms collected from the unstimulated column for the same respective five days. Black vertical line on Day 1 scan shows the data location for the waveform plot; black box on Day 29 scan denotes location of data plotted in Figure 3.4 and ESEM images shown in Figure 3.7.

Through five days prior to experimental stimulation, the temporal percent change in compressional wave amplitude was relatively similar for both the biostimulated (Figure 3.4a) and unstimulated (Figure 3.4b) samples. However, one day after biostimulation, the transmitted amplitudes deviate from the baseline values observed for the unstimulated column. By Day 5, the wave amplitudes observed from the biostimulated column are highly variable, both increasing and decreasing in amplitude in the select region (Figure 3.2a; Locations A-E). After Day 6, the trend in amplitude continued through the end of the experiment with the exception of one data location from

the select region. Data location C exhibited increased values through Day 12 before decreasing to near baseline values on Day 29. The relatively small overall variation in amplitude (<37%) relative to Day -1 observed from the unstimulated column is consistent for all of the select data points plotted (Figure 3.3a; Locations A-E) and does not exhibit the same behavior as observed for the biostimulated column (Figure 3.4).

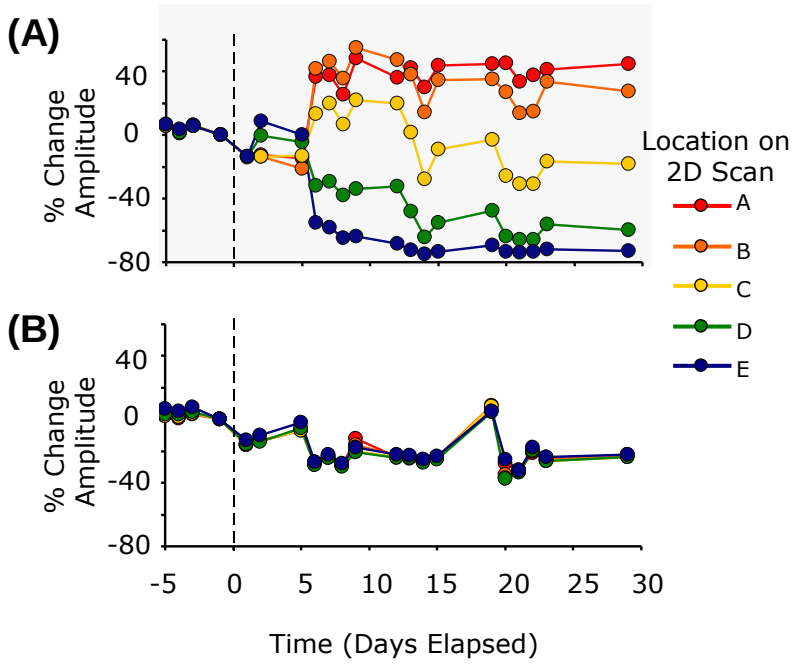

Figure 3.4. Graphs showing the temporal percent change in acoustic wave amplitude relative to Day -1 for the (a) biostimulated column, and (b) unstimulated column. Locations of the data points plotted here are shown in Figure 3.2 and 3.3 for the biostimulated and unstimulated columns, respectively.

3.4.2. Complex Conductivity and Geochemical Measurements. The results of the calibration tests conducted prior to the experiment indicate that experimental uncertainty associated with the φ measurements were generally less than 0.5 mrad at 10 Hz. The experimental σ" results are reported at 10 Hz, as this is the frequency where the lowest phase shift error was observed during calibration measurements, and this frequency is close to typical frequencies used in field electrical measurements.

The results of the temporal σ" and geochemical measurements are shown in Figure 3.5. The σ" measured from the biostimulated column (Figure 3.5a) increased by ~220% to peak values (2.29×10^{-5} S/m) on Day 5 relative to pre-injection (Day -1) values (7.16×10^{-6} S/m), before steadily decreasing to near baseline values on Day 20, and remained relatively consistent through Day 23. The magnitude of the σ" response measured from the unstimulated column was relatively small compared to the biostimulated column, varying by ~1.09×10^{-6} S/m over the duration of the experiment compared to 1.57×10^{-5} S/m for the biostimulated column. Relative to pre-injection values, σ" from the unstimulated column decreased by ~9.55×10^{-7} S/m (~89%) through Day 5, before steadily increasing to 2.17×10^{-6} S/m on Day 23, nearly ~103% above baseline values. Initial fluid conductivity values (Figure 3.5b) measured ~17% lower in the biostimulated column compared to the unstimulated column, and steadily increased from ~9.22×10^{-2} S/m through the end of the experiment. In contrast, the fluid conductivity values measured from the unstimulated column remained nearly constant around 1.13×10^{-1} S/m throughout the experiment, only decreasing slightly (by ~9%) between Day 15 and 20. Like that of the fluid conductivity values measured for the unstimulated column, the pH values remained steady near a pH of 7 throughout the experiment (Figure 3.5c). The pH values measured from the biostimulated column, however, steadily decreased from a baseline pH value of 7 to near 4.4 on Day 12, and remained steady at a pH of 4.4 through Day 20.

3.4.3. Sand Surface Imaging. ESEM images obtained from sand samples collected from the biostimulated and unstimulated columns are shown in Figure 3.6. The ESEM images of sand sampled from an area of increased acoustic amplitude in the biostimulated column (Figure 3.2; Location A) were imaged with ESEM operating condition of 25 kV, 14%, 20°C, for accelerating voltage, relative humidity, and temperature, respectively. An ESEM image that is representative of the increased acoustic amplitude samples is shown in Figure 3.6a. This image shows a rough textured surface which appears to have a patchy covering of 'biomaterial' over some portions of the sand grain, while on other portions of the image the silica sand surface is clearly visible. Rod-shaped bacterial cells are present in this biomaterial, but not clearly distinguishable in this image (Figure 3.6a). The ESEM images of sand sampled from an

area of decreased acoustic amplitude in the biostimulated column (Figure 3.2; Location E) were imaged with ESEM operating condition of 25 kV, 89%, 5°C, for accelerating voltage, relative humidity, and temperature, respectively. An ESEM image that is representative of the decreased acoustic amplitude samples is shown in Figure 3.6b. In contrast to the previous ESEM image (Figure 3.6a), the images obtained from the area of decreased acoustic amplitude (Figure 3.6b) show the surface of a sand grain which appears to be completely draped or covered in a smooth biomaterial, with several holes and void-spaces. This image also shows the presence of attached rod-shaped bacteria on top of the biomaterial as well as what appears to be a layering of bacteria cells seen on the inner sides of the void-spaces. We note that during ESEM imaging of the increased amplitude sand samples (Figure 3.2a; Location A), individual bacterial cells were not clearly distinguishable until the operating temperature of the ESEM was raised from 5 to 20°C, and the relative humidity was decreased from 89% to 14%, which effectively dried out the sample/biomaterial. However, individual cells and attached biomass on sand samples collected from Location E (Figure 3.2a), were evident immediately upon viewing with the ESEM (at 5°C and 89%) and remained virtually the same in appearance when the temperature was increased to 20°C (images not shown).

The ESEM images of sand samples obtained from the unstimulated column (Figure 3.3a; Location C) were imaged with ESEM operating conditions of 25 kV, 89%, 5°C, for accelerating voltage, relative humidity, and temperature, respectively, and a representative image is shown in Figure 3.6c. This image shows the irregular or hummocky surface of a silica sand grain (Figure 3.6c), with no apparent bacteria cells or biomass.

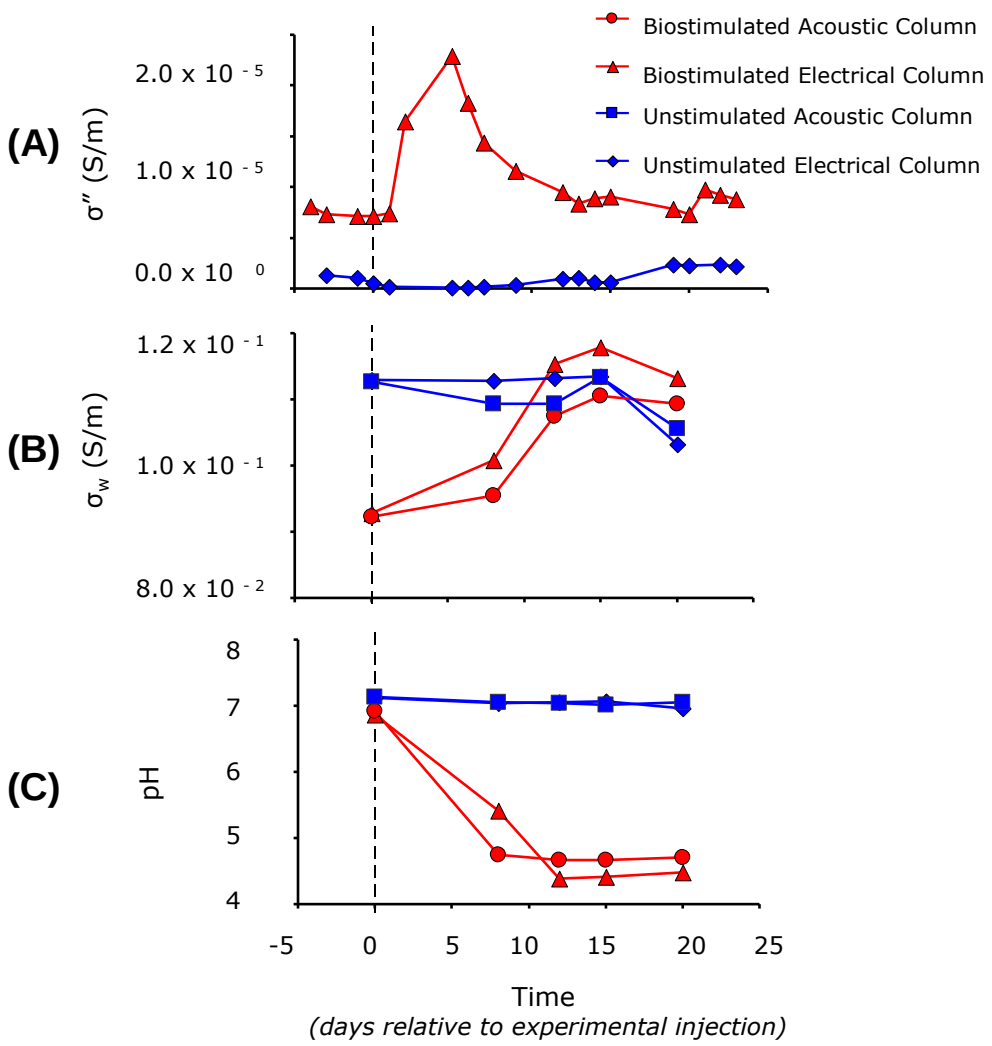

Figure 3.5. Temporal results of the (a) imaginary conductivity (σ"), (b) fluid conductivity (σ_w), and (c) pH measurements. Complex conductivity results shown at 10 Hz. Vertical dashed line represents experimental injection.

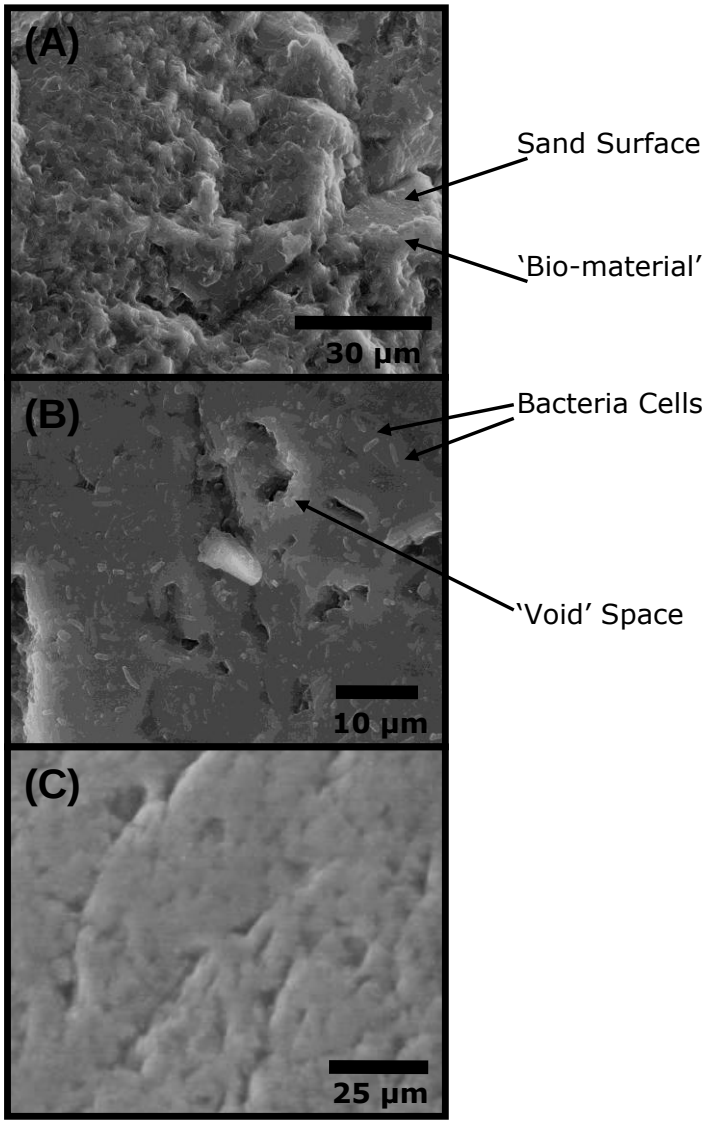

Figure 3.6. Environmental scanning electron microscope (ESEM) images of sand samples collected from the biostimulated column (a & b) and unstimulated column (c). Images obtained from the biostimulated column from an area of (a) increased amplitude (Location A; Figure 3.2a), and (b) decreased amplitude (Location E; Figure 3.2a) on the 2D acoustic scan. Location of the sand samples on the 2D scan are shown in Figure 3.2.

3.5. DISCUSSION AND CONCLUSIONS

The experimental results presented in this study show a significant difference in the temporal and spatial acoustic amplitude between the biostimulated and unstimulated columns. The biostimulated column became more spatially variable over time and the unstimulated column more homogeneous over time. Differences or variability in acoustic amplitude can result from a number of various factors. Acoustic properties of porous media are generally dependant on the bulk modulus of the saturating fluid [e.g., *Knight and Nolen-Hoeksema*, 1990], the elastic moduli of the solid media [e.g., *Ecker et al.*, 1998], and the solid-fluid interactions [e.g., *Clark et al.*, 1980]. Thus, changes in the elastic properties of a saturated porous medium will result in changes in the acoustic properties of the medium. Generally, decreases in acoustic amplitude result from biogenic gas production or the weakening of grain contacts in porous media, both of which reduce the elastic moduli and are manifested by delays and attenuation of acoustic waves. Increases in acoustic amplitude may result from increases in the bulk modulus of the solid media [e.g., *Li et al.*, 2001] through the stiffening of grain contacts. The variability in the acoustic wave measurements presented here from the biostimulated column (e.g., Figure 3.2) suggests that more than one mechanism may be responsible for the variability in the spatiotemporal acoustic amplitude.

Previous seismic studies have demonstrated that seismic methods are sensitive to the products of microbial activity in porous media, such as the production of biogenic gas [*Williams*, 2002] and enhanced biomineralization [*Williams et al.*, 2005; *DeJong et al.*, 2006]. In a column-scale experiment, *Williams* [2002] investigated the effect of stimulated microbial biogenic gas (N_2) production on acoustic (compressional) wave propagation in porous media. *Williams* [2002] observed gas bubble accumulation which was visible on the sides of the column, and strong attenuation of the acoustic wave signals consistent with regions of gas accumulation. In another column-scale experiment, *Williams et al.* [2005] observed strong attenuation of the compressional wave signals associated with microbial-mediated precipitation of sulfide minerals. They attributed the variations in attenuation of the acoustic signals to changes in the aggregation state of the crystalline sulfides and the non-uniformity of biomineralization along the length of the column which produced a heterogeneous distribution of elastic properties and pore

geometries [*Williams et al.*, 2005]. *DeJong et al.* [2006] used a bender element method to monitor shear waves in soils undergoing microbial-induced calcite precipitation and to nondestructively assess the engineering properties of the soil. The authors observed an increase in the shear wave velocity following nutrient injection and the progressive microbial-induced cementation of the soil particles [*DeJong et al.*, 2006]. Based on the fact that mineral precipitation was not induced or enhanced in our current experiment, and no large gas bubble formation was observed on the sides of the biostimulated columns (unlike that of *Williams* [2002]), we suggest that a different mechanism or mechanisms may be responsible for the observed amplitude variability in the biostimulated sample.

ESEM imaging of sand grain surface characteristics from the biostimulated column confirm microbial cell and attachment of biomaterial (Figure 3.6a & b), and show that no enhanced microbial growth was present in the unstimulated column (Figure 3.6c). The bacteria culture stimulated in this study (*P. aeruginosa*) is capable of producing different forms of biofilms, depending on the environment [e.g., *Friedman and Kolter*, 2004], and formation of these biofilms is documented to occur in a sequential process [e.g., *Davey et al.*, 2003; *Klausen et al.*, 2003]. *Davey et al.* [2003] describes five different physiologies over the course of biofilm development by *P. aeruginosa*, including: (1) initial reversible attachment, (2) irreversible attachment, (3) maturation through layering of bacterial cell clusters, (4) maturation of cell clusters and maximum layer thickness, and (5) dispersion of bacteria cells from within the inner portion of the biofilm. In addition to the relative sequence of biofilm development described *Davey et al.* [2003], the authors also provided a relative timeframe for this development, where the third stage (or physiology) occurred at ~3 days of growth, the fourth stage after ~6 days of growth, and the fifth stage after ~9-12 days. *Klausen et al.* [2003] observed that the basic *P. aeruginosa* biofilm structure did not change appreciably after day 7, although the accumulation of biomass within the biofilm on day 7 had not yet reached a plateau. Therefore, the authors referred to the 7 day old biofilms as being mature biofilms. Further, *Davey et al.* [2003] stated that all stages of the sequential development may be present at the same time during the maturation of the biofilm. In addition, one characteristic of the *P. aeruginosa* biofilms described in the literature [e.g., *Davey et al.*,

2003; *Pamp and Tolker-Nielsen*, 2007] is the presence of macrocolonies surrounded by large void spaces or open, dark fluid-filled channels, through which the lower levels of bacteria in the biofilm are thought to dispose of accumulating waste products. The results of the ESEM images obtained from the biostimulated column reflect these observations, showing apparent qualitative differences in the type and/or texture of the attached biomass or biofilms on the surface of the sand grains by the end of the 29 day experiment. Consequently, differences in the type and/or texture of the attached biomass/biofilms in the biostimulated column appear to reflect differences in the measured acoustic amplitude.

The thickness and morphology of biofilms can be readily quantified using a variety of microscopy techniques such as a confocal scanning laser or atomic force microscopy. Unfortunately, due to the roughness of the sand grains and the inherent difficulties of making such measurements when biofilms are found in geologic material we are unable to use the above microscopy techniques to measure or quantify the amount of biofilm (i.e., thickness) between areas of variable acoustic amplitudes. Hence, we present a qualitative interpretation based on our analysis of a library of ESEM images obtained from areas of different amplitude variations in the columns and provide representative images to illustrate our point. We observe that areas of increased amplitude were shown to have cells embedded in a highly hydrated matrix of biomaterial/film (Figure 3.6a) with a very rough texture, and discontinuous in coverage of surface of the sand grains. Whereas areas of decreased amplitude were observed to show bacterial cells within a continuous covering of biomaterial having a smoother texture (Figure 3.6b), with numerous void spaces or channels present. In contrast, the acoustic results from the unstimulated column show the acoustic properties of the sand homogenized over time which is attributed to settling within the sample (Figure 3.3a) and the ESEM shows a sand surface devoid of bacterial cells. We infer from these results that spatial variations in acoustic amplitude may result from the non-uniform distribution of biomass in porous media which affect the grain-to-grain coupling, pore geometry and elastic/viscoelastic response of the medium.

Physically, the presence of biofilms may alter grain contact coupling by decreasing the volume and size of pores, altering the pore throat geometry or providing

additional coupling among grains, all of which affect the sediment matrix stiffness and the elastic and/or visco-elastic moduli of the media. In addition, if the microbial-induced alterations are not uniformly distributed throughout the sediment, then the sediment textural and mechanical properties may vary spatially leading to spatial heterogeneity in the seismic signatures (i.e., scattering). Variations in pore geometries and elastic properties between regions of highly colonized, dense areas of biofilm and those with a patchy distribution of biomass may affect local permeability and pore pressure. When the porous media is excited by the passing acoustic wave, grain scale heterogeneities (i.e., pore shape, saturation) will induce pressure gradients and cause pore fluid to be squeezed from compliant to less compliant regions. This movement of fluid results in viscous dissipation or 'squirt-flow' mechanisms [e.g., *Palmer and Traviolia*, 1980, *Mavko and Jizba*, 1991]. Thus, we propose that spatially non-uniform biofilm formation alters the pore geometry and elastic moduli that results in heterogeneous attenuation.

In addition to the spatial variability in the acoustic wave amplitude, there is also significant temporal variability measured in the biostimulated column, as shown in the time-progression 2D acoustic maps (Figure 3.2a). Significant changes in the acoustic wave properties occurred in the biostimulated column between Day 5 and Day 7 of the experiment (Figure 3.2a; 3.4a). These observed acoustic changes are consistent with a peak in the imaginary conductivity values on Day 5 (Figure 3.5a). In our earlier work [*Davis et al.*, 2006], we demonstrated that imaginary conductivity measurements are uniquely sensitive to the physicochemical properties at grain-fluid interfaces, and showed that imaginary conductivity measurements may be used as a proxy indicator of microbial growth, attachment, and biofilm formation in porous media. In this earlier work, we observed peak increases in imaginary conductivity that generally paralleled peak increases in attached microbial cell concentrations and biofilms. While we did not measure the concentration of attached biomass in the current experiment, our complex conductivity results are identical to the study by *Davis et al.* [2006]. Thus we suggest that the peak changes observed in the imaginary conductivity response may reflect a peak in the concentration of attached biomass on Day 5. Based on this assumption, we infer that the variations in the acoustic amplitude that occurred between Day 5 and 7 are associated with the change in physical properties of the medium caused by peak microbial

attachment and biofilm formation. We also note that there is a remarkable similarity in the temporal acoustic and electrical data presented here, and the relative timeframe for biofilm development presented by *Davey et al.* [2003]. This may be further evidence that biofilm development is a primary contributor to the observed geophysical response.

Similar to *Davis et al.* [2006], we observed a consistent decrease in the imaginary conductivity after peak values were observed and for the remaining duration of the experiment. This decrease in the imaginary conductivity may be attributed to increased rates of detachment, dispersion, and/or cell death potentially due to nutrient limitations [*Davis et al.*, 2006; *Abdel Aal et al.*, 2008]. A possible reason for the suggested increase in cell death or detachment may be the result of the accumulation of waste products (e.g., organic acids) and that the low pH conditions that developed over time in the biostimulated column contributed to the death of the cells. In contrast to the imaginary conductivity, the acoustic wave amplitude after Day 10, remained relatively constant through the end of the experiment (Figure 3.4a). While dead cells have no electrical properties and hence the decrease in imaginary conductivity after day 5 [e.g., *Abdel Aal et al.*, 2008], it is possible that the EPS and biomass remained in the pore spaces and continued to affect the elastic properties and pore geometries of the porous media. The initial lower fluid conductivity values measured in the biostimulated columns, compared to the unstimulated columns, may have been the result of microbial utilization of the nutrient media in the biostimulation fluid prior to injection, and before microbial production/accumulation of waste products, such as organic acids. Temporal increases in the fluid conductivity values may be related to the accumulation of these waste products, and is consistent with the temporal decrease in pH resulting from organic acid production. *Davis* [2009; Chapter 2] show that increases in organic acid concentration increases fluid conductivity, which would be consistent with the data presented in this study.

Understanding the mechanical properties of biofilms is important for assessing biofilm processes and behavior, as well as for the control of biofilms in industrial and medical environments (attachment and detachment) [*Stoodley et al.*, 1999; *Ahimou et al.*, 2007]. Rheological measurements of biofilms have shown that biofilms exhibit linear viscoelastic behavior [*Stoodley et al.*, 1999; *Klapper et al.*, 2002; *Ahimou et al.*, 2007]

and the acoustic/seismic response of a medium depends on the rheological properties of the medium. Thus the changes in viscoelastic properties of biofilms as they develop and evolve over time suggest that seismic geophysical techniques can be used to assess biofilm distribution and processes in field situations. Biofilms are soft and gelatinous in nature [*Ahimou et al.*, 2007]. Although several studies have investigated the rheological properties of biofilms in laboratory settings [e.g., *Ahimou et al.*, 2007], it is not known how such soft gelatinous material affect seismic wave propagation in porous media in the absence of mineral precipitation. Such an understanding is critical for assessing the utility of seismic geophysical techniques for imaging biofilm spatial heterogeneity and their effects in porous media in field settings.

The results presented in our study suggest acoustic imaging techniques are sensitive to spatiotemporal changes in porous media that result from enhanced microbial growth of a biofilm forming bacteria culture, in the absence of biomineralization. We observe relatively high spatial variability in the acoustic amplitude measured from initial conditions of nearly homogeneous amplitudes in the biostimulated column (Figure 3.2a), while no significant changes were observed in the unstimulated column (Figure 3.3a). The relative high spatial variability observed in the acoustic data from our current study suggests that enhanced microbial growth has a variable effect on the elastic properties of porous media. We note that a recent numerical model study by *Brovelli et al.* [2009] to simulate bioclogging in porous media demonstrated that the rate and patterns of bioclogging development were sensitive to the initial distribution of the biomass. Hence, while the exact microbial-induced mechanisms for the variations in amplitude are yet unclear, we speculate that the differences in amplitude may arise from a non-uniform distribution of microbial activity or possible heterogeneity in the biomass distribution and biofilm morphology (e.g., variations in biofilm thickness, roughness, hydration, simultaneous attachment to multiple grains, etc).

The results presented in Figure 3.2a are qualitatively similar to porosity and hydraulic conductivity evolution due to biomass distribution as observed in *Brovelli et al.*, [2009, Figure 13]. Thus, we suggest that the acoustic wave spatial and temporal results presented here would be beneficial as an additional tool for bioclogging model/simulation validation. Hence up-scaling to field scale could help provide

information on spatiotemporal distribution of biomass/bioclogging development and changes in hydraulic properties allowing for the optimization of amendment-based in situ remedial strategies. Further, MEOR activities involving the in-situ growth of microorganisms and biofilm formation for the selective plugging of highly permeable zones may also benefit from such techniques as acoustic wave measurements.

3.6. ACKNOWLEDGMENTS

This material is based in part on work supported by the Environmental Protection Agency Student Services Contract EP07D000660, and the National Science Foundation under Grant No. OCE-0729642, EAR-0525316, and NSF REU Award # 0552918. Notice: Although this work was reviewed by EPA and approved for publication, it may not necessarily reflect official Agency policy. Mention of trade names or commercial products does not constitute endorsement or recommendation by EPA for use.

3.7. REFERENCES

Ahimou, F., Semmens, M.J., Novak, P.J., and Haugstad, G. (2007), Biofilm cohesiveness measurement using a novel atomic force microscopy methodology, Appl. Environ. Microbiol., 73(9), 2897-2904.

Abdel Aal, G.Z., Slater, L.D., and Atekwana, E.A. (2006), Induced-polarization measurements on unconsolidated sediments from a site of active hydrocarbon biodegradation, Geophysics, 71(2), H13-H24.

Abdel Aal, G.Z. (2008), Electrical properties of bacteria in sand columns: live vs. dead cells, AGU Chapman Conference on Biogeophysics, Portland, ME.

Atekwana, E.A., Atekwana, E.A., and Werkema, D.D. (2006), Biogeophysics: the effects of microbial processes on geophysical properties of the shallow subsurface. In Applied Hydrogeophysics, Vereecken, H., Binley, A., Cassiani, G., Revil, A., and Titov, K., (eds.), NATO Sci. Ser. IV, Springer: New York, pp. 161–193.

Baveye, P., Vandevivere, P., Hoyle, B.L., DeLeo, P.C., and Sanchez de Lozada, D. (1998), Environmental impact and mechanisms of the biological clogging of saturated soils and aquifer materials, Crit. Rev. Environ. Sci. Tech., 28(2), 123-191.

Brovelli, A., Malaguerra, F., and Barry, D.A. (2009), Bioclogging in porous media: model development and sensitivity to initial conditions, Environ. Model. Software, 24, 611-626.

Clark, V.A., Tittman, B.R., and Spencer, T.W. (1980), Effect of volatiles on attenuation (Q-1) and velocity in sedimentary rocks, J. Geophys. Res., 85, 5190-5198.

Davey, M.E., Caiazza, N.C., and O'Toole, G.A. (2003), Rhamnolipid surfactant production affects biofilm architecture in *Pseudomonas aeruginosa* PAO1, J. Bacteriol., 185(3), 1027-1036, doi:10.1128/JB.185.3.1027–1036.2003.

Davis, C.A., Atekwana, E.A., Atekwana, E.A., Slater, L.D., Rossbach, S., and Mormile, M.R. (2006), Microbial growth and biofilm formation in geologic media is detected with complex conductivity measurements, Geophys. Res. Lett., 33, L18403, doi:10.1029/2006GL027312.

DeJong, J.T., Fritzges, M.B., and Nusslein, K. (2006), Microbially induced cementation to control sand response to undrained shear, J. Geotech. Geoenviron. Eng., 132(11), 1381-1392.

DeJong, J.T., Mortensen, B.M., Martinez, B.C., and Nelson, D.C. (2009), Bio-mediated soil improvement, Ecol. Eng., *In Press*, doi:10.1016/j.ecoleng.2008.12.029.

Dupin, H.J., and McCarty, P.L. (2000), Impact of colony morphologies and disinfection on biological clogging in porous media, Environ. Sci. Technol., 34(8), 1513-1520, doi:10.1021/es990452f.

Ecker, C., Dvorkin, J., and Nur, A. (1998), Sediments with gas hydrates: internal structure from seismic AVO, Geophysics, 63, 1659-1669.

Friedman, L., and Kolter, R. (2004), Genes involved in matrix formation in *Pseudomonas aeruginosa* PA14 biofilms, Molec. Microbio., 51(3), 675–690 doi:10.1046/j.1365-2958.2003.03877.x.

Kildsgaard, J., and Engesgaard, P. (2002), Numerical analysis of biological clogging in two-dimensional sand box experiments, J. Contam. Hydrol., 50, 261-285.

Klapper, I., Rupp, C.J., Cargo, R., Purvedorj, B., and Stoodley, P. (2002), Viscoelastic fluid description of bacterial biofilm material properties, Biotech. Bioeng., 80(3), 289-296.

Klausen, M., Heydorn, A., Ragas, P., Lambertsen, L., Aaes-Jørgensen, A., Molin, S., and Tolker-Nielsen, T. (2003), Biofilm formation by Pseudomonas aeruginosa wild type, flagella and type IV pili mutants, Molecular Microbiol., 48(6), 1511–1524.

Knight, R., and Nolen-Hoeksema, R. (1990), A laboratory study of the dependence of elastic wave velocities on pore scale fluid distribution, Geophys. Res. Lett., 17, 1529-1532.

Lesmes, D.P., and Frye, K.M. (2001), Influence of pore fluid chemistry on the complex conductivity and induced polarization responses of Berea sandstone, J. Geophys. Res., 106, 4079-4090.

Li, X., Zhong, L.R., and Pyrak-Nolte, L.J. (2001), Physics of partially saturated porous media: residual saturation and seismic-wave propagation, Ann. Rev. Earth Planet. Sci., 29, 419-460.

Mavko, G., and Jizba, D. (1991), Estimating grain-scale fluid effects on velocity dispersion in rocks, Geophysics, 56, 1940–49.

Ntarlagiannis, D., Yee, N., and Slater, L. (2005), On the low frequency induced polarization of bacterial cells in sands, Geophys. Res. Lett., 32, L24402, doi:10.1029/2005GL024751.

Palmer, I.D., and Traviolia, M.L. (1980), Attenuation by squirt flow in undersaturated gas sands, Geophysics, 45, 1780–1792.

Pamp, S.J., and Tolker-Nielsen, T. (2007), Multiple roles of biosurfactants in structural biofilm development by *Pseudomonas aeruginosa*, J. Bacteriol., 189(6), 2531–2539, doi:10.1128/JB.01515-06.

Pyrak-Nolte, L.J., Mullenbach, B.L., Li, X., Nolte, D.D., and Grader, A.S. (1999), Detecting sub-wavelength layers and interfaces in synthetic sediments using seismic wave transmission, Geophys. Res. Lett., 26, 127-130.

Rinck-Pfeiffer, S.M., Ragusa, S.R., Sztajnbok, P., and Vandevelde, T. (2000), Interrelationships between biological, chemical and physical processes as an analog to clogging in Aquifer Storage and Recovery (ASR) wells, Wat. Res., 34(7), 2110-2118.

Slater, L., and Lesmes, D.P. (2002), IP interpretation in environmental investigations, Geophysics, 67, 77-88.

Stoodley, P., Lewandowksi, Z., Boyle, J.D., and Lappin-Scott, H.M. (1999), Structural deformation of bacterial biofilms caused by short-term fluctuations in fluid shear: an in situ investigation of biofilm rheology, Biotech. Bioeng., 65(1), 83-92.

Taylor, S.W., and Jaffé, P.R. (1990), Substrate and biomass transport in a porous medium, Water Resour. Res., 26(9), 2181–2194.

Thullner, M., Schroth, M.H., Zeyer, J., and Kinzelbach, W. (2004), Modeling of a microbial growth experiment with bioclogging in a two-dimensional saturated porous media flow field, J. Contam. Hydrol., 70, 37-62.

Vandevivere, P., and Baveye, P. (1992), Effect of bacterial extracellular polymers on the saturated hydraulic conductivity of sand columns, Appl. Environ. Microbiol., 58(5), 1690-1698.

Williams, K.H. (2002), Monitoring microbe-induced physical property changes using high-frequency acoustic waveform data: toward the development of a microbial megascope, M.S. Thesis, University of California, Berkeley, CA.

Williams, K.H., Ntarlagiannis, D., Slater, L.D., Dohnalkova, A., Hubbard, S.S., and Banfield, J.F. (2005), Geophysical imaging of stimulated microbial biomineralization, Environ. Sci. Technol., 39(19), 7592-7600.

4. SELF-POTENTIAL SIGNATURES ASSOCIATED WITH AN INJECTION EXPERIMENT AT AN IN-SITU BIOLOGICAL PERMEABLE REACTIVE BARRIER

4.1. ABSTRACT

Strategies available to evaluate the performance of *in-situ* permeable reactive barriers (PRB) are currently not well developed, and often rely on fluid and media sampling directly from the PRB. Here, we report on the results of a field experiment conducted to investigate the utility of the self-potential (SP) method as a minimally invasive technique to monitor in-situ PRB performance. Our field study was conducted at an in-situ biological PRB in Portadown, Northern Ireland, that was emplaced to assist in the remediation of groundwater contamination (e.g., hydrocarbons, ammonia) that resulted from the operations and waste disposal practices of a former gasworks. Borehole SP measurements were collected during the injection of contaminant groundwater slugs in an attempt to monitor/detect the response of the microbial activity associated with the breakdown of the added contaminants into the PRB. In addition, an uncontaminated groundwater slug was injected into a different portion of the PRB as a 'control', and SP measurements were collected for comparison to the SP response of the contaminant slugs. The results of the SP signals due to the contaminant injections show that the magnitude of the response was a relatively small (<10 mV) yet consistent decrease during both contaminant injections. The net decrease in SP recorded during the contaminant injections slowly rebounded to near background values through ~44 hours post-injection. The SP response during the uncontaminated injection, however, showed a slight though negligible increase (~1 mV which was within our margin of error) in the measured SP signals, in contrast to the contaminant injections. Based on the difference in SP response between the contaminated and uncontaminated injections, we suggest that the responses are likely the result of differences in the chemistry of the injection types (contaminated vs. uncontaminated) and *in-situ* PRB groundwater. We argue that the SP signals associated with the contaminated injections are dominated by diffusion (electrochemical) potential, possibly enhanced by a microbial effect.

4.2. INTRODUCTION

In recent years, permeable reactive barrier (PRB) systems have become a reasonable and cost-effective approach for the passive in-situ treatment of contaminated groundwater. The basis of PRB technology requires that contaminated groundwater flows through a confined area of reactive material whereby contaminants are retained or degraded by the treatment media through chemical, physical, or biological processes [e.g., *Scherer et al.*, 2000; *USEPA*, 2001; 2002; *Boshoff and Bone*, 2005]. A variety of reactive media have been used in PRB applications, depending on the target contaminant, including zero-valent iron (ZVI), activated carbon, zeolites, organic materials, and synthetic media [*USEPA*, 2001; 2002]. In the case of biological PRB's, the treatment material is essentially any media in which microbial activity is enhanced by the delivery of oxygen and/or nutrients to the system, thereby encouraging the biodegradation of contaminants [e.g., *Shirazi*, 1997; *Sturman et al.*, 1995].

Irrespective of the type of reactive media, PRB applications are generally used for long-term remediation efforts, on the order of decades. Current strategies available to evaluate long-term PRB performance, however, are not well developed and often require the direct collection of groundwater for analysis of target contaminants and geochemical indicators, as well as the physical analysis of core samples [e.g., *McMahon et al.*, 1999; *Puls et al.*, 1999; *Liang et al.*, 2001; *Beck et al.*, 2002]. While few studies have been conducted to evaluate the long-term efficacy of PRB systems, recent evidence suggests that secondary biogeochemical processes (e.g., mineral precipitation, gas accumulation) may have negative affects on barrier media [e.g., *Zolla et al.*, 2007]. Mineral precipitation, for example, can clog the pore spaces of barrier materials over time. This pore clogging can lead to reductions in porosity, hydraulic conductivity, and chemical reactivity [e.g., *Liang et al.*, 2003; *Phillips et al.*, 2003; *Zolla et al.*, 2007], and thus degrade the efficiency of the PRB system. In addition to the need for chemical and physical studies to investigate the long-term effectiveness of PRB media, there is also a need for the development of methods/tools to assist in the assessment of in situ barrier performance. Here, we investigate the potential utility for the minimally invasive self-potential (SP) geophysical method to be used as a tool for monitoring PRB performance.

In recent years, the SP method has received greater attention for its potential

application to environmental characterization, as it is directly sensitive to variations in subsurface parameters such as groundwater flow and chemistry. The SP method has been successfully applied to a variety of environmental field investigations, including the detection/approximation of water table location [e.g., *Sailhac and Marquis*, 2001; *Darnet et al.*, 2003], delineation of preferential water flow pathways [e.g., *Bogoslovsky and Ogilvy*, 1970; *Song et al.*, 2005], and delineation of contaminant plumes [e.g., *Arora et al.*, 2007; *Naudet et al.*, 2003; 2004]. In addition, there is increasing interest in SP to detect and monitor subsurface microbial processes [e.g., *Arora et al.*, 2007; *Ntarlagiannis et al.*, 2007; *Slater et al.*, 2007b], as well as the performance and long-term monitoring capabilities of SP electrodes [e.g., *Minsley et al.*, 2007; *Slater et al.*, 2007b]. Further, previous studies have shown a strong relationship between self-potential signals and redox potential measurements [e.g., *Naudet et al.*, 2004; *Arora et al.*, 2007], particularly with respect to contaminant plumes. *Arora et al.* [2007] proposed a geobattery model in association with biodegradation of subsurface organic contaminants and attributed to strong microbial-induced redox gradients. *Arora et al.* [2007] hypothesized this natural battery to exist at contaminant plume boundaries between highly reduced, oxygen depleted areas within the plume and oxygen-rich conditions surrounding the contaminant plume. In order to complete the geobattery circuit, *Arora et al.* [2007] hypothesized that the presence of biomass and metallic mineral precipitates would act as an electron conductor.

Based on the ideas presented by *Arora et al.* [2007], we hypothesized that the SP method may be useful for the delineation of microbial activity within an in-situ biological PRB, and in particular, microbial-induced redox gradients associated with the microbial break down of contaminants. To test this hypothesis, we conducted a field experiment where contaminant slugs were injected into a PRB and the SP signals were recorded in attempt to monitor the progress of the biodegradation of the addition contaminants. As such, the primary objective of this study was to investigate the potential for the minimally invasive self-potential (SP) geophysical method to be used as an indirect proxy of biological PRB performance. More specifically, we were interested in answering the following questions: (1) what is the magnitude of the SP signals associated with the injection of added contaminants into a biological PRB? (2) Will microbial activity

associated with the breakdown of the added contaminants in the PRB have a measurable effect on SP signals? Here, we report on the results of two injection experiments performed to investigate the SP signatures associated with the in-situ response of a biological PRB. The first experiment was designed to investigate the basic effect of added contaminants on SP signals in the PRB, possibly associated with microbial degradation of the additional contaminants. The second experiment (served as a control), which consisted of separate injections of contaminated and uncontaminated groundwater, was designed to: (1) confirm or refute the results of the first contaminant injection experiment, and (2) compare the SP signals associated with uncontaminated groundwater to that contaminated groundwater.

The results of our investigation show that while we did not observe a measurable response in the SP signals that could be attributed to microbial activity, we did observe a persistent SP signal associated with the contaminant injections. Qualitative analysis and comparison of the SP datasets for the contaminated vs. uncontaminated injections suggests that the SP signals recorded in this study are primarily dominated by electrochemical (i.e., diffusion) potentials, similar to that of *Maineult et al.* [2006] due to differences in the chemistry of the injected slug(s) and resident PRB water.

4.3. BACKGROUND

4.3.1. Self-potential Method. The SP technique is based upon the passive measurement of naturally occurring electric potentials in the subsurface with non-polarizable electrodes in contact with the ground surface (or down borehole). Electrodes placed at the ground surface are connected via wire to a high impedance (>10 MΩ) voltmeter, and the electric potential is measured. The naturally occurring potentials can result from a variety of factors and/or mechanisms, and include electrokinetic, electrochemical, mineralization, redox, thermoelectric, and bioelectric potentials [e.g., *Nyquist and Corry*, 2002]. In natural environments, however, the SP response often results from a combination of mechanisms [e.g., *Darnet and Marquis*, 2004; *Kulessa et al.*, 2003; *Maineult et al.*, 2004]. We chose the SP method as a tool to monitor the response of the PRB for the current study because of the sensitivity of this method to groundwater fluxes (electrokinetic/streaming potential), ionic gradients

(electrochemical/diffusion potential) and redox potential gradients (electro-redox potential), all three of which may dominate the measured SP signals in this field study.

4.3.1.1 Streaming Potentials. An electrical field that develops in association with the flow of fluid through a porous medium is often called a streaming potential [e.g., *Ernstson and Scherer*, 1986]. Streaming potentials can arise from the drag of excess charge of the pore fluid during fluid flow through a porous medium [see description in *Boleve et al.*, 2007], and the resultant electrical field commonly parallels the direction of fluid flow. Based on the classical description of electrokinetic theory [e.g., *Sill*, 1983], the current density is related to pore fluid pressure gradients and a streaming current coupling coefficient which is dependent on the zeta-potential (ζ), an interfacial property of the porous media [e.g., *Boleve et al.*, 2007]. A proportional relationship exists between hydraulic gradient (Δh) and SP, which is described by a streaming coupling coefficient (C) [*Fournier*, 1989; *Revil et al.*, 2003]. Thus, streaming potential is equal to:

$$\Delta SP = C\Delta h \tag{1}$$

where

$$C = \frac{L}{\sigma_w}, \tag{2}$$

and

$$L = -\frac{c_0 n \varepsilon \zeta}{\eta}. \tag{3}$$

Where L is the reduced coupling coefficient, σ_w is fluid conductivity, c_0 is material medium tortuosity, n is medium porosity, ε is fluid dielectric constant, η is fluid viscosity.

A recently revised formulation of the electrokinetic theory developed by *Revil and Leroy* [2004] and *Revil et al.* [2005], and presented in *Boleve et al.* [2007], describes a direct dependence of streaming (electrokinetic) potential on the microstructure of porous media, and more specifically permeability. Herein, we will focus on the classic formulation of the electrokinetic theory, but it is worth mentioning the importance of the new formulation for investigating the effect of microstructure on SP signals.

4.3.1.2 Electrochemical Potentials. An electrical field that develops in association with the flow of fluid through a porous medium is often called a streaming potential [e.g., *Ernstson and Scherer*, 1986]. Electrochemical potentials can arise from differences in chemical composition, such as concentration gradients and redox gradients, known as diffusion potentials and electro-redox potentials, respectively. Diffusion potentials can result from ionic concentration gradients in solutions with ions of differing ionic mobilities. This electrochemical effect is related to differences in fluid conductivity (σ_1/σ_2), and can be described by a combined electrochemical coupling coefficient (C_{comb}) [*Kulessa et al.*, 2003], where:

$$\Delta SP = C_{comb} \ln (\sigma_1/\sigma_2) \tag{4}$$

Naudet et al. [2004] describe a relationship between SP and redox gradient (ΔEh), which is related through a redox coupling coefficient (C_{Eh}):

$$\Delta SP = C_{Eh} \Delta Eh \tag{5}$$

A 'geobattery' model has been used to describe the strong SP response measured over subsurface ore deposits, associated with oxidation-reduction reactions [e.g., *Sato and Mooney*, 1960]. Previous researchers have described this geobattery model as being the shuttling of electrons from oxidized zones above the water table to reduced zones below the water table [e.g., *Sato and Mooney*, 1960; *Timm and Moller*, 2001]. Previous studies have also observed a similar relationship between SP signals and redox potential gradients associated with contaminant plumes [e.g., *Naudet et al.*, 2003; 2004; *Arora et al.*, 2007]. While the mechanisms responsible for this relationship are still not well understood, it has been suggested that a geobattery model may be used to explain this phenomena [e.g., *Naudet et al.*, 2004]. According to *Naudet and Revil* [2005], biomass may act as a conductor to electrically connect the oxidized and reduced zones of contaminant plumes.

4.3.2. Field Site. The study site was located on the property of a former manufactured gasworks plant (~15,000 m^2) in the town of Portadown, Northern Ireland

(Figure 4.1). Historical groundwater contamination at the site includes sulfate, cyanide, ammonia, and hydrocarbons [*Doherty et al.*, 2006; *Doherty*, 2002]. The contamination resulted from the operation and waste disposal practices during the 150 year lifespan of the gasworks facility. The geology, hydrogeology, and microbiology of the site have been described previously by *Doherty et al.* [2006], *Ferguson et al.* [2003], and *Doherty* [2002].

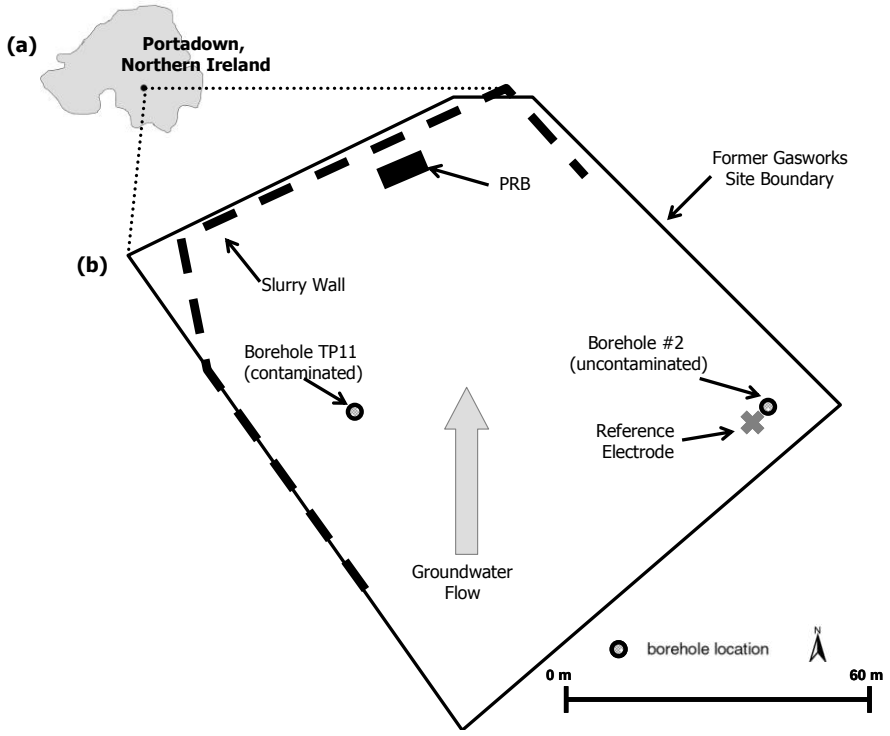

Figure 4.1. (a) Location of the field site in Portadown, Northern Ireland, and (b) diagram showing the location of the PRB on the property of the former gasworks (modified after *Doherty* [2002]).

Laboratory-scale and on-site assessments concluded that enhanced monitored natural attenuation was the best approach to remediate the contaminated groundwater [*CL:AIRE*, 2005; *Doherty*, 2002]. To this end, a sequential biological permeable reactive

barrier was installed on the former gasworks site (Figure 4.1) perpendicular to the direction of groundwater flow. Installed in 2001, the PRB consisted of a pre-cast concrete box (4.8m length, 2.4m width, 2.5m depth) filled with treatment media. Prior to entering the PRB, groundwater flows through the interceptor (I), which is a concrete manhole with no granular fill, to separate the light non-aqueous phase liquid (LNAPL) from the bulk fluid. Flow then enters the weir (W) which is a concrete manhole filled with coarse sand prior to entering the initial stage of the PRB. The initial stage of the sequential PRB (Figure 4.2) was filled with coarse sand, and aerobic biodegradation was encouraged through the addition of oxygen to the groundwater by air sparging. The final stage was filled with granular activated carbon (GAC) which acted as a back-up approach to sorb any organic contaminants not degraded by the initial biological unit. A slotted sheet of plastic separates the initial (sand) and final (GAC) stages of the barrier. Groundwater flow (estimated flow rate ~3.75 L/day; *CL:AIRE* [2005]) is directed to the PRB by slurry walls surrounding the former gasworks site (Figure 4.1), through the 20m3 reactor from west to east. Pea-gravel acts as a mixing zone at both the entrance and exit of the reactor. The treated groundwater is then discharged from the PRB to the east-northeast of the reactor. Fourteen permanent boreholes, installed during the emplacement of the PRB, are located over the length of the PRB (Figure 4.2). Each borehole consisted of solid plastic pipe (~6.5 cm inner diameter; ~3.5m length; ~12L volume) that extended from the bottom of the barrier to ~1 m above the ground surface.

4.4. FIELD METHODS

4.4.1. Self-potential Surveys. SP measurements were collected using lead-lead chloride non-polarizing electrodes (after *Petiau* [2000]) emplaced down the 14 permanent boreholes installed in the PRB. One electrode was installed in each borehole, raised ~0.1m off the barrier floor, and the connecting cable was secured in place with electrical tape. The borehole electrodes remained down-hole for the duration of the study (~10 days). All SP data were collected as differential values relative to the reference electrode, located to the southeast of the PRB, in the uncontaminated portion of the site (Figure 4.1). By convention, the reference electrode was connected to the negative terminal of the voltmeter. One surface SP electrode placed next to the reference electrode, was used to

measure diurnal SP variations at the beginning and end of each survey day to calculate and correct for average daily SP variations. Borehole electrodes were tested at the reference electrode before being placed and after removal from the boreholes to calculate electrode drift associated with the borehole SP measurements (+/- 1 mV). SP measurements were collected (manually) from each borehole before, during, and after the experimental injections.

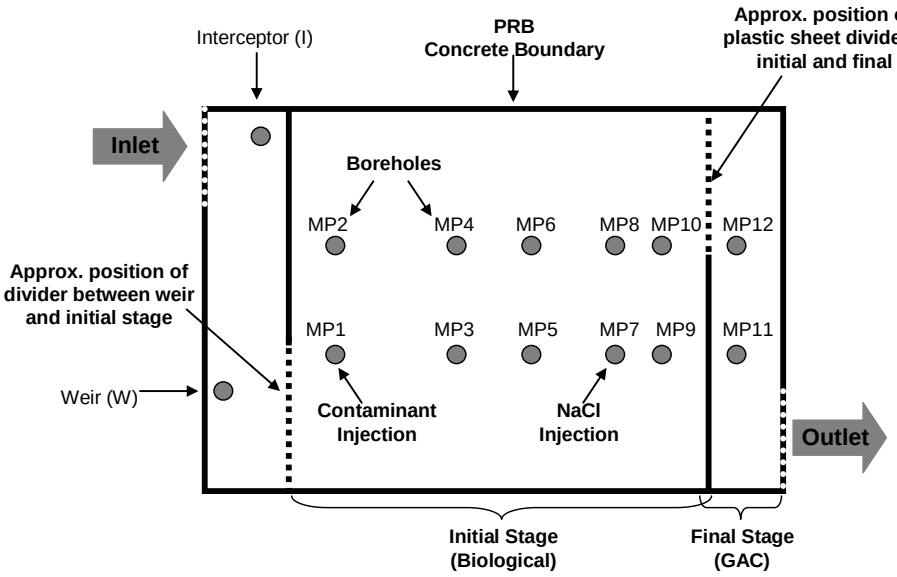

Figure 4.2. Diagram showing the design of the sequential PRB, the location of boreholes, and direction of groundwater flow in-to and out-of the PRB.

4.4.2. Water Quality Measurements. Oxidation-reduction potential (Eh) and fluid conductivity measurements were performed on-site from fluid samples (~50 mL) collected from each of the 14 boreholes located on the PRB (except borehole MP5 which was not filled with water, but rather only slightly saturated at the bottom of the borehole). Prior to fluid sampling, each borehole was purged using a peristaltic pump to allow for representative sample collection. Water quality measurements were collected before and after the experimental injections.

4.4.3. Field Experiment. The field study consisted of two phases, referred to as Experiment #1 and Experiment #2, to investigate the SP response of transient flow induced by the injection of groundwater. During Experiment #1, 50L of contaminated groundwater was injected near the entrance of the PRB (MP1), and the SP signals and water quality were monitored for two days following the injection. Experiment #2 consisted of an injection of uncontaminated groundwater (50 L) into the middle of the barrier (MP7), followed by the injection of another 50L slug of contaminated groundwater (~2.5 hrs after the uncontaminated groundwater injection) at the entrance (MP1), and the SP and water quality were again monitored for two days following the injection(s). The contaminated groundwater used for the experimental slugs was collected from contaminated borehole TP11 (Table 4.1), located in the center of the contaminant plume to the southwest of the PRB (Figure 4.1). Prior to collection, the borehole was purged using a peristaltic pump. The contaminated groundwater from TP11 was collected in 10L increments. The 10L slug of contaminated groundwater was poured into the top of borehole MP1 near the inlet of the PRB (Figure 4.2). While the 10L slug was being injected, the TP11 borehole was allowed to recharge (~15 min) and this procedure was repeated until a total volume of 50L was injected.

The uncontaminated groundwater used for Experiment #2 was collected from borehole BH2 (Table 4.1), located in an uncontaminated portion of the field site near the reference electrode (Figure 4.1). The sample collection and injection procedure was similar to that of the contaminant injections, except the fluid conductivity of the clean groundwater slug was adjusted artificially using NaCl(s) (~0.4g NaCl per 1L clean groundwater). The fluid conductivity was adjusted to simulate a fluid conductivity near that of the contaminated groundwater slug to more directly compare the effect of the contaminated versus uncontaminated injection response. Due to equipment malfunction, the uncontaminated slug was not injected immediately after being pumped out of the uncontaminated borehole. The uncontaminated slug was allowed to sit out overnight (under ambient conditions), and after the equipment was fixed, the uncontaminated slug was injected into MP7 ~24 hours after withdrawal from BH2.

Table 4.1. Geochemical data collected from the uncontaminated borehole (BH2) and contaminated borehole (TP11) locations. Data compiled from unpublished data courtesy of Queen's University Belfast, and *Doherty et al.* [2006] which is denoted with an asterisk symbol.

Component	Borehole	
	BH2	TP11
Eh (mV)	162	-106
Fluid Conductivity (uS/cm)	709	3710
pH	7.27	7.39
DO	2.77	-0.06
TOC (ppm)	6	57
Ammoniacal Nitrogen (as NH4-N)	1.13	342.3
Nitrate (mg/L)	6.61	-
Sulfate (mg/L)	82.38	* 669
Sodium (mg/L)	62	* 33
Magnesium (mg/L)	11	* 22
Calcium (mg/L)	36	* 112
Chloride (mg/L)	41	* 39
Iron (mg/L)	<0.05	* 0.95

BH2 samples collected 9/19/2000
TP11 samples collected 10/4/2000

4.5. RESULTS

The average diurnal SP values, measured using one roving surface electrode positioned at the reference electrode, varied by ~4 mV over the duration of the field study, and all borehole SP data presented here have been corrected for diurnal SP variations.

4.5.1. Experiment #1. Initial borehole self-potential (BHSP) data collected prior to the injection experiment ranged from 43-109 mV and are shown in Table 4.2. During the injection of the contaminant slug at MP1 the BHSP values decreased at the injection site by ~9mV (Figure 4.3). The SP and water quality data collected for Experiment #1 are presented in Figure 4.4 as kriged contour plots showing the percent change relative to two hours before the contaminant injection. One hour after injection the BHSP values (Figure 4.4a) showed a decrease at the injection borehole MP1 (~11%; 9 mV), and adjacent boreholes MP3 (~3%; 3 mV) and W (~2%; 2 mV), while all other boreholes

remained within +/- 1 mV of pre-injection SP values. BHSP values recorded 20 hours post-injection (Figure 4.4b) show that the injection borehole MP1 rebounded to pre-injection values, while all other boreholes increased by 2-6% compared to pre-injection values. The BHSP values continued to increase (up to ~12%) surrounding the injection borehole MP1 through 44 hours post-injection (Figure 4.4c).

Table 4.2. Initial borehole SP, fluid conductivity, and Eh data collected from the PRB boreholes ~2hr prior to Experiment #1.

Borehole	SP (mV)	Fluid Conductivity (µS/cm)	Eh (mV)
I	46	1276	-119.5
W	43	1276	-82.9
MP1	85	1311	-28.9
MP2	92	1176	-108.6
MP3	72	1063	73.4
MP4	72	1070	24
MP5	71	-	-
MP6	90	1132	46.7
MP7	96	1278	77.5
MP8	109	1127	66.5
MP9	66	1083	90.9
MP10	78	1118	74.5
MP11	84	1145	78.1
MP12	80	1120	73.5

Initial water quality data collected from the PRB boreholes and contaminant slug prior to injection are shown in Table 4.2 and Table 4.3, respectively. Fluid conductivity values recorded ~2 hrs prior to the injection experiment ranged from ~1063-1311 µS/cm over the PRB. Fluid conductivity values recorded ~1 hour after injection increased at the injection borehole MP1 and adjacent borehole MP3 (Figure 4.4d) by ~53% and 26%, respectively, while all other boreholes varied by <15% (+/- 100 µS/cm). Fluid

conductivity values remained elevated at the injection borehole MP1 20 hours after the injection (Figure 4.4e) and to a lesser extent 44 hours post-injection (Figure 4.4f). Eh data collected from the PRB boreholes ~2hrs prior to the injection experiment ranged from ~ -120mV to 91mV over the PRB (Table 4.2). Eh values recorded ~1 hour after injection increased by ~180% (~50 mV) at the injection borehole MP1 (Figure 4.4g), and ~105% at MP4, while decreased Eh values were observed at the interceptor (171%), weir (-172%), and MP3 (-109%). The trend of the Eh values remained relatively similar after ~20 hours (Figure 4.4h). The Eh values recorded ~44 hours post-injection show increased Eh values (~50-300%) at MP2, MP4, and MP6, while decreased Eh values are observed at all other boreholes (Figure 4.4i).

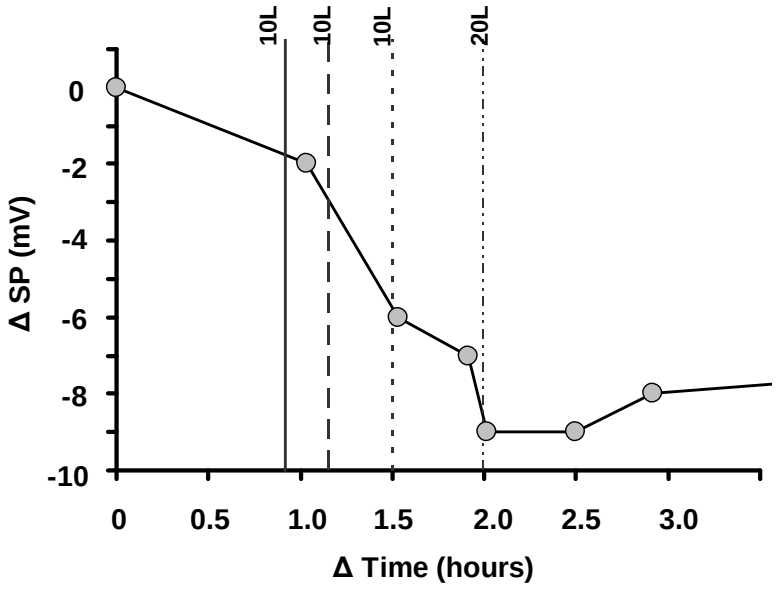

Figure 4.3. Plot showing the borehole SP data collected at the injection borehole (MP1) during the Experiment #1 contaminant injection. Vertical lines represent injection times.

Table 4.3. Initial fluid conductivity and Eh measured from the contaminant slug (TP11) and uncontaminated slug (BH2) prior to injection for Experiment #1 and #2.

	Experiment #1		Experiment #2	
Borehole	Fluid Conductivity (μS/cm)	Eh (mV)	Fluid Conductivity (μS/cm)	Eh (mV)
TP 11	1919	-109.9	2297	-59.8
BH2	-	-	2559	-16.1

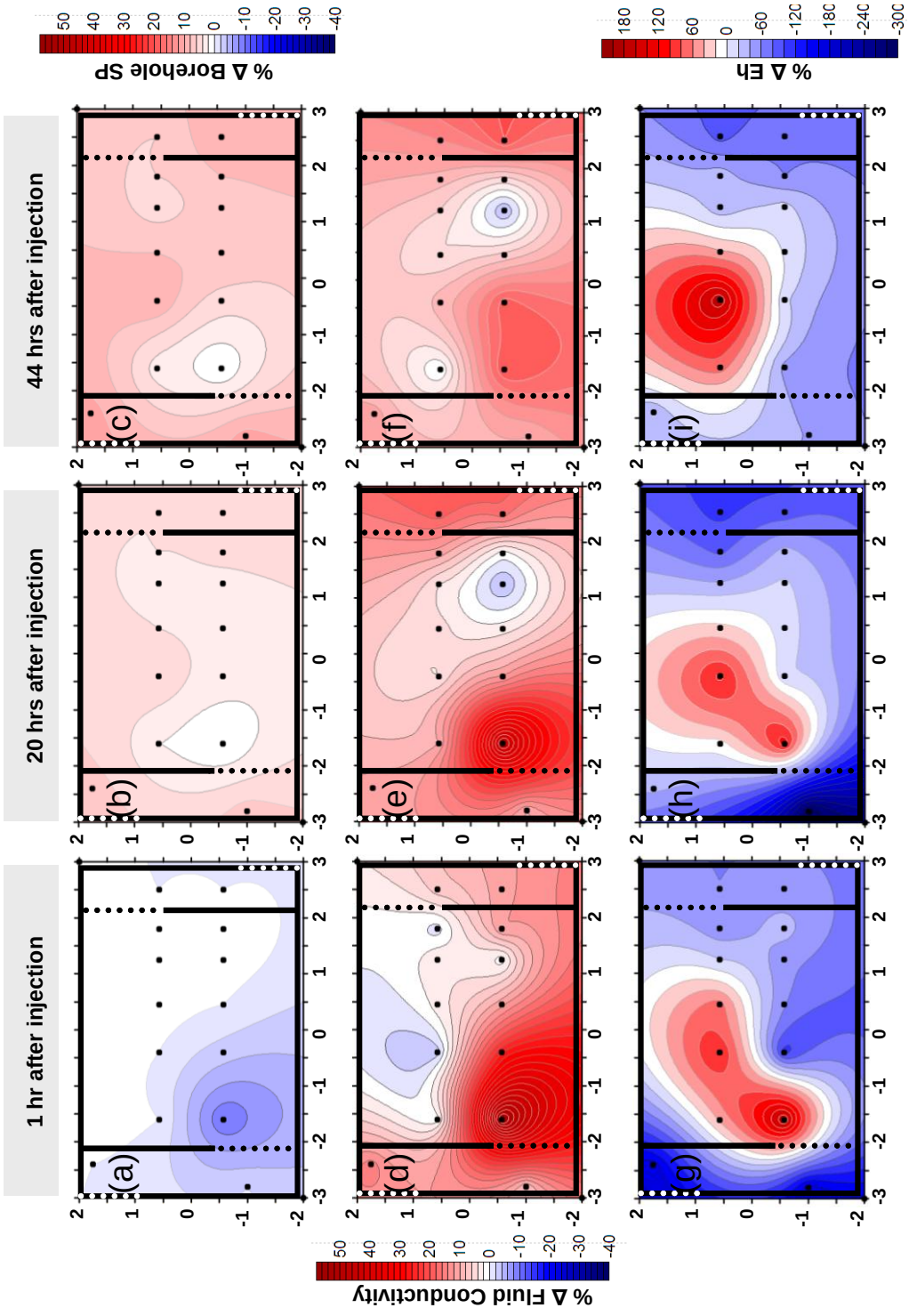

Figure 4.4. Kriged contour plots showing the percent change in borehole SP (a-c), fluid conductivity (d-f), and Eh (g-i) at 1 hour, 20 hours, and 44 hours after the Experiment #1 contaminant injection, relative to two hours before injection. Coordinates (0, 0) represent approximate center of PRB survey area.

4.5.2. Experiment #2. Initial BHSP data collected prior to the Experiment #2 injections ranged from ~52-114 mV and are shown in Table 4.4. During the Experiment #2 injections, the BHSP values showed an overall increase of ~1mV at the uncontaminated injection borehole MP7 (Figure 4.5a), and a decrease of ~9mV at the contaminant injection borehole MP1 (Figure 4.5b). The BHSP and water quality data collected during Experiment #2 are presented in Figure 4.6 as kriged contour plots showing the percent change relative to 1.5 hours prior to the clean groundwater injection (or ~4 hrs prior to contaminant injection). BHSP values recorded ~0.5 and ~3 hours post-injection (Figure 4.6a) for the NaCl and contaminant injections, respectively, showed an increase of ~3% (3 mV) at MP7, and a decrease of ~11% (9 mV) at MP1. The BHSP values recorded through ~20-44 hours post-injection (Figure 4.6b&c) continued to show increased BHSP values at the uncontaminated injection borehole (MP7). The decreased BHSP values also persisted through ~20-44 hours at the contaminant injection borehole MP1, though to a lesser extent (~3%).

Table 4.4. Initial borehole SP, fluid conductivity, and Eh data collected from the PRB boreholes ~1.5hr prior to Experiment #2.

Borehole	SP (mV)	Fluid Conductivity (µS/cm)	Eh (mV)
I	51	1419	-134.4
W	49	1392	-79
MP1	89	1618	-107.1
MP2	95	1409	-136.2
MP3	73	1379	95.6
MP4	79	1285	87.5
MP5	77	-	-
MP6	97	1451	75.7
MP7	100	1544	77.4
MP8	114	1479	67.2
MP9	68	1591	62.7
MP10	82	1395	78.5
MP11	95	1607	102.7
MP12	85	1520	14

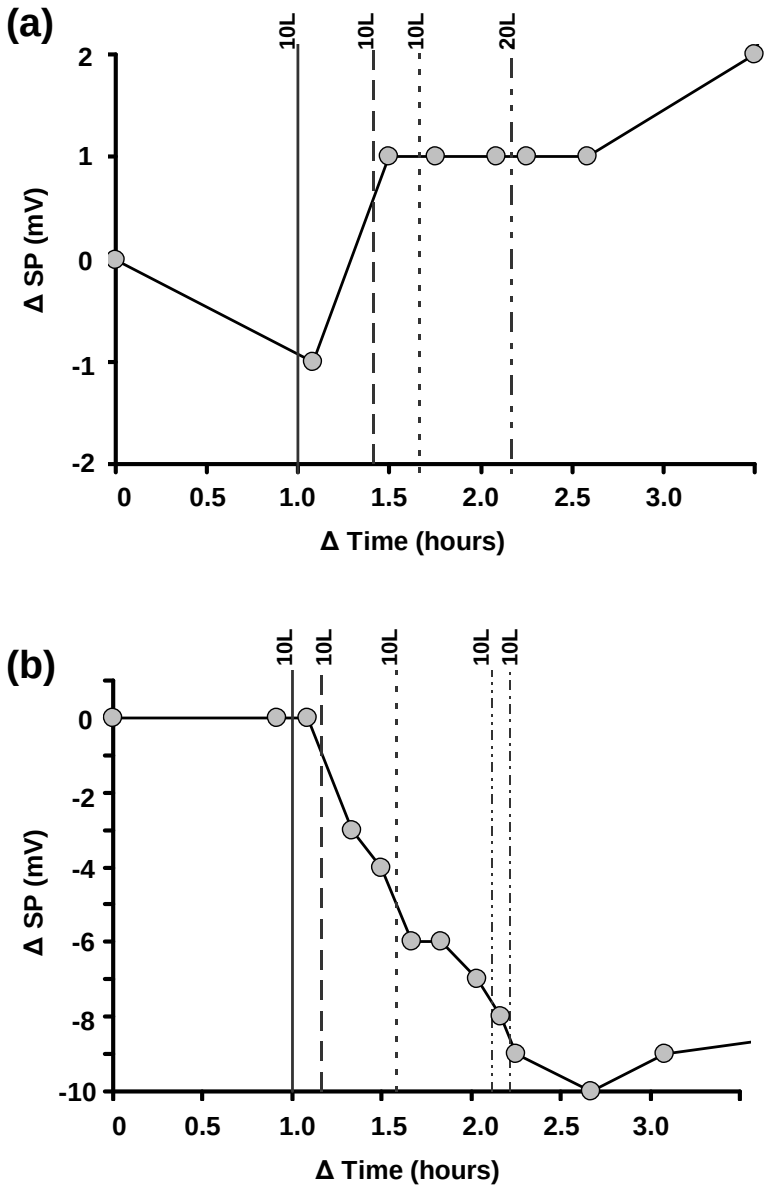

Figure 4.5. Plots showing the borehole SP data collected during the Experiment #2 (a) uncontaminated injection at borehole MP7, and (b) contaminant injection at borehole MP1. Vertical lines represent injection times.

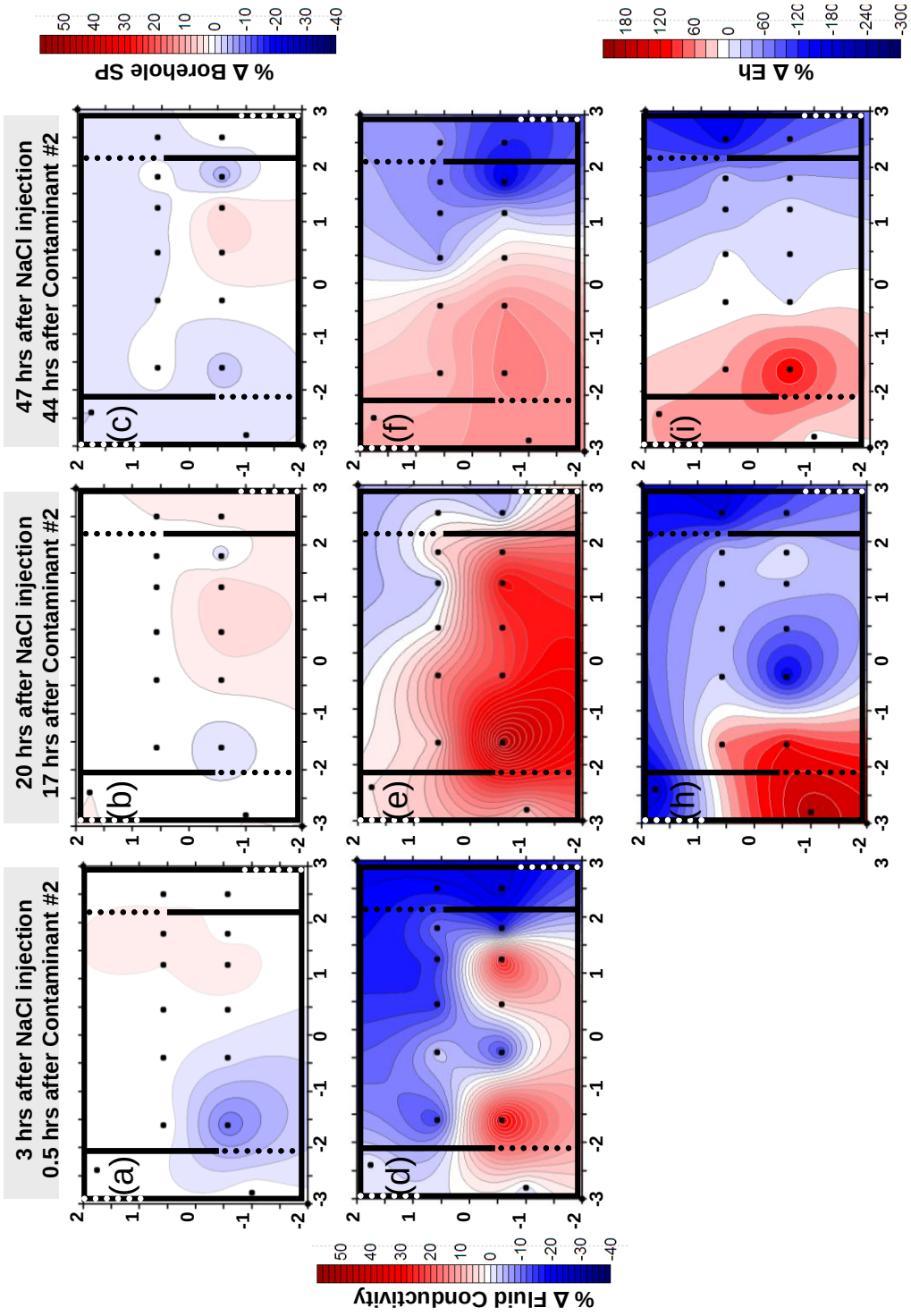

Figure 4.6. Kriged contour plots showing the percent change in borehole SP (a-c), fluid conductivity (d-f), and Eh (h-i) after the Experiment #2 uncontaminated (3, 20, and 47 hours) and contaminant (0.5, 17, and 44 hours) slug injections. Coordinates (0, 0) represent approximate center of PRB survey area.

Initial water quality data collected during the uncontaminated/contaminant slugs and PRB boreholes prior to injection are shown in Table 4.3 and Table 4.4, respectively. Fluid conductivity values recorded ~1.5 hrs prior to the injection experiment ranged from ~1285-1618 µS/cm over the PRB. Fluid conductivity values recorded after both uncontaminated and contaminant injections increased at both injection boreholes (Figure 4.6d) by ~25 – 30% (~300 µS/cm), and continued to increase at the contaminant injection borehole (MP1) through 17-20 hrs post-injection (Figure 4.6e) to ~45% (600 µS/cm). The fluid conductivity values recorded ~44-47 hours post-injection (Figure 4.6f) show a slight increase (<15%) near the entrance of the PRB, and a slight decrease (up to ~25%) near the exit of the PRB, relative to pre-injection values. Initial Eh measurements collected ~1.5hrs prior to the injections ranged from ~ -136mV to 103 mV over the PRB. Measurement of Eh immediately after the Experiment #2 injections were not available, but through 17-20 hrs post-injection (Figure 4.6h) Eh values at the uncontaminated injection borehole had decreased by ~50% (30 mV) and increased at the contaminant injection borehole ~100% (130 mV). The increased Eh measured at MP1, and decreased values measured at MP7 persisted through ~44-47 hours post-injection (Figure 4.6i), though to a lesser extent.

4.6. DISCUSSION

The results of our field study show that the injected contaminant groundwater slugs clearly affected the temporal BHSP signals at the injection boreholes. The source of the SP signals, however, is not immediately evident upon inspection of the BHSP data sets. Prior to the injection experiments, the BHSP values display relatively small spatial variations (~50-63 mV) through the barrier, and no apparent gradient (from PRB entrance to exit) which would indicate an electrokinetic potential due to natural groundwater flow. We speculate that the absence of an electrokinetic potential from natural fluid flow may be due to the discontinuous nature of the PRB design, where water is required to flow or lap over a wall between the weir and the biological stage of the PRB, instead of a continuous flow regime.

The water quality measurements, however, show that the Eh values (Table 4.2) become increasingly positive spatially through the PRB from entrance (I) to the exit (MP12), which generally suggests a change in the redox environment associated with air sparging in the biological stage of the PRB.

During the injection of the groundwater slugs, we observe consistent yet relatively small (<10 mV) decreases in SP (Figure 4.3 & 4.5b) associated with the contaminant injections, and a negligible (within our margin of error) 1 mV increase in SP (Figure 4.5a) associated with the uncontaminated injection. Previous injection studies [e.g., *Sill*, 1983] have reported decreased SP signals which were attributed to electrokinetic effects due to increased hydraulic head at the injection site, associated with the addition of the volume of the injected slug. In our current injection experiments, however, we do not observe decreased BHSP signals associated with the uncontaminated injection, although the method and volume of the injected slugs were similar for both the contaminant and uncontaminated injections. This would suggest that we are dealing with an effect other than a dominant electrokinetic potential during the injection of the groundwater slugs.

The SP signals recorded from the contaminant injection experiments are much lower in magnitude (<10 mV) than that of the relatively strong SP response (> 50 mV) observed in previous field studies, attributed to redox gradients associated with subsurface microbial activity [e.g., *Naudet et al.*, 2003; *Arora et al.*, 2007]. While we do observe sharp changes in the redox values post-injection (Figure 4.4g-i & 4.6h-i) at MP1, we do not measure a corresponding strong (i.e, >50 mV) change in the measured BHSP signals (Figure 4.4a-c & 4.6a-c). Further, we observe a rough inverse relationship between variations in BHSP and Eh (Figure 4.7) for both the contaminant and uncontaminated injections. This relationship is inconsistent with previous studies [e.g., *Naudet et al.*, 2004; *Arora et al.*, 2007] which show a relatively good positive correlation between variations in SP and Eh. In addition, the rough inverse relationship we observe between BHSP and Eh was not expected as the injected contaminated water had a lower measured Eh value compared to that measured in MP1 prior to the injections. For example, during the Experiment #1 we injected a contaminant slug with an Eh of ~ -59.8 mV into MP1 with an Eh of -28.9 mV. The increased Eh values measured at MP1 post-injection may be explained by the possible aeration of the contaminant slug while it was

being injected down the borehole. As a result of these observations, we tentatively rule out electro-redox potential as being a primary contributor to the measured SP response in our experiments. Further, based on the relative magnitude of the SP response in comparison with previous studies [e.g., *Arora et al.*, 2007], it is unlikely that the SP signals measured here can be attributed to geobattery effects.

In the absence of a dominant electrokinetic or electro-redox/geobattery effect, we next examine the possible presence of electro-diffusion effects as being a contributor to the SP signals associated with the contaminant injections. *Maineult et al.* [2006] conducted a laboratory study of the effect of strong abiotic redox gradients on SP signals. The authors observed relatively small SP signals (< 10 mV) were produced along a reaction front between two parallel solutions ($KMnO_4$ and $FeCl_2$). The study by *Maineult et al.* [2006] suggests that an additional source mechanism is necessary to account for the large SP response (> 10mV) measured at biodegradation field sites, and that this SP source mechanism is absent in their abiotic study. We note the similarity in the magnitude of the SP signals in our current study to that of the Maineult et al. [2006] study. In addition, in our current study, we observe increased Eh values at the contaminant injection borehole (MP1) after the injection (e.g., Figure 4.4g & Figure 4.6h), consistent with decreased BHSP signals (Figure 4.4a & Figure 4.6a). In contrast we do not observe increased Eh values at the uncontaminated injection borehole (MP7; Figure 4.6h), and a slight increase (~2 mV) in the BHSP signals (Figure 4.6b). We speculate that the difference in the Eh values, and difference in the chemical species driving the reactions between the uncontaminated and contaminated injections may be responsible for the difference in the BHSP response. Thus, it is possible that we observe a dominant electrochemical (electro-diffusion) potential associated with the different injection types, similar to that of the abiotic study by *Maineult et al.* [2006].

In addition to the rough inverse relationship we observe between variations in Eh and BHSP signals, we also observe a rough inverse correlation between fluid conductivity variations and BHSP signals measured from the contaminant injections (Figure 4.8). We suggest that differences in the chemical composition between the injected slugs and the resident PRB water, and the concentration gradients and chemical reactions that developed as a result of the injections are responsible for the difference in

BHSP response between the contaminated and uncontaminated injections. While we attribute the dominant BHSP response of the contaminant injections to electro-diffusional effects, we cannot rule out the possible contribution of a microbial effect.

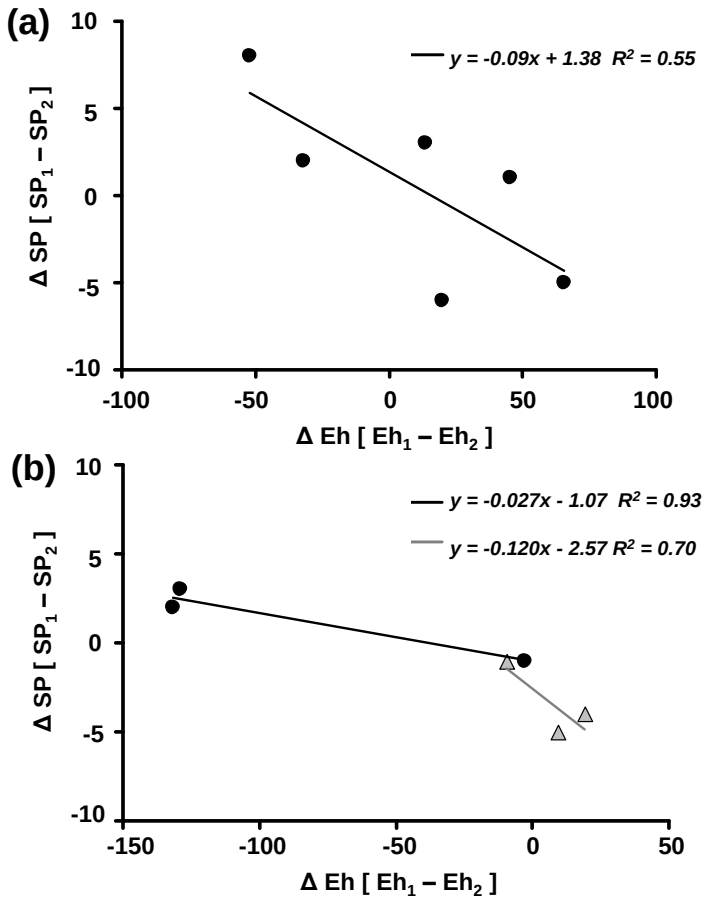

Figure 4.7. Plots showing the relationship between borehole SP and Eh for the (a) Experiment #1 and (b) Experiment #2 injections. Black filled circles represent the contaminant injections, and the gray filled triangles represent the uncontaminated injection.

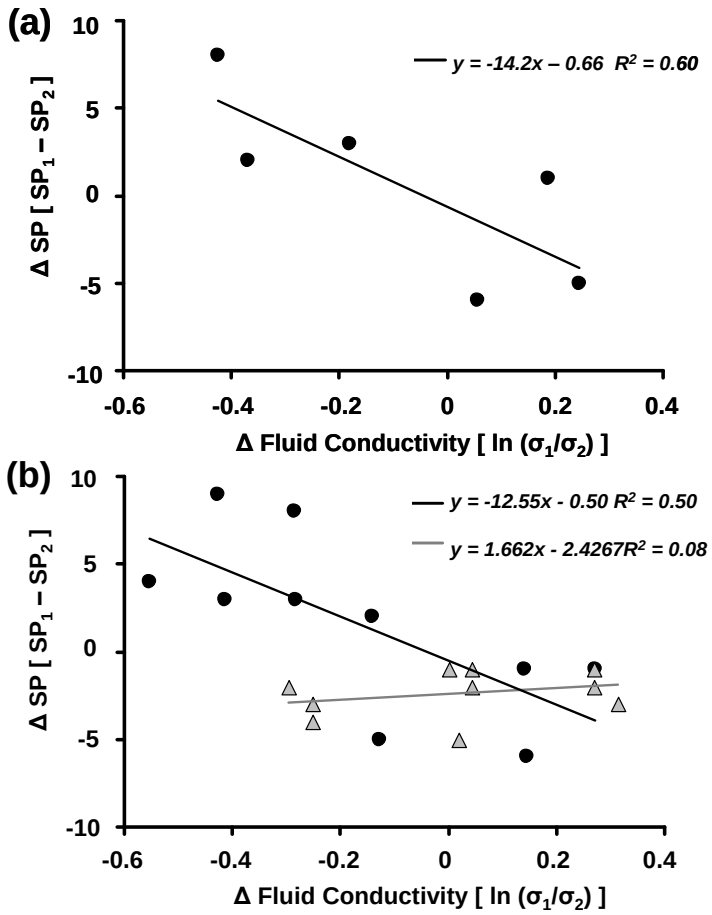

Figure 4.8. Plots showing the relationship between borehole SP and fluid conductivity for the (a) Experiment #1 and (b) Experiment #2 injections. Black filled circles represent the contaminant injections, and the gray filled triangles represent the uncontaminated injection.

4.7. SUMMARY AND CONCLUSIONS

A summary of the results of this study with regard to are initial objectives are as follows:

1. The magnitude of the SP signals associated with the injections were similar for both contaminant injections (~ -9 mV), but different for the uncontaminated (NaCl) injection (~ +1 mV).
2. Based on the relatively small, yet consistent 9 mV decrease we observe for the contaminant injections, we do not observe a measurable effect on the

SP signals that can be attributed to geobattery effects. While our study measured SP signals <10mV, previous studies of redox gradients associated with subsurface microbial activity measured SP variations well beyond 50 mV [e.g., *Naudet et al.*, 2003; *Arora et al.*, 2007].

3. The injection of the uncontaminated groundwater (NaCl) slug did not result in the same measured SP response as the contaminant injections. We suggest that the difference in SP response is likely due to differences in the chemical composition of the different slugs and electro-diffusion effects with respect to the resident PRB water.

Questions raised from this study include: (1) why did we not observe a strong microbial-induced response in the SP data? (2) Can measurement of electro-diffusional effects be used to detect and monitor microbial-induced changes within a biological PRB? Further studies are required to better understand the effect of microbial activity on SP signals associated with biological PRB's and the potential utility for the SP method to detect/monitor changes that may be indicative of PRB performance.

4.8. ACKNOWLEDGMENTS

I would like to sincerely thank Lee Slater for the opportunity to conduct this work in Northern Ireland, and J. Graber, A. Ferguson, and R. Doherty for their assistance with field data collection. I also acknowledge B. Kulessa for helping to facilitate the field work in Northern Ireland, advisement during the field study, and assistance in helping with the preparation of previous versions of this manuscript.

4.9. REFERENCES

Arora, T., Linde, N., Revil, A., and Castermant, J. (2007), Non-intrusive characterization of the redox potential of landfill leachate plumes from self-potential data, J. Contam. Hydrol., doi:10.1016/j.conhyd.2007.01.018.

Beck, F.P., Clark, P.J., and Puls, R.W. (2002), Direct push methods for locating and collecting cores of aquifer sediment and zero-valent iron from a permeable reactive barrier, Ground Water Monit. Remed., 22,165-168.

Bogoslovsky, V.A., and Ogilvy, A.A. (1970), Natural potential anomalies as a quantitative index of the rate of seepage from water reservoirs, Geophys. Propect., 18, 261-268.

Boleve, A., Revil, A., Janod, F., Mattiuzzo, J.L., and Jardani, A. (2007), Forward modeling and validation of a new formulation to compute self-potential signals associated with ground water flow, Hydrol. Earth Syst. Sci., 11, 1661–1671.

Boshoff, G.A., and Bone, B.D. (eds.) (2005), Permeable reactive barriers, International Association of Hydrological Sciences, Publication 298, 163 p.

CL:AIRE (Contaminated Land: Applications in Real Environments), (2005), Laboratory and field evaluation of a biological permeable reactive barrier for remediation of organic contaminants in soil and groundwater, CL:AIRE Case Study Bulletin, CSB 3, 4 p.

Darnet, M., Marquis, G., and Sailhac, P. (2003), Estimating aquifer hydraulic properties from the inversion of surface streaming potential (SP) anomalies, Geophys. Res. Lett., 30, 1679-1682, doi:10.1029/2003GL 017631.

Darnet, M., and Marquis, G. (2004), Modelling streaming potential (SP) signals induced by water movement in the vadose zone, J. Hydrol. (Amsterdam), 285, 114-124.

Doherty, R. (2002), Modeling of a permeable reactive barrier (PRB) at a manufactured gas plant site in Portadown, Northern Ireland, U.K., Ph.D. Thesis, The Queen's University of Belfast.

Doherty, R., Phillips, D.H., McGeough, K.L., Walsh, K.P., and Kalin, R.M. [2006], Development of modified flyash as a permeable reactive barrier medium for a former manufactured gas plant site, Northern Ireland, Environ. Geol., 50, 37-46.

Ernstson, K., and Scherer, H.U. (1986), Self-potential variations with time and their relation to hydrogeologic and meteorological parameters, Geophysics, 51, 1967–1977.

Ferguson, A.S., Doherty, R., Larkin, M.J., Kalin, R.M., Irvine, V., and Ofterdinger, U.S. (2003), Toxicity Assessment of a Former Manufactured Gas Plant, Bulletin of Environmental Contamination and Toxicology, 71 (1).

Fournier, C. (1989), Spontaneous potentials and resistivity surveys applied to hydrogeology in a volcanic area: case history of the Chaine des Puys (Puy-de-Dome, France), Geophys. Prospecting, 37, 647–668, 1989.

Kulessa, B., Hubbard, B., and Brown, G.H. (2003), Cross-coupled flow modeling of coincident streaming and electrochemical potentials and application to subglacial self-potential data, J. Geophys. Res., 108(B8), 2381, doi:10.1029/2001JB001167.

Liang, L., Korte, N.E., Moline, G.R., and West, O.R. (2001), Long-term monitoring of permeable reactive barriers, ORNL/TM-2001/1. Oak Ridge National Laboratory, Oak Ridge, Tennessee.

Liang, L., Sullivan, A.B., West, O.R., Kamolpornwijit, W., and Moline, G.R. (2003), Predicting the precipitation of mineral phases in permeable reactive barriers, Environ. Eng. Sci., 20(6), 635-653.

Maineult, A., Bernabe, Y., and Ackerer, P. (2004), Electrical response of flow, diffusion, and advection in a laboratory sand box, Vadose Zone Journal, 3, 1180-1192.

Maineult, A., Bernabé, Y., and Ackerer, P. (2006), Detection of advected, reacting redox fronts from self-potential measurements, J. Contam. Hydrol., 86, 32–52.

McMahon, P.B., Dennehy, K.F., and Sandstrom, M.W. (1999), Hydraulic and geochemical performance of a permeable reactive barrier containing zero-valent iron, Denver Federal Center, Ground Water, 37(3), 396-404.

Minsley, B.J. (2007), Modeling and inversion of self-potential data, Ph.D. Thesis, Massachusetts Institute of Technology, Cambridge, MA.

Naudet, V., and Revil, A. (2005), A sandbox experiment to investigate bacteria-mediated redox processes on self-potential signals, Geophys. Res. Lett., 32, L11405, doi:10.1029/2005GL022735.

Naudet, V., Revil, A., Bottero, J., and Begassat, P. (2003), Relationship between self-potential (SP) signals and redox conditions in contaminated groundwater, Geophys. Res. Lett., 30(21), 2091, doi:10.1029/2003GL018096.

Naudet, V., Revil, A., Rizzo, E., Bottero, J., and Begassat, P. (2004), Groundwater redox conditions and conductivity in a contaminant plume from geoelectrical investigations, Hydrol. Earth Sys. Sci., 8(1), 8-22.

Ntarlagiannis, D., Atekwana, E.A., Hill, E.A., and Gorby, Y. (2007), Microbial nanowires: Is the subsurface "hardwired"?, Geophys. Res. Lett., 34(17).

Nyquist, J.E., and Corry, C.E. (2002), Self-potential: the ugly duckling of environmental geophysics, Leading Edge, 446-451.

Petiau, G. (2000), Second generation of lead-lead chloride electrodes for geophysical applications, Pure Appl. Geophys., 157, 357-382.

Phillips, D.H., Watson, D.B., Roh, Y., and Gu, B. (2003), Mineralogical characteristics and transformations during long-term operation of zerovalent iron reactive barrier, J. Environ, Qual., 32(6), 2033-2045.

Puls, R., Paul, C., and Powell, R. (1999), The application of in situ permeable reactive (zero-valent iron) barrier technology for the remediation of chlorate contaminated groundwater: a field test, Appl. Geochem., 14, 989-1000.

Revil, A., Naudet, V., Nouzaret, J., and Pessel, M. (2003), Principles of electrography applied to self-potential electrokinetic sources and hydrogeological applications, Water Resour. Res., 39(5), 1114, doi:10.1029/2001WR000916.

Revil, A., and Leroy, P. (2004), Governing equations for ionic transport in porous shales, J. Geophys. Res., 109, B03208, doi:10.1029/2003JB002755.

Revil, A., Cary, L., Fan, Q., Finizola, A., and Trolard, F. (2005), Self potential signals associated with preferential ground water flow pathways in a buried paleo-channel, Geophys. Res. Lett., 32, L07401, doi:10.1029/2004GL022124.

Sailhac, P., and Marquis, G. (2001), Analytic potentials for the forward and inverse modeling of SP anomalies caused by subsurface fluid flow, Geophys. Res. Lett., 28, 1851-1854.

Sato, M., and Mooney, H.M. (1960), The electrochemical mechanism of sulfide self-potentials, Geophysics, 25(1), 226-249.

Scherer, M.M., Richter, S., Valentine, R.L., Alvarez, P.J.J. (2000), Chemistry and microbiology of permeable reactive barriers for in situ groundwater clean up, Crit. Rev. Microbiol., 26, 221–264.

Shirazi, F. (1997), Development of biological permeable reactive barriers for removal of Chlorophenols (2,4,6-Trichlorophenol) in contaminated groundwater, Ph.D. Thesis, Oklahoma State University, Stillwater, OK.

Sill, W.R. (1983), Self-potential modeling from primary flows, Geophysics, 48, 76-86.

Slater, L., Ntarlagiannis, D., Yee, N., O'Brien, M, Zhang, C., and Williams, K.H. (2007b), Electrodic voltages in the presence of sulfide: implications for (1) monitoring natural microbial activity, and (2) SP electrode performance, Geophysics, 73(2), F65-F70.

Song, S., Song, Y., and Kwon, B. (2005), Application of hydrogeological and geophysical methods to delineate leakage pathways in an earth fill dam, Explor. Geophys., 36, 92-96.

Sturman, P.J., Stewart, P.S., Cunningham, A.B., Bouwer, E.J., and Wolfram, J.H. (1995), Engineering scale-up of in situ bioremediation processes: a review, J. Contam. Hydrol., 19, 171-203.

Timm, F., and Moller, P. (2001), The relation between electric and redox potential: evidence from laboratory and field measurements, J. Geochem. Explor., 72(2), 115-128.

USEPA (2001), A Citizen's Guide to Permeable Reactive Barriers (PRBs), United States Environmental Protection Agency, USA. EPA/542/F-01-005.

USEPA (2002), Field Applications of In Situ Remediation Technologies: Permeable Reactive Barriers, United States Environmental Protection Agency, USA.

Zolla, V., Sethi, R., and Di Molfetta, A. (2007), Performance assessment and monitoring of a permeable reactive barrier for the remediation of a contaminated site, Am. J. Environ. Sci., 3, 158-165.

3. CONCLUSIONS

3.1. SUMMARY

Previous geophysical studies have greatly advanced the field of biogeophysics, however this subdiscipline of geophysics is still in its infancy, and hence provides for a wealth of opportunities to explore the effects of microbial-induced phenomena on geophysical signatures. Some of the outstanding questions that remain from previous investigations include: (1) What are the relative contributions of microbial metabolic byproducts on geophysical signatures? (2) What is the effect of microbial growth and biofilm formation on geophysical properties? (3) What geophysical techniques are best suited for assessing microbial-geologic interactions? To this end, the primary goal of this thesis was to test the hypothesis that microbial growth and activity in geologic media can result in measurable changes to the geophysical properties of the media. This was accomplished through a series of geophysical laboratory experiments and a field-scale study. A review of the objectives for this thesis, general observations and conclusions are summarized below:

Contribution of metabolic byproducts (organic acids and biosurfactants) to electrical conductivity magnitude. The results of this experiment show that increases in electrolytic (fluid and real) conductivity are consistent with increases in concentrations of organic acids and biosurfactant. Increases in the electrolytic conductivity are also consistent with temporal increases major cation concentrations, which is indicative of mineral weathering, with a secondary affect on the interfacial conductivity. The results of this experiment suggest that electrolytic conductivity measurements may be useful as an indicator of microbial metabolism.

Direct contribution and relative magnitude of the effect of microbial growth and biofilm formation on the low-frequency electrical properties of porous media. The results of this experiment show that interfacial conductivity generally paralleled the attached microbial cell concentrations in the biostimulated (bacteria + nutrients + diesel) columns. The results suggest that interfacial conductivity measurements may be used as proxy indicator for microbial growth and biofilm formation in porous media.

Spatiotemporal changes in acoustic wave propagation associated with microbial growth and biofilm formation in porous media. The results from the biostimulated column show an overall temporal decrease in acoustic wave velocity and exhibit variations in acoustic wave amplitude spatially over a 2D area of the column. While the exact mechanisms responsible for the differences in velocity and amplitude are yet unclear, the spatial variations appear to correlate with differences in the amount of attached biofilm and/or biofilm architecture.

Natural electrical signatures associated with an in-situ biological permeable reactive barrier in response to the injection of contaminated groundwater. The results of this experiment show that the measured self-potential (SP) signals are dominated by electrochemical or diffusion potentials induced by the injections, though the effect of microbial activity can not be completely ruled out.

In summary, the findings presented in this thesis provide an additional fundamental understanding of the influence of microbial growth and activity on geophysical properties. Understanding the geophysical response of microbial biosignatures in controlled investigations, such as those presented here, is the first step toward recognizing these biosignatures in field geophysical data. Furthermore, the results of this study may allow for more accurate interpretation of geophysical data from near-surface environments where microbial activity is enhanced or stimulated.

3.2. RECOMMENDATIONS AND FUTURE WORK

While this study has provided useful information regarding the influence of microbial growth and activity on geophysical signatures, several questions have been raised and remain unanswered. Further research is recommended to resolve these new questions and obtain a better understanding of not only the geophysical signatures associated with microorganisms, but also the mechanisms responsible for the observed biogeophysical response. As such, a list of questions that have been raised from this study are outlined below, along with additional ideas for future studies.

1. What is the effect of oil mobilization by biosurfactants, and the physicochemical changes imparted during oil mobilization (i.e., changes in wettability) on the electrical properties of porous media?

2. What is the magnitude of the electrical response due to biogenic gas production?
3. What is the contribution of microorganisms themselves on the elevated bulk conductivity response observed at hydrocarbon biodegradation field sites?
4. What are the mechanisms responsible for the observed polarization response at the fluid-mineral interface due to microbial attachment and biofilm formation?
5. Do different types of biofilms (i.e., different biofilm structures/architecture) have a variable effect on geophysical response?
6. What are the mechanisms responsible for the variable acoustic wave propagation due to biofilm formation?

As eluded to above, the research opportunities at this point in the progression of the field of biogeophysics are seemingly endless. Since geophysical processes are often coupled, like those of the complex/dynamic microbial-induced changes to the physicochemical properties of geologic media, more studies are needed to decouple these effects and quantify the magnitude of contributions. Knowledge of the biogeophysical signatures in the laboratory setting will allow for better interpretation of geophysical data due to microbial-induced changes in natural environments. Limitations exist with current geophysical studies, however, as most of the work to date has been largely experimental. Thus, there is also a need for additional numerical modeling studies to better describe bio-geophysical relationships. Looking forward, this work in addition to the previous biogeophysical studies, demonstrates the potential application of biogeophysical studies towards field-scale environmental problems, such as those associated with bioremediation, microbial enhanced oil recovery, and gas hydrate studies.

APPENDIX

JOURNAL REPRINT PERMISSION FORMS

Included with this dissertation is the written letter used to request permission from the American Geophysical Union (AGU) to use the article I had published in 2006 in the Geophysical Research Letters journal for this dissertation.

July 13, 2009

Dear AGU,

I am writing to request permission to use the 2006 article I have published in the Geophysical Research Letters journal for my dissertation at Missouri University of Science and Technology. The citation for the article I am requesting permission for is as follows:

Davis, C. A., E. Atekwana, E. Atekwana, L. D. Slater, S. Rossbach, and M. R. Mormile (2006), Microbial growth and biofilm formation in geologic media is detected with complex conductivity measurements, *Geophys. Res. Lett.*, 33, L18403, doi:10.1029/2006GL027312.

Please sign and date the fields below and return to me at cadk9d@mst.edu (or by fax to 319-378-5927). Thank you in advance for your assistance.

Sincerely,
Caroline A. Davis

The undersigned copyright owner of the material described herein grants permission for the above detailed use.

Owner

13 July 2009
Date

please see attached information.

BIBLIOGRAPHY

Abdel Aal, G., Atekwana, E., Radzikowski, S., Rossbach, S. (2009), Effect of bacterial adsorption on low frequency electrical properties of clean quartz sands and iron-oxide coated sands, Geophys. Res. Lett., 36, L04403, doi:10.1029/2008GL036196.

Abdel Aal, G.Z. (2008), Electrical properties of bacteria in sand columns: live vs. dead cells, AGU Chapman Conference on Biogeophysics, Portland, ME.

Abdel Aal, G.Z., Atekwana, E.A., Slater, L.D., and Atekwana E.A. (2004), Effects of microbial processes on electrolytic and interfacial electrical properties of unconsolidated sediments, Geophys. Res. Lett., 31(12), L12505, doi:10.1029/2004GL020030.

Abdel Aal, G.Z., Slater, L.D., Atekwana, E.A. (2006), Induced-polarization measurements on unconsolidated sediments from a site of active hydrocarbon biodegradation, Geophysics, 71, H13-H24.

Ahimou, F., Semmens, M.J., Novak, P.J., and Haugstad, G. (2007), Biofilm cohesiveness measurement using a novel atomic force microscopy methodology, Appl. Environ. Microbiol., 73(9), 2897-2904.

Allen, J.P., Atekwana, E.A., Atekwana, E.A., Duris, J.W., Werkema, D.D., and Rossbach, S. (2007), The microbial community structure in petroleum-contaminated sediments corresponds to geophysical signatures, Appl. Environ. Microbiol., 73, 2860-2870.

Archie, G.E. (1942), The electrical resistivity log as an aid in determining some reservoir characteristics, Transactions of the American Institute of Mining, Metallurgical and Petroleum Engineers, 146, 54-62.

Arora, T., Linde, N., Revil, A., and Castermant, J. (2007), Non-intrusive characterization of the redox potential of landfill leachate plumes from self-potential data, J. Contam. Hydrol., doi:10.1016/j.conhyd.2007.01.018.

Atekwana, E.A., Atekwana, E.A., and Werkema, D.D. (2006), Biogeophysics: the effects of microbial processes on geophysical properties of the shallow subsurface. In Applied Hydrogeophysics, Vereecken, H., Binley, A., Cassiani, G., Revil, A., and Titov, K., (eds.), NATO Sci. Ser. IV, Springer: New York, pp. 161–193.

Atekwana, E.A., Atekwana, E.A., Legall, F.D., and Krishnamurthy, R.V. (2004a), Field evidence for geophysical detection of microbial activity, Geophys. Res. Lett., 31, L23603, doi:10.1029/2004GL021576.

Atekwana, E.A., Atekwana, E.A., Legall, F.D., and Krishnamurthy, R.V. (2005), Biodegradation and mineral weathering controls on bulk electrical conductivity in a shallow hydrocarbon contaminated aquifer, J. Contam. Hydrol., 80, 149-167.

Atekwana, E.A., Atekwana, E.A., Rowe, R.S., Werkema, D.D., and Legall, F.D. (2004b), Total dissolved solids in groundwater and its relationship to bulk conductivity of soils contaminated with hydrocarbon, J. Appl. Geophys., 56, 281-294.

Atekwana, E.A., Atekwana, E.A., Werkema, D.D., Allen, J.P., Smart, L.A., Duris, J.W., Cassidy, D.P., Sauck, W.A., and Rossbach, S. (2004c), Evidence for microbial enhanced electrical conductivity in hydrocarbon-contaminated sediments, Geophys. Res. Lett., 31, L23501.

Atekwana, E.A., Atekwana, E.A., Werkema, D.D., Allen, J.P., Smart, L.A., Duris, J.W., Cassidy, D.P., Sauck, W.A., and Rossbach, S. (2004c), Evidence for microbial enhanced electrical conductivity in hydrocarbon-contaminated sediments, Geophys. Res. Lett., 31, L23501.

Atekwana, E.A., Sauck, W.A., and Werkema Jr., D.D. (2000), Investigations of geoelectrical signatures at a hydrocarbon contaminated site, J. Appl. Geophys., 44, 167-180.

Atekwana, E.A., Werkema, D.D., Duris, J.W., Rossbach, S., Atekwana, E.A., Sauck, W.A., Cassidy, J.P., Means, J., and Legall, F.D. (2004d), In-situ apparent conductivity measurements and microbial population distribution at a hydrocarbon-contaminated site, Geophysics, 69, 56-63.

Bartha, R., and Atlas, R.M. (1987), Transport and transformations of petroleum: biological processes. In Boesch, D.F., and Rabalais, N.N. (eds.), Long-term environmental effects of offshore oil and gas development, Elsevier Applied Science, London, pp. 287-341.

Baveye, P., Vandevivere, P., Hoyle, B.L., DeLeo, P.C., and Sanchez de Lozada, D. (1998), Environmental impact and mechanisms of the biological clogging of saturated soils and aquifer materials, Crit. Rev. Environ. Sci. Tech., 28(2), 123-191.

Beck, F.P., Clark, P.J., and Puls, R.W. (2002), Direct push methods for locating and collecting cores of aquifer sediment and zero-valent iron from a permeable reactive barrier, Ground Water Monit. Remed., 22,165-168.

Bennett, P.C., Hiebert, F.K., Choi, W.J. (1996), Microbial colonization and weathering of silicates in a petroleum-contaminated groundwater, Chem. Geol., 132, 45-53.

Bermejo, J.L., Sauck, W.A., and Atekwana, E.A. (1997), Geophysical discovery of a new LNAPL plume at the former Wurtsmith AFB, Ground Water Monit. Remed., 17, 131-137.

Blitz, J., and Simpson, G. (1996), Ultrasonic methods of non-destructive testing, Springer, 264 p.

Bogoslovsky, V.A., and Ogilvy, A.A. (1970), Natural potential anomalies as a quantitative index of the rate of seepage from water reservoirs, Geophys. Propect., 18, 261-268.

Boleve, A., Revil, A., Janod, F., Mattiuzzo, J.L., and Jardani, A. (2007), Forward modeling and validation of a new formulation to compute self-potential signals associated with ground water flow, Hydrol. Earth Syst. Sci., 11, 1661–1671.

Boshoff, G.A., and Bone, B.D. (eds.) (2005), Permeable reactive barriers, International Association of Hydrological Sciences, Publication 298, 163 p.

Brovelli, A., Malaguerra, F., and Barry, D.A. (2009), Bioclogging in porous media: model development and sensitivity to initial conditions, Environ. Model. Software, 24, 611-626.

Bryant, S.L., and Lockhart, T.P. (2002), Reservoir engineering analysis of microbial enhanced oil recovery, SPE Reservoir Eval. Eng., 5, 365-374

Bunthof, C.J., van Schalkwijk, S., Meijer, W., Abee, T., and Hugenholtz, J. (2001), Fluorescent method for monitoring cheese starter permeabilization and lysis, Appl. Environ. Microbiol., 67, 4264-4271.

Cassidy, D.P., Hudak, A.J., Werkema, D.D., Atekwana, E.A., Rossbach, S., Duris, J.W., Atekwana, E.A., and Sauck, W.A. (2002), In-situ rhamnolipid production at an abandoned petroleum refinery by Pseudomonas aeruginosa, J. Soil Sed. Contam., 11, 769-787.

Cassidy, D.P., Werkema, D.D., Sauck, W.A., Atekwana, E.A., Rossbach, S., and Duris, J. (2001), The effects of LNAPL biodegradation products on electrical conductivity measurements, J. Env. Eng. Geophysics, 6, 47-52.

Chapelle, F.H., and Bradley, P.M. (1997), Alteration of aquifer geochemistry by microorganisms. In Hurst, C.J. (ed.), Manual of Environmental Microbiology, ASM Press, Washington, DC, pp. 558-564.

CL:AIRE (Contaminated Land: Applications in Real Environments), (2005), Laboratory and field evaluation of a biological permeable reactive barrier for remediation of organic contaminants in soil and groundwater, CL:AIRE Case Study Bulletin, CSB 3, 4 p.

Clark, V.A., Tittman, B.R., and Spencer, T.W. (1980), Effect of volatiles on attenuation (Q-1) and velocity in sedimentary rocks, J. Geophys. Res., 85, 5190-5198.

Cozzarelli, I.M., Baedecker, M.J., Eganhouse, R.P., and Goerlitz, D.F. (1994), The geochemical evolution of low-molecular-weight organic acids derived from the degradation of petroleum contaminants in groundwater, Geochim. Cosmo. Acta, 58, 863-877.

Cozzarelli, I.M., Herman, J.S., and Baedecker, M.J. (1995), Fate of microbial metabolites of hydrocarbons in a coastal plain aquifer: the role of electron acceptors, Environ. Sci. Tech., 29, 458-469.

Darnet, M., and Marquis, G. (2004), Modelling streaming potential (SP) signals induced by water movement in the vadose zone, J. Hydrol. (Amsterdam), 285, 114-124.

Darnet, M., Marquis, G., and Sailhac, P. (2003), Estimating aquifer hydraulic properties from the inversion of surface streaming potential (SP) anomalies, Geophys. Res. Lett., 30, 1679-1682, doi:10.1029/2003GL 017631.

Davey, M.E., Caiazza, N.C., and O'Toole, G.A. (2003), Rhamnolipid surfactant production affects biofilm architecture in *Pseudomonas aeruginosa* PAO1, J. Bacteriol., 185(3), 1027-1036, doi:10.1128/JB.185.3.1027–1036.2003.

Davis, C.A., Atekwana, E.A., Atekwana, E.A., Slater, L.D., Rossbach, S., and Mormile, M.R. (2006), Microbial growth and biofilm formation in geologic media is detected with complex conductivity measurements, Geophys. Res. Lett., 33, L18403, doi:10.1029/2006GL027312.

DeJong, J.T., Fritzges, M.B., and Nusslein, K. (2006), Microbially induced cementation to control sand response to undrained shear, J. Geotech. Geoenviron. Eng., 132(11), 1381-1392.

DeJong, J.T., Mortensen, B.M., Martinez, B.C., and Nelson, D.C. (2009), Bio-mediated soil improvement, Ecol. Eng., *In Press*, doi:10.1016/j.ecoleng.2008.12.029.

Desai, J.D., and Banat, I.M. (1997), Microbial production of surfactants and their commercial potential, Microbiol. Mol. Bio. Rev., 61(1), 47-64.

Doherty, R. (2002), Modeling of a permeable reactive barrier (PRB) at a manufactured gas plant site in Portadown, Northern Ireland, U.K., Ph.D. Thesis, The Queen's University of Belfast.

Doherty, R., Phillips, D.H., McGeough, K.L., Walsh, K.P., and Kalin, R.M. [2006], Development of modified flyash as a permeable reactive barrier medium for a former manufactured gas plant site, Northern Ireland, Environ. Geol., 50, 37-46.

Dupin, H.J., and McCarty, P.L. (2000), Impact of colony morphologies and disinfection on biological clogging in porous media, Environ. Sci. Technol., 34(8), 1513-1520, doi:10.1021/es990452f.

Ecker, C., Dvorkin, J., and Nur, A. (1998), Sediments with gas hydrates: internal structure from seismic AVO, Geophysics, 63, 1659-1669.

Ernstson, K., and Scherer, H.U. (1986), Self-potential variations with time and their relation to hydrogeologic and meteorological parameters, Geophysics, 51, 1967–1977.

Ferguson, A.S., Doherty, R., Larkin, M.J., Kalin, R.M., Irvine, V., and Ofterdinger, U.S. (2003), Toxicity Assessment of a Former Manufactured Gas Plant, Bulletin of Environmental Contamination and Toxicology, 71 (1).

Fournier, C. (1989), Spontaneous potentials and resistivity surveys applied to hydrogeology in a volcanic area: case history of the Chaine des Puys (Puy-de-Dome, France), Geophys. Prospecting, 37, 647–668, 1989.

Friedman, L., and Kolter, R. (2004), Genes involved in matrix formation in *Pseudomonas aeruginosa* PA14 biofilms, Molec. Microbio., 51(3), 675–690 doi:10.1046/j.1365-2958.2003.03877.x.

Gorby, Y.A., Yanina, S., McLean, J.S., Rosso, K.M., Moyles, D., Dohnalkova, A., Beveridge, T.J., Chang, I., Kim, B.H., Kim, K.S., Culley, D.E., Reed, S.B., Romine, M.F., Saffarini, D.A., Hill, E.A., Shi, L, Elias, D.A., Kennedy, D.W., Pinchuk, G., Watanabe, K., Ishii, S., Logan, B., Nealson, K.H., and Fredrickson, J.K. (2006), Electrically conductive bacterial nanowires produced by Shewanella oneidensis strain MR-1 and other microorganisms, Proc. Natl. Acad. Sci. USA, 103(30), 11358-11363.

Hiebert, F.K., and Bennett, P.C. (1992), Microbial control of silicate weathering in organic-rich groundwater, Science, 258, 278-281.

Huang, W.H., and Keller, W.D. (1970), Dissolution of rock-forming silicate minerals in organic acids: simulated first-stage weathering of fresh mineral surfaces, Amer. Mineral., 55, 2076-2094.

Kearey, P., Brooks, M., and Hill, I. (2002), An introduction to geophysical exploration, Blackwell Publishing, 262 p.

Kildsgaard, J., and Engesgaard, P. (2002), Numerical analysis of biological clogging in two-dimensional sand box experiments, J. Contam. Hydrol., 50, 261-285.

Klapper, I., Rupp, C.J., Cargo, R., Purvedorj, B., and Stoodley, P. (2002), Viscoelastic fluid description of bacterial biofilm material properties, Biotech. Bioeng., 80(3), 289-296.

Klausen, M., Heydorn, A., Ragas, P., Lambertsen, L., Aaes-Jørgensen, A., Molin, S., and Tolker-Nielsen, T. (2003), Biofilm formation by Pseudomonas aeruginosa wild type, flagella and type IV pili mutants, Molecular Microbiol., 48(6), 1511–1524.

Knight, R., and Nolen-Hoeksema, R. (1990), A laboratory study of the dependence of elastic wave velocities on pore scale fluid distribution, Geophys. Res. Lett., 17, 1529-1532.

Kolev, V. L., Danov, K.D., Kralchevsky, P.A., Broze, G., and Mehreteab, A., (2002), Comparison of the van der waals and frumkin adsorption isotherms for sodium dodecyl sulfate at various salt concentrations, Langmuir, 18(23), 9106-9109, doi:10.1021/la0259858.

Kulessa, B., Hubbard, B., and Brown, G.H. (2003), Cross-coupled flow modeling of coincident streaming and electrochemical potentials and application to subglacial self-potential data, J. Geophys. Res., 108(B8), 2381, doi:10.1029/2001JB001167.

Lehman, M.R., Colwell, F.S., and Bala, G.A. (2001), Attached and unattached microbial communities in a simulated basalt aquifer under fracture- and porous-flow conditions, Appl. Environ. Microbiol., 67(6), 2799-2809.

Lesmes, D.P., and Frye, K.M. (2001), Influence of pore fluid chemistry on the complex conductivity and induced polarization responses of Berea sandstone, J. Geophys. Res., 106, 4079-4090.

Lesmes, D.P., and Morgan, F.D. (2001), Dielectric spectroscopy of sedimentary rocks, J. Geophys. Res., 106, 13329-13346.

Li, X., Zhong, L.R., and Pyrak-Nolte, L.J. (2001), Physics of partially saturated porous media: residual saturation and seismic-wave propagation, Ann. Rev. Earth Planet. Sci., 29, 419-460.

Liang, L., Korte, N.E., Moline, G.R., and West, O.R. (2001), Long-term monitoring of permeable reactive barriers, ORNL/TM-2001/1. Oak Ridge National Laboratory, Oak Ridge, Tennessee.

Liang, L., Sullivan, A.B., West, O.R., Kamolpornwijit, W., and Moline, G.R. (2003), Predicting the precipitation of mineral phases in permeable reactive barriers, Environ. Eng. Sci., 20(6), 635-653.

Lundegard, P.D., and Land, L.S. (1986), Carbon dioxide and organic acids: their role in porosity enhancement and cementation, Paleogene of the Texas Gulf Coast. In Gautier, D.L. (ed.), Roles of Organic Matter in Sediment Diagenesis, SEPM Special Pub., 38, pp. 129-146.

Maier, R.M., Pepper, I.L., and Gerba, C.P. (2000), Environmental Microbiology, Academic Press, San Diego, CA, 585 p.

Maineult, A., Bernabe, Y., and Ackerer, P. (2004), Electrical response of flow, diffusion, and advection in a laboratory sand box, Vadose Zone Journal, 3, 1180-1192.

Maineult, A., Bernabé, Y., and Ackerer, P. (2006), Detection of advected, reacting redox fronts from self-potential measurements, J. Contam. Hydrol., 86, 32–52.

Mai-Prochnow, A., Evans, F., Dalisay-Saludes, D., Stelzer, S., Egan, S., James, S., Webb, J.S., and Kjelleberg, S. (2004), Biofilm development and cell death in the marine bacterium Pseudoaltermonas tunicate, Appl. Environ. Microbiol., 70, 3232-3238.

Mavko, G., and Jizba, D. (1991), Estimating grain-scale fluid effects on velocity dispersion in rocks, Geophysics, 56, 1940–49.

Mázac, O., Benes, L., Landa, I., and Maskova, A. (1990), Determination of the extent of oil contamination in groundwater by geoelectrical methods. In Ward, S.H. (ed.), Geotechnical. Env. Geo., 2, pp. 107-112.

McInerney, M.J., Nagle, D.P., and Knapp, R.M. (2005), Microbially enhanced oil recovery: past, present, and future. In Ollivier, B., and Magot, M. (eds.), Petroleum Microbiology, ASM Press, 365 p.

McMahon, P.B., and Chapelle, F.H. (1991), Microbial production of organic acids in aquitard sediments and its role in aquifer geochemistry, Nature, 349, 233-235.

McMahon, P.B., Dennehy, K.F., and Sandstrom, M.W. (1999), Hydraulic and geochemical performance of a permeable reactive barrier containing zero-valent iron, Denver Federal Center, Ground Water, 37(3), 396-404.

McMahon, P.B., Vroblesky, D.A., Bradley, P.M., Chapelle, F.H., and Gullet, C.D. (1995), Evidence for enhanced mineral dissolution in organic acid-rich shallow groundwater, Ground Water, 33, 207-216.

Meshri, I.D. (1986), On the reactivity of carbonic and organic acids and generation of secondary porosity, SEPM Special Pub., 38, pp. 123-128.

Minsley, B.J. (2007), Modeling and inversion of self-potential data, Ph.D. Thesis, Massachusetts Institute of Technology, Cambridge, MA.

Murphy III, W.F., Winkler, K.W., and Kleinberg, R.L. (1984), Frame modulus reduction in sedimentary rocks: the effect of adsorption on grain contacts, Geophys. Res. Lett., 1(9), 805-808.

Naudet, V., and Revil, A. (2005), A sandbox experiment to investigate bacteria mediated redox processes on self-potential signals, Geophys. Res. Lett., 32, L11405, doi:10.1029/2005GL022735.

Naudet, V., Revil, A., Bottero, J., and Begassat, P. (2003), Relationship between self-potential (SP) signals and redox conditions in contaminated groundwater, Geophys. Res. Lett., 30(21), 2091, doi:10.1029/2003GL018096.

Naudet, V., Revil, A., Rizzo, E., Bottero, J., and Begassat, P. (2004), Groundwater redox conditions and conductivity in a contaminant plume from geoelectrical investigations, Hydrol. Earth Sys. Sci., 8(1), 8-22.

Ntarlagiannis, D., and Ferguson, A. (2009), SIP response of artificial biofilms, Geophysics, 74(1), A1-A5.

Ntarlagiannis, D., Atekwana, E.A., Hill, E.A., and Gorby, Y. (2007), Microbial nanowires: Is the subsurface "hardwired"?, Geophys. Res. Lett., 34(17).

Ntarlagiannis, D., Williams, K.H., Slater, L., and Hubbard, S. (2005a), The low frequency electrical response to microbially induced sulfide precipitation, J. Geophys. Res., 110, G02009, doi:10.1029/2005JG000024.

Ntarlagiannis, D., Yee, N., and Slater, L. (2005b), On the low frequency induced polarization of bacterial cells in sands, Geophys. Res. Lett., 32, L24402, doi:10.1029/2005GL024751.

Nyquist, J.E., and Corry, C.E. (2002), Self-potential: the ugly duckling of environmental geophysics, Leading Edge, 446-451.

Olhoeft, G.R. (1985), Low-frequency electrical properties, Geophysics, 50(12), 2492-2503.

Ollivier, B., and Magot, M., (eds.) (2005), Petroleum Microbiology, ASM Press, 365 p.

Palmer, I.D., and Traviolia, M.L. (1980), Attenuation by squirt flow in undersaturated gas sands, Geophysics, 45, 1780–1792.

Pamp, S.J., and Tolker-Nielsen, T. (2007), Multiple roles of biosurfactants in structural biofilm development by *Pseudomonas aeruginosa*, J. Bacteriol., 189(6), 2531–2539, doi:10.1128/JB.01515-06.

Personna Y.R., Ntarlagiannis, D., Slater, L., Yee, N., O'Brien, M., and Hubbard, S. (2008), Spectral induced polarization and electrodic potential monitoring of microbially mediated iron sulfide transformations, J. Geophys. Res., 113, G02020, doi:10.1029/2007JG000614.

Petiau, G. (2000), Second generation of lead-lead chloride electrodes for geophysical applications, Pure Appl. Geophys., 157, 357-382.

Phillips, D.H., Watson, D.B., Roh, Y., and Gu, B. (2003), Mineralogical characteristics and transformations during long-term operation of zerovalent iron reactive barrier, J. Environ, Qual., 32(6), 2033-2045.

Prodan, C., F. Mayo, J. R. Claycomb, J. H. Miller, and Benedik, M.J. (2004), Low-frequency, low-field dielectric spectroscopy of living cell suspensions, J. Appl. Phys., 95, 3754-3756.

Puls, R., Paul, C., and Powell, R. (1999), The application of in situ permeable reactive (zero-valent iron) barrier technology for the remediation of chlorate contaminated groundwater: a field test, Appl. Geochem., 14, 989-1000.

Pyrak-Nolte, L.J., Mullenbach, B.L., Li, X., Nolte, D.D., and Grader, A.S. (1999), Detecting sub-wavelength layers and interfaces in synthetic sediments using seismic wave transmission, Geophys. Res. Lett., 26, 127-130.

Reguera, G., McCarthy, K.D., Mehta, T., Nicoll, J.S., Tuominen, M.T., and Lovely, D.R. (2005), Extracellular electron transfer via microbial nanowires, Nat. Lett., 435(23), 1098-1101.

Revil, A., and Glover, P.W.J. (1998), Nature of surface electrical conductivity in natural sands, sandstones, and clays, Geophys. Res. Lett., 25, 691-694.

Revil, A., and Leroy, P. (2004), Governing equations for ionic transport in porous shales, J. Geophys. Res., 109, B03208, doi:10.1029/2003JB002755.

Revil, A., Cary, L., Fan, Q., Finizola, A., and Trolard, F. (2005), Self potential signals associated with preferential ground water flow pathways in a buried paleo-channel, Geophys. Res. Lett., 32, L07401, doi:10.1029/2004GL022124.

Revil, A., Naudet, V., Nouzaret, J., and Pessel, M. (2003), Principles of electrography applied to self-potential electrokinetic sources and hydrogeological applications, Water Resour. Res., 39(5), 1114, doi:10.1029/2001WR000916.

Reynolds, J.M. (1997), An introduction to applied and environmental geophysics, John Wiley and Sons, 806p.

Rinck-Pfeiffer, S.M., Ragusa, S.R., Sztajnbok, P., and Vandevelde, T. (2000), Interrelationships between biological, chemical and physical processes as an analog to clogging in Aquifer Storage and Recovery (ASR) wells, Wat. Res., 34(7), 2110-2118.

Ron, E.Z., and Rosenberg, E. (2001), Natural roles of biosurfactants, Environ. Microbiol., 3(4), 229, doi:10.1046/j.1462-2920.2001.00190.x.

Rosen, MJ. (1989), Surfactants and Interfacial Phenomena. 2nd Ed. New York: Wiley-Interscience, 393–419.

Sailhac, P., and Marquis, G. (2001), Analytic potentials for the forward and inverse modeling of SP anomalies caused by subsurface fluid flow, Geophys. Res. Lett., 28, 1851-1854.

Sato, M., and Mooney, H.M. (1960), The electrochemical mechanism of sulfide self-potentials, Geophysics, 25(1), 226-249.

Sauck, W.A., Atekwana, E.A., and Nash, M.S. (1998), High conductivities associated with an LNAPL plume imaged by integrated geophysical techniques, J. Env. Eng. Geophys., 2, 203-212.

Scherer, M.M., Richter, S., Valentine, R.L., Alvarez, P.J.J. (2000), Chemistry and microbiology of permeable reactive barriers for in situ groundwater clean up, Crit. Rev. Microbiol., 26, 221–264.

Shirazi, F. (1997), Development of biological permeable reactive barriers for removal of Chlorophenols (2,4,6-Trichlorophenol) in contaminated groundwater, Ph.D. Thesis, Oklahoma State University, Stillwater, OK.

Sill, W.R. (1983), Self-potential modeling from primary flows, Geophysics, 48, 76-86.

Silverman, M.P., and Munoz, E.F. (1974), Microbial metabolism and dynamic changes in the electrical conductivity of soil solutions: a method for detecting extraterrestrial life, Appl. Microbiol., 28(6), 960-967.

Slater, L., (2006), Near surface electrical characterization of hydraulic conductivity: from petrophysical properties to aquifer geometries - a review, Surv. Geophys., 28, 169-197.

Slater, L., and Lesmes, D.P. (2002), IP interpretation in environmental investigations, Geophysics, 67, 77-88.

Slater, L., Ntarlagiannis, D., Personna, Y.R., and Hubbard, S. (2007a), Pore-scale spectral induced polarization signatures associated with FeS biomineral transformations, Geophys. Res. Lett., 34, L21404, doi: 10.1029/2007GL031840.

Slater, L., Ntarlagiannis, Yee, N., O'Brien, M., Zhang, C., and Williams, K.H. (2007b), Electrodic voltages in the presence of dissolved sulfide: Implications for monitoring natural microbial activity, Geophysics, 73(2), 65-70.

Song, S., Song, Y., and Kwon, B. (2005), Application of hydrogeological and geophysical methods to delineate leakage pathways in an earth fill dam, Explor. Geophys., 36, 92-96.

Stoodley, P., Lewandowksi, Z., Boyle, J.D., and Lappin-Scott, H.M. (1999), Structural deformation of bacterial biofilms caused by short-term fluctuations in fluid shear: an in situ investigation of biofilm rheology, Biotech. Bioeng., 65(1), 83-92.

Sturman, P.J., Stewart, P.S., Cunningham, A.B., Bouwer, E.J., and Wolfram, J.H. (1995), Engineering scale-up of in situ bioremediation processes: a review, J. Contam. Hydrol., 19, 171-203.

Taylor, S.W., and Jaffé, P.R. (1990), Substrate and biomass transport in a porous medium, Water Resour. Res., 26(9), 2181–2194.

Telford, W.M., Geldart, I.P., and Sheriff, R.E. (1991), Applied geophysics, Cambridge University Press, 770 p.

Thullner, M., Schroth, M.H., Zeyer, J., and Kinzelbach, W. (2004), Modeling of a microbial growth experiment with bioclogging in a two-dimensional saturated porous media flow field, J. Contam. Hydrol., 70, 37-62.

Timm, F., and Moller, P. (2001), The relation between electric and redox potential: evidence from laboratory and field measurements, J. Geochem. Explor., 72(2), 115-128.

Tower, O.F. (1905), The conductivity of liquids: methods, results, chemical applications, and theoretical considerations, Chemical Publishing Co., Easton, PA., 182.

USEPA (2001), A Citizen's Guide to Permeable Reactive Barriers (PRBs), United States Environmental Protection Agency, USA. EPA/542/F-01-005.

USEPA (2002), Field Applications of In Situ Remediation Technologies: Permeable Reactive Barriers, United States Environmental Protection Agency, USA.

Vandevivere, P., and Baveye, P. (1992), Effect of bacterial extracellular polymers on the saturated hydraulic conductivity of sand columns, Appl. Environ. Microbiol., 58(5), 1690-1698.

Vanhala, H., and Soininen, H. (1995), Laboratory technique for measurement of spectral induced polarization response of soil samples, Geophys. Prospect., 43, 655-676.

Vinegar, H.J., and Waxman, M.H. (1984), Induced polarization of shaly sands, Geophysics, 49(8), 1267-1287.

Volkering, F., Breure, A.M., and Rulkens, W.H. (1998), Microbiological aspects of surfactant use for biological soil remediation, Biodegradation, 8, 401-417.

Watnick, P., and Kolter, R. (2000), Biofilm, city of microbes, J. Bacteriol., 182(10), 2675-2679.

Waxman, M.H., and Smits, L.J.M. (1968), Electrical conductivities in oil-bearing shaly sands, Soc. Petrol. Eng. Journal, 8, 107-122.

Welch, S.A., and Ullman, W.J. (1993), The effect of organic acids on feldspar dissolution rates and stoichiometry, Geochim. Cosmo. Acta, 57, 2725-2736.

Werkema, D.D., Atekwana, E.A., Enders, A., Sauck, W.A., and Cassidy, D.P. (2003), Investigating the geoelectrical response of hydrocarbon contamination undergoing biodegradation, Geophys. Res. Lett., 30, 1647, doi: 10.1029/2003GL017346.

Williams, K.H. (2002), Monitoring microbe-induced physical property changes using high-frequency acoustic waveform data: toward the development of a microbial megascope, M.S. Thesis, University of California, Berkeley, CA.

Williams, K.H., Ntarlagiannis, D., Slater, L.D., Dohnalkova, A., Hubbard, S.S., and Banfield, J.F. (2005), Geophysical imaging of stimulated microbial biomineralization, Environ. Sci. Technol., 39(19), 7592-7600.

Youssef, N., Simpson, D.R., Duncan, K.E., McInerney, M.J., Folmsbee, M., Fincher, T., and Knapp, R.M. (2007), In Situ Biosurfactant Production by *Bacillus* Strains Injected into a Limestone Petroleum Reservoir, Appl. Environ. Microbiol., 73(4), 1239–1247, doi:10.1128/AEM.02264-06.

Zhang, Y., and Miller, R.M. (1995), Effect of rhamnolipid (biosurfactant) structure on solubilization and biodegradation of n-alkanes, Appl. Environ. Microbiol., 61, 2247-2251.

Zolla, V., Sethi, R., and Di Molfetta, A. (2007), Performance assessment and monitoring of a permeable reactive barrier for the remediation of a contaminated site, Am. J. Environ. Sci., 3, 158-165.

VITA

Caroline Ann Davis was born August 8, 1978. In 1996, she graduated from Linn-Mar High School located in Marion, IA. She then went on to acquire her A.A. degree (1998) in International Business from Kirkwood Community College, Cedar Rapids, IA. She earned her B.S. (2001) in Geology from Iowa State University, Ames, IA, and an M.S. (2003) in Geology from Fort Hays State University, located in Hays, KS. Her Ph.D. in Geophysics was awarded in August 2009 from the Missouri University of Science and Technology.